

# Study of the Influence of Different Electrolyte Salts on the Performance of Lithium-Sulfur Batteries

by

Chenyang Guo

A thesis

presented to the University of Waterloo

in fulfillment of the

thesis requirement for the degree of

Master of Applied Science

in

Chemical Engineering

Waterloo, Ontario, Canada, 2021

©Chenyang Guo 2021

## **Author's Declaration**

I hereby declare that I am the sole author of this thesis. This is a true copy of the thesis, including any required final revisions, as accepted by my examiners.

I understand that my thesis may be made electronically available to the public.

## Abstract

Lithium-sulfur batteries (LSBs) have advantages of extremely high theoretical specific capacity and energy density, environmental friendliness and low cost, making it one of the top candidates for the next-generation energy storage systems. However, there are still some issues that hinder the commercialization of LSBs, including low practical energy density, short cycle life and safety hazards. These issues are directly caused by the insulating properties of sulfur and its discharge products, the dissolution and shuttle of reaction intermediates as well as the unstable interface between metallic lithium anode and electrolyte. The liquid electrolyte plays a pivotal role in the operation of Li-S batteries, which provides ions and promotes the transfer of ions between the sulfur cathode and the lithium anode. Therefore, the liquid electrolyte has a great influence on the performance of LSB. While there are many lithium salts that may be suitable for LSBs, the use of lithium electrolyte salts has been limited to a few, such as lithium bis(trifluoromethanesulfonyl)imide (LiTFSI). There is still a lack of a comprehensive understanding of the performance of Li-S batteries with lithium electrolyte salts commonly used in lithium-ion batteries. Therefore, the purpose of this thesis is to study the influence of several lithium salts in the electrolyte on the specific capacity and stability of LSBs.

The first part of this thesis is to systematically investigate the influence of five different lithium salts, namely, LiTFSI, lithium bromide (LiBr), lithium perchlorate (LiClO<sub>4</sub>), lithium trifluoromethanesulfonate (LiTf), and lithium hexafluorophosphate (LiPF<sub>6</sub>), in the electrolyte on the performance of LSBs. The effects of electrolytes with different lithium salts on the electrochemical performance of Li-S batteries are evaluated, including long-term cycling and rate performance, sulfur utilization, compatibility with lithium metal anode, reversibility, and redox reactions. It is found that the rate capability is highly dependent on the ionic conductivity of the electrolyte imparted by the lithium salt. Among the five lithium salts used, the battery using lithium bromide (LiBr) shows

the highest initial capacity and best 0.2C galvanostatic cycling stability and sulfur utilization. On the other hand, batteries using LiBr experience overcharge and voltage fluctuations during electrochemical cycling, severe surges during cyclic voltammetry testing, and poor high c-rate performance. The second part of the thesis focuses on troubleshooting and optimization of most promising LiBr-based LSBs. Firstly, the possible causes of the overcharging and current surge problems associated with LiBr-based batteries are studied. It is found that the cathode side rather than the anode side causes the problems. By replacing the PVDF binder with a crosslinked PEI-Araldite 506 epoxy resin binder, the overcharging and current surge problems are solved. In addition, the cycling performance is improved, and the longer cycle life is achieved. Unexpectedly, the high c-rate performance is also greatly improved. Finally, cathodes with higher areal sulfur loading of  $6.3 \text{ mg cm}^{-2}$  using PEI-Araldite 506 epoxy resin are tested in the LiBr electrolyte. The initial specific capacity of the battery is as high as  $1090.2 \text{ mAh g}^{-1}$ , and it remains above  $523 \text{ mAh g}^{-1}$  after 100 cycles at 0.1 C.

Therefore, this work provided insights on the effects of different electrolyte salts on the specific capacity, rate performance and cycle stability of LSBs, and determined that LiBr is a promising electrolyte salt for achieving improved performance of LSBs. After solving problems induced by LiBr electrolyte, a baseline research combination was established for future LiBr-based optimization work. Besides, the way those problems were solved helps contribute more insights to a common challenge that LSBs must be faced with in the process of continuous advancement, e.g., adopting the strategy to realize controllable electrodeposition of discharge products during charge in this case.

## **Acknowledgements**

The work reported herein was financially supported by Discovery Grants (RGPIN-2016-04366) of the Natural Sciences and Engineering Research Council (NSERC) of Canada.

I would like to express my sincere gratitude to my supervisors, Dr. Yuning Li and Dr. Bo Cui, for the great support and patient guidance, and for assisting me to forward my research efficiently and to enjoy the process of research throughout my master period. I feel very lucky and honored to work with them. I would also like to thank Prof. Eric Croiset for reviewing my thesis and providing precious suggestions and comments.

I am very thankful to Xiguang Gao who taught me laboratory skills and helped my research on Li-S batteries. I also would like to thank Dr. Zhong Ma, Dr. Guan Xi, Dr. Fengmei Li for giving me valuable advice during the research. My thanks also go to Pankaj Kumar for helping me test the XRD of samples.

Finally, I would like to show great thankfulness to my family and friends for their constant support.

## Table of Contents

Author's Declaration .....	ii
Abstract .....	iii
Acknowledgements .....	v
List of Figures .....	ix
List of Tables .....	xiv
List of Abbreviations .....	xv
List of Symbols .....	xvi
Chapter 1. Introduction .....	1
1.1 Research background .....	1
1.2 Overview of lithium-based rechargeable batteries .....	2
1.2.1 Fundamental concepts of lithium-based rechargeable batteries .....	3
1.2.2 Principles and limitations of current lithium-ion battery .....	5
1.3 General concept of lithium-sulfur battery .....	8
1.3.1 Working principles of Li-S battery .....	9
1.3.2 Great challenges towards Li-S battery .....	11
1.4 Current approaches on electrolyte and binder .....	14
1.4.1 Functional electrolyte solvent .....	14
1.4.2 Lithium salt and its concentration .....	18
1.4.3 Additive and anode protection .....	20
1.4.4 Functional binder .....	21
1.5 Objective and structure of this thesis .....	24

Chapter 2. Electrochemical Characterization Methods and Other Techniques .....	25
2.1 Coin cell configuration .....	25
2.2 Galvanostatic discharge/ charge .....	26
2.3 Cyclic voltammetry .....	26
2.4 Potentiostatic electrochemical impedance spectroscopy (PEIS) .....	27
2.5 Ultraviolet–visible absorption spectroscopy (UV-vis) .....	28
Chapter 3. Impact of Different Lithium Salts on the Cycling Performance of Li-S Batteries .....	30
3.1 Introduction .....	30
3.2 Experimental section .....	34
3.3 Results and discussion .....	36
3.3.1 Cycling performance comparison of five lithium salts .....	36
3.3.2 Voltage barrier at the beginning of oxidizing $\text{Li}_2\text{S}$ .....	41
3.3.3 Compatibility with lithium anodes and self-discharge behavior .....	43
3.3.4 Kinetics of electrochemical reactions for different lithium salts .....	46
3.3.5 Charge transfer process of batteries with different lithium salts .....	50
3.4 Conclusion .....	53
Chapter 4. Troubleshooting and Optimization for LiBr-based Li-S Batteries .....	54
4.1 Introduction .....	54
4.2 Experimental section .....	54
4.3 Results and discussion .....	55
4.3.1 Exploration of possible reasons for problems of Li-S cells using LiBr salt .....	55
4.3.2 Attempts to solve the cathode structural problem .....	64

4.3.3 The solution to the structural problem of sulfur cathode .....	67
4.4 Conclusion.....	74
Chapter 5. Summary and Future Directions .....	76
Bibliography .....	78



## List of Figures

<b>Figure 1-1. (a) Annual total carbon dioxide emissions divided by world region.</b> (Reference: Carbon Dioxide Information Analysis Center (CDAIAC) from Global Carbon Project). <b>(b) Air pollution.</b> (Reference: conserve-energy-future.com).....	1
<b>Figure 1-2. Schematic of structure and operating principle of Li-ion battery</b> <sup>6</sup> . Reproduced from Reference 6. ....	7
<b>Figure 1-3. (a) A comparison of the average discharge potentials and specific capacities for two types of electrodes used in lithium-based batteries.</b> <sup>7</sup> <b>(b) An overview of the theoretical and practical energy density of different types of batteries belonging to integration or intercalation electrochemistry</b> <sup>8</sup> . Reproduced from reference 7 and 8. ....	9
<b>Figure 1-4. Schematic of material change during electrochemical process and the structure of a Li-S cell</b> <sup>11</sup> . Reproduced from reference 11. ....	10
<b>Figure 1-5. The relationship between calculated gravimetric energy densities and E/S ratio as well as areal sulfur loading</b> <sup>16</sup> . Reproduced from reference 16. ....	12
<b>Figure 1-6. A schematic illustration of surface film formation on Li electrodes in DOL solutions</b> <sup>25</sup> . Reproduced from reference 25. ....	15
<b>Figure 1-7. Three types of electrochemical reaction schemes for LSBs</b> <sup>26</sup> . (a) Di-anion route in conventional ether-based electrolyte with poor solubility of short-chain polysulfides and Li <sub>2</sub> S causes early passivation of the cathode surface. (b) Quasi-solid-state route in non/sparsely-solvating electrolyte with negligible soluble intermediates. (c) Radical route in high DN or dielectric constant electrolyte with S <sub>3</sub> <sup>•-</sup> radical intermediate. Reproduced from reference 26.....	16
<b>Figure 1-8. Scanning electron microscopy images of metallic lithium anodes</b> <sup>37</sup> . (a) Fresh lithium metal, (b) Lithium metal with 2M LiTFSI after 278 cycles. (c) Lithium metal with 4M LiTFSI after 183 cycles. (d) Lithium metal with 7M LiTFSI electrolyte after 280 cycles. Reproduced from reference 37. ....	19

<b>Figure 1-9.</b> A schematic illustration of the cross-linking of CMC binder with CA as the linker, based on the esterification of the –OH groups in CMC and the –COOH groups in CA at 150 °C, and the SEM images of sulfur cathode surface using PVDF and cross-linked CMC–CA binder <sup>49</sup> . Reproduced from reference 45. ....	22
<b>Figure 2-1.</b> Schematic diagram of the Li-S coin cell adopted for this research <sup>58</sup> . Reproduced from reference 58.....	25
<b>Figure 3-1. Charge and discharge voltage profiles of several overcharged cycles for LiBr battery during (a) 0.2C galvanostatic cycling and (b) rate performance test.</b> The fluctuation of voltage would not stop unless a cut-off charging time was set before the cycling.....	37
<b>Figure 3-2. Electrochemical characteristics of Li-S batteries with different lithium salts.</b> Electrolyte comprises following compositions, 1 M lithium salt in 1,3-dioxolane (DOL) + 1,2-dimethoxyethane (DME), (1:1 by volume) and 2wt% LiNO <sub>3</sub> as additive. <b>a)</b> Specific discharge capacity of batteries over 100 cycles at 0.2C. <b>b)</b> Coulombic efficiency values for 100 charge/discharge cycles at 0.2C. <b>c)</b> Charge and discharge voltage profile of batteries for 1 <sup>st</sup> cycle at 0.2C. <b>d)</b> Elemental sulfur utilization defined by specific discharge capacity drawn from first discharge plateau divided by theoretical value for 100 cycles at 0.2C. <b>e)</b> Capacity ratio of batteries with different lithium salts for 100 discharge/charge cycles. <b>f)</b> Rate performance test for 30 discharge/charge cycles in total with current density ranging from 0.1C to 2C, then returning to 0.1C.....	39
<b>Figure 3-3.</b> Variation trend of voltage spike at onset of charge for batteries with different electrolytes. ....	42
<b>Figure 3-4. Compatibility of lithium metal electrode and electrolyte with varying lithium salts.</b> Voltage variation curves of Li/Li symmetric cell during Li plating and stripping process in different electrolyte at a galvanostatic condition of 0.5 mA cm <sup>-2</sup> . Electrolyte system includes 1 M varying lithium salt + 2wt% LiNO <sub>3</sub> in DOL/DME (1:1 by volume ratio). Five lithium salts were presented in two separate figure for the purpose of clarity. ....	44

<b>Figure 3-5. Variation of open circuit voltages (<math>V_{oc}</math>) of LSBs using different lithium salts during the self-discharge measurement.</b> Electrolyte system includes 1 M varying lithium salt + 2wt% $\text{LiNO}_3$ in DOL/DME (1:1 by volume ratio).....	45
<b>Figure 3-6. Cyclic voltammograms of Li-S batteries with varying lithium electrolyte salts.</b> a) 2 <sup>nd</sup> cycle of cyclic voltammetry (CV) at a sweep rate of 0.2 mV/s. b) Peak potential obtained from Zone I, II and III. c) Onset potential extracted from Zone I, II and III. d) Overpotential drawn from cyclic voltammograms of five different batteries where peak potential of Zone III minus peak potential of Zone II. ....	47
<b>Figure 3-7. Onset potential for electrochemical reactions of Li-S battery with <math>\text{LiClO}_4</math> electrolyte.</b> a) Differential CV curves. b) Normal CV curves with $\text{mA}/\text{cm}^2$ unit for y-axis. ....	48
<b>Figure 3-8. (a) Electrochemical impedance spectrum</b> of batteries after cyclic voltammetry test for four cycles. <b>(b) The equivalent circuit model</b> for EIS analysis based on two-electrode Li-S coin cells. ....	51
<b>Figure 4-1. Voltage profiles of Li-S cell using electrolyte without adding <math>\text{LiNO}_3</math> at 0.2C.</b> The electrolyte composition includes 1M $\text{LiBr}$ in DOL/DME (1:1 by volume ratio).....	57
<b>Figure 4-2. Voltage profiles of Li-S batteries using different E/S ratios at 0.2C.</b> (a) $5\mu\text{L mg}^{-1}$ . (b) $8\mu\text{L mg}^{-1}$ . (c) $12\mu\text{L mg}^{-1}$ . The electrolyte composition includes 1M $\text{LiTFSI}+2\text{wt}\% \text{LiNO}_3$ in DOL/DME ( $v/v=1:1$ ). ....	59
<b>Figure 4-3. Comparison of conventional Li-S cell and Li-Polysulfide liquid cell.</b> (a) 0.2C galvanostatic cycling. (b) Rate performance test. (c, d) Voltage profile of Li-Polysulfide liquid cell from 0.2C cycling and rate performance. (e, f) CV scan results. The electrolyte composition for conventional Li-S cell includes 1M $\text{LiBr}+2\text{wt}\% \text{LiNO}_3$ in DOL/DME ( $v/v=1:1$ ), while the catholyte composition for Li-Polysulfide liquid cell 1M $\text{LiBr}+0.3\text{M LiNO}_3+0.3\text{MLi}_2\text{S}_6$ in DOL/DME ( $v/v=1:1$ ). The scan rate for CV was 0.2mV/s. ....	62

**Figure 4-4. Comparison of conventional Li-S cells using LiBr electrolyte and PVDF/Na-alginate/SBR-CMC binder.** (a) 0.2C galvanostatic cycling. (b) rate performance test. (c, d) CV scan results. The electrolyte composition includes 1M LiBr+2wt% LiNO<sub>3</sub> in DOL/DME (v/v=1:1). The scan rate for CV was 0.2mV/s.....65

**Figure 4-5. Schematics of in situ step-growth polymerization of polyethylenimine (PEI) and Araldite 506 epoxy resin (ER) in the presence of sulfur (S) and conductive carbon black (C) to form a PEI-ER:S:C cathode composite material.** S and C particles are tightly held by the cross-linked 3D PEI-506 network <sup>125</sup>. Reproduced from reference 125. ....69

**Figure 4-6. Comparison of conventional Li-S batteries using LiBr electrolyte and crosslinked binders with different mass ratios of PEI to Araldite 506.** (a) 0.2C galvanostatic cycling. (b) rate performance. (c-f) CV scan results. The electrolyte composition includes 1M LiBr+2wt% LiN;O<sub>3</sub> in DOL/DME (v/v=1:1). (a) 0.2C cycling performance. (b) Rate performance. (c-f) Cyclic voltammogram at the scan rate of 0.2 mV s<sup>-1</sup>.....70

**Figure 4-7. Comparison of conventional Li-S batteries using PEI-Araldite 506 binder with different lithium electrolyte salts during 0.2C.** The electrolyte composition includes 1M LiX+2wt% LiNO<sub>3</sub> in DOL/DME (v/v=1:1).....71

**Figure 4-8. Comparison of conventional Li-S batteries using LiBr electrolyte and PVDF binder/ PEI-Araldite 506 binder** during (a) 0.2C galvanostatic cycling and (b) rate performance test. (c) Elemental sulfur utilization and (d) capacity (plateau) ratio under three different combinations. The electrolyte composition includes 1M LiBr/LiTFSI+2wt% LiNO<sub>3</sub> in DOL/DME (v/v=1:1). ....72

**Figure 4-9. (a) Comparison of 0.2C cycle performance of LSBs using LiBr electrolyte with PVDF binder and PEI-506 binder (different mass ratios) at extended cycles.** Batteries were kept cycling until being subject to a sharp decline of capacity, which were considered as “dead”. **(b) 0.1C cycle performance of LSBs using**

<b>LiBr electrolyte with higher sulfur loading based on carbon paper.</b> First several cycles were for activation at 0.05C.....	72
--	----

## List of Tables

<b>Table 3-1.</b> A summary of basic information and properties of different lithium salts in this work <sup>78-80</sup> .....	31
<b>Table 3-2.</b> A summary of resistance values simulated by ZView for batteries with different electrolytes. ....	51
<b>Table 3-3.</b> The comparison of key performance parameters of LSBs with different lithium salts .....	52
<b>Table 4-1.</b> A comparison of particle size of conductive agent and pore diameter of separator <sup>114, 115</sup> .....	63

## List of Abbreviations

CE	Coulombic efficiency
CMC	Carboxymethyl cellulose
CNT	Carbon nanotube
CV	Cyclic voltammetry
DN	Gutmann donor number
EIS	Electrochemical impedance spectroscopy
EV	Electric vehicles
HOMO	Highest occupied molecular orbital
LSB(s)	Lithium-sulfur (Li-S) batteries
LIB(s)	Lithium-ion (Li-ion) batteries
LMB(s)	Lithium-metal batteries
LUMO	Lowest unoccupied molecular orbital
SA	Sodium alginate
SBR	Styrene butadiene rubber
SEI	Solid electrolyte interface
SEM	Scanning electron microscopy
TEGDME	Tetraethylene glycol dimethyl ether
TEM	Transmission electron microscopy
UV-Vis	Ultraviolet-visible
XANES	X-ray absorption near-edge structure
XAS	X-ray absorption spectroscopy
XPS	X-ray photoelectron spectroscopy
XRD	X-ray diffraction

## List of Symbols

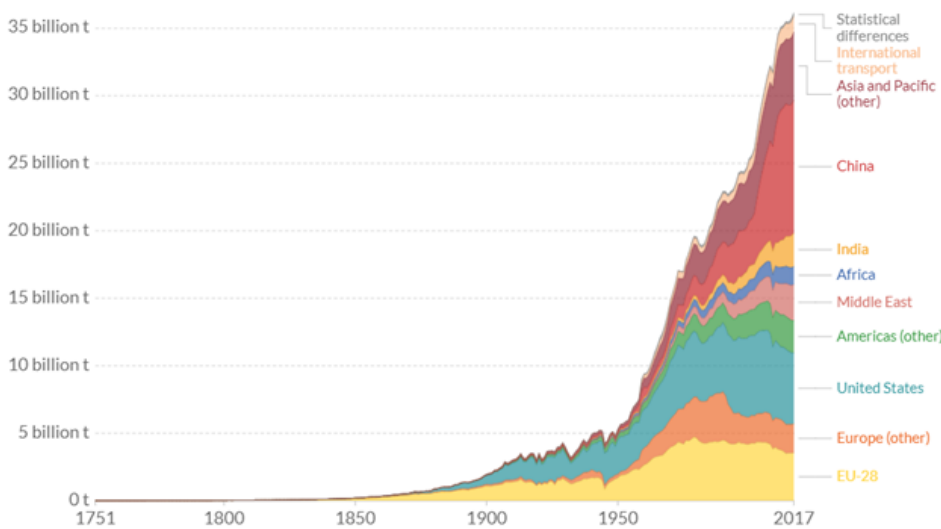
BTFE	Bis(2,2,2-trifluoroethyl) ether
DMA	Dimethylacetamide
DME	Dimethoxymethane
DMSO	Dimethyl sulfoxide
DOL	1,3-dioxolane
E/S ratio	Ratio of volume of electrolyte added to sulfur loading on the cathode
LiFSI	Lithium bis(trifluoromethanesulfonyl)imide
LiHFDF	Lithium 1, 1, 2, 2, 3, 3-hexafluoropropane-1, 3-disulfonimide
LiPS(s)	Lithium polysulfides
LiTFSI	Bis(trifluoromethanesulfonyl)imide lithium
LiTNFSI	Lithium (trifluoromethanesulfonyl)(n-nonafluorobutanesulfonyl)imide
LiBr	Lithium bromide
LiClO <sub>4</sub>	Lithium perchlorate
LiTf	Lithium trifluoromethanesulfonate
LiPF <sub>6</sub>	Lithium hexafluorophosphate
LiNO <sub>3</sub>	Lithium nitrate
NMP	N-Methyl-2-pyrrolidone
OFE	1H,1H,5H-octafluoropentyl-1,1,2,2-tetrafluoroethyl ether
PVDF	Polyvinylidene fluoride
PVP	Polyvinylpyrrolidone
TFEE	1,2-(1,1,2,2-tetrafluoroethoxy)ethane
TFTFE	1,1,2,2-Tetrafluoroethyl 2,2,2-trifluoroethyl ether
TTE	1,1,2,2-tetra-fluoroethyl 2,2,3,3-tetrafluoropropyl ether
V <sub>oc</sub>	Open-circuit voltage



# Chapter 1. Introduction

## 1.1 Research background

Starting from the second industrial revolution, electricity and oil have gradually become the main new energy sources used by human society after the invention of generators. Fueled by coal and gasoline, the invention of internal combustion engines and diesel engines promoted the development of petroleum extraction industry and the emergence of petrochemical industry. Although the industrialization greatly promoted productivity, the rapid economic development was accompanied not only by the global warming but also the severe air pollution due to the consumption of fossil fuel. As shown in **Figure 1-1a**, the annual total carbon dioxide emission has been starting to skyrocket ever since the early twentieth century.



(a)



(b)

**Figure 1-1. (a) Annual total carbon dioxide emissions divided by world region.** (Reference: Carbon Dioxide Information Analysis Center (CDIAC) from Global Carbon Project). **(b) Air pollution.** (Reference: conserve-energy-future.com)

Thus, renewable clean energy such as hydropower, wind or the solar energy gradually enter people's field of vision as possible alternatives to the fossil fuels. The produced energy is transformed into electricity and then transferred to the large-scale electric grid to facilitate transportation. But all those renewable energy have the disadvantages of

being intermittent and require good energy storage system with as high energy conversion efficiency as possible. Moreover, the popularization of electric vehicles is also an important step to combat the use of fossil fuels, which further accelerates the development of energy storage system. Rechargeable batteries store the electric energy in the form of chemical energy with advantages of low cost, high energy density and environmental friendliness.

## **1.2 Overview of lithium-based rechargeable batteries**

There has been a long history since people started using batteries as the energy storage system. According to the records, the Baghdad battery was regarded as the first electrochemical cell that people knew of, which was about 2500 years old. It is basically a clay pot sealed with bitumen, inside which an iron rod was surrounded by copper cylinders. At present, cells can be categorized as either primary batteries or secondary batteries.

Secondary batteries are also called rechargeable batteries in contrast to the primary battery or one-shot battery. Instead of just single use for the latter one, rechargeable batteries are capable of having reversible charge and discharge that sustain for a certain life span. This ability originates from the reversible nature of redox reactions. Due to this important advantage, rechargeable batteries are right now more efficient and popular than primary batteries such as zinc-carbon and alkaline batteries that used to be dominant in the market.

There are many types of common rechargeable batteries, e.g. nickel-cadmium (NiCd), nickel-metal hydride (NiMH), lead-acid, lithium-based batteries (lithium-ion, lithium-ion polymer, lithium-metal). Lead-acid was the first rechargeable battery invented in 1859 by Gaston Planté. Followed by this invention, the first alkaline battery (NiCd) was developed in 1899, and the emergence of NiMH on the market was in 1989. NiMH battery gradually substituted the use of NiCd because of the toxic cadmium. As people are entering the information era, the outbreak of portable electronics and electric

vehicles triggered the appearance of batteries with higher energy density, environmental friendliness and safety. Lithium-based rechargeable batteries have been receiving the most attention by researchers. Among all the metals, lithium has the lightest mass (density =  $0.53 \text{ g cm}^{-3}$ ) and the lowest electrochemical potential, which are very attractive characteristics for the promising energy storage system. Since the invention of LIBs in 1980 and commercialization in 1991, LIBs have snatched a great portion of the battery market share. The development of LIBs was also recognized by Nobel Prize in Chemistry in 2019.

#### 1.2.1 Fundamental concepts of lithium-based rechargeable batteries

A rechargeable battery is usually comprised of a certain number of electrochemical cells connected in parallel or series <sup>1</sup> for the purpose of attaining required voltage and current output. Therefore, researchers in relevant areas put their emphasis on the advancement of a single electrochemical cell, e.g. optimizing the system and improving electrochemical performance. A single electrochemical cell includes one positive electrode and one negative electrode, also called a cathode and an anode. They are divided by an insulating separator to avoid short-circuiting and with a lot of nanopores to allow liquid electrolyte permeation. In some cases, two electrodes are directly separated by the solid electrolyte. To ensure the successful operation of an electrochemical cell, the conduction of electrons and transport of ions both happen but in different locations. An exterior electric circuit links two electrodes, providing path for the conduction of electrons during the electrochemical process. Meanwhile, the transport of ions occurs in the electrolyte, stemming from the disparity of chemical potentials between the anode and cathode. Thus, there are reduction half-reaction and oxidation half-reaction in positive electrode and negative electrode during discharge and the other way around during charge.

Before digging into the world of lithium-based rechargeable batteries, it is very important to define and illustrate some fundamental concepts in order to get the work

across in this thesis. These concepts are usually used for describing or assessing the performance of an electrochemical cell.

◆ Potential (V, volt). Its value is dictated by the potential difference of redox reactions happening at two electrodes within an electrochemical cell. The redox potential of each electrode is defined by the law of thermodynamics and is inherent depending on active material. Larger potential difference between the cathode and anode signifies the higher output power since it is equal to the product of current and voltage. Therefore, the electrolyte must be carefully selected to be stable within the electrochemical voltage window of the battery to prevent the possible decomposition.

◆ Current Density ( $I$ ,  $\text{mA g}^{-1}$ ). When taking power density into account, the battery discharge/charge current is an important parameter. The "C/m" rate represents the "speed" ( $\text{mA g}^{-1}$ ) at which the theoretical specific capacity is reached within m hours during discharge. The advantage of using higher rates is higher power rendered but at the cost of higher polarization and lower specific capacity. With the increase of c-rate, one electrochemical cell is deemed to possess high rate capability if it could maintain the capacity and degree of polarization .

◆ Specific/Volumetric Capacity ( $\text{mA h g}^{-1}$  or  $\text{mA h cm}^{-3}$ ). It is defined by the amount of charge ( $\text{mA h}$ ) stored per full mass or volume of electrode for one discharge/charge. Similarly, energy density is also used often with the unit of  $\text{Wh/kg}$  or  $\text{Wh/L}$  for evaluating the battery performance. Two parameters are both the higher the better for a newly developed battery system.

◆ Discharge/Charge Voltage Profile. The graph shows the evolution of voltage with specific capacity for the battery in the galvanostatic mode that constant discharge/charge current density is imposed. Different redox reactions can be identified and analyzed by looking at the voltage range that they occur. The voltage plateau on the curve symbolizes the occurrence of a two-phase transition reaction,

while the slope represents a homogeneous reaction. It is expected that smaller voltage hysteresis between the discharge curve and charge curve (indicating lower polarization) achieves the maximum energy efficiency.

◆ **Cycling Life.** It is an indicator used for measuring the duration that a battery can last before being regarded as reaching the limit. Essentially, cycling life could be quantified by the number of cycle corresponding to a certain capacity retention. This parameter is crucial at the industrial level, but in laboratory scale there are so many factors that influence the final result so that it is not always easy to obtain satisfactory reproducibility. For laboratory experiments, a certain value of capacity retention is usually set for the galvanostatic cycling. If the capacity retention of a battery has dropped to this specified percentage, this battery is regarded as reaching its cycling life.

◆ **Coulombic Efficiency (CE, %).** It is defined by the ratio of discharge specific capacity to charge specific capacity in the same cycle, which gives researchers a sense on how much charge is released during the discharge process.

◆ **Capacity Retention (%).** Within a specified number of cycles, capacity retention describes the degree of reversibility of a battery by comparing current discharge specific capacity to that of the initial one or the cycle that has the highest discharge specific capacity. It is mostly expressed in the form of a percentage or fraction.

### 1.2.2 Principles and limitations of current lithium-ion battery

As mentioned earlier in **section 1.2**, lithium has the most negative standard electrode potential (- 3.045V vs. Standard hydrogen electrode) among all the metal elements, and its lowest atomic weight ( $6.941 \text{ g mol}^{-1}$ ) suggests that lightest mass was needed for the gain or loss of electrons of lithium atom. As a result, theoretical specific capacity of metallic lithium is up to  $3860 \text{ mA h g}^{-1}$ , while other metals like zinc and lead can only get to  $825 \text{ mA h g}^{-1}$  and  $260 \text{ mA h g}^{-1}$ , respectively. The commercial application of

lithium-based batteries started by primary batteries, including but not limited to Li-FeS<sub>2</sub>, Li-MnO<sub>2</sub>, Li-SOCl<sub>2</sub> et al. Considering the huge potential of metallic lithium and limited reserves of lithium resources, the use of primary cell could no longer satisfy the requirement for sustainable development.

Rechargeable lithium battery system can be divided into two categories based on different electrochemistry. For the intercalation electrochemistry, the battery realizes the charge/ discharge process through topotactic insertion/ extraction of the lithium ions on both electrodes. For the integration electrochemistry, it depends on the reversible reaction of Li<sup>+</sup> with active material and corresponding chemical conversion (Li-O<sub>2</sub> and Li-S batteries). LIBs fall into the first category mentioned in last paragraph. The intercalation electrochemistry was firstly investigated in 1976 by M. Stanley Whittingham <sup>2</sup> using layered TiS<sub>2</sub> and cathode material combined with lithium metal as the anode. This type of lithium metal battery was always haunted by the safety problem due to the growth of lithium dendrite. In 1990, a Canadian company called Moli Energy went bankruptcy caused by an explosion in the battery warehouse. The first attempt to commercialize the lithium metal batteries failed and resulted in a low tide for the development of LMBs. During the same period, the LIBs underwent rapid progress. In 1977, Armand et al. <sup>3</sup> reported lithium-graphite intercalation compounds, which laid the ground for using graphite as anode material of LIBs in the future. Subsequently, Goodenough et al. <sup>4</sup> synthesized the ideal cathode material for LIBs in 1980 that was Li<sub>x</sub>CoO<sub>2</sub> compound with layered intercalated structure where they observed the reversible de/intercalation process of Li<sup>+</sup> in this compound. Combining the LiCoO<sub>2</sub> with a type of novel one-dimensional graphite as anode developed by Akira et al. <sup>5</sup>, the first prototype of LIB was built up in 1985. Finally, the mass production was realized by Sony company in 1991.

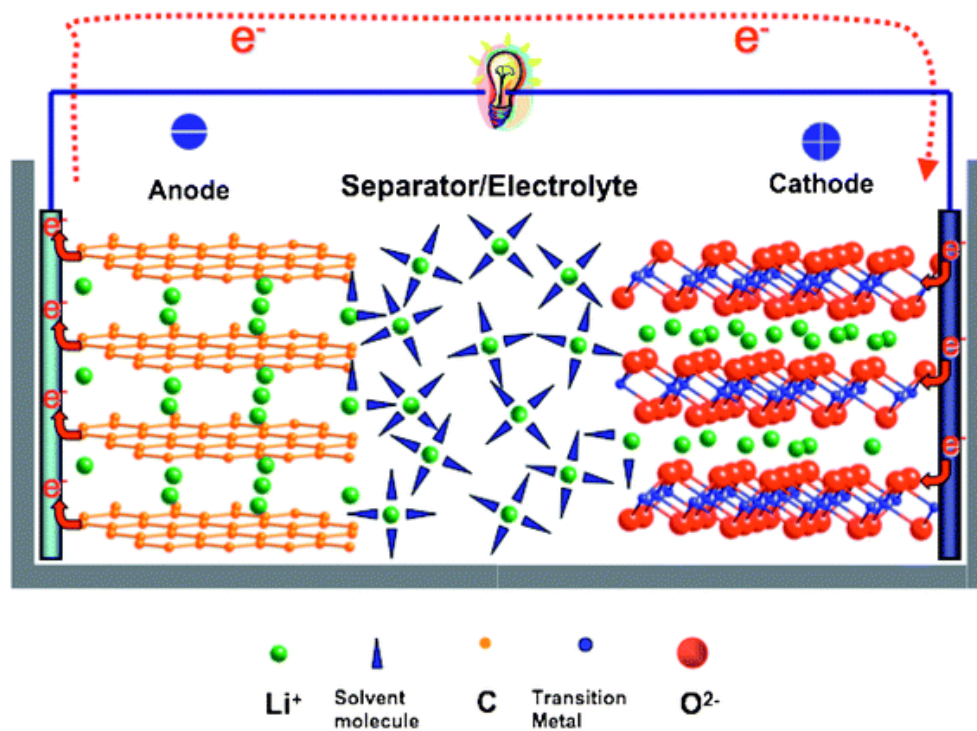


**Figure 1-2. Schematic of structure and operating principle of Li-ion battery** <sup>6</sup>. Reproduced from Reference 6.

The structure and working principle of LIBs is outlined in **Figure 1-2**. Generally, the negative electrode of the battery is carbonaceous material, while the positive electrode is lithium-containing transition metal oxide such as  $\text{LiCoO}_2$ ,  $\text{LiMn}_2\text{O}_4$  or  $\text{LiFePO}_4$ , etc. The electrolyte is either an organic solution or polymer with lithium salt. During charging process, lithium ions de-intercalate from the  $\text{LiCoO}_2$  or  $\text{LiMn}_2\text{O}_4$  crystals and intercalate to the layered carbonaceous cathode in the lattice structure through the electrolyte and vice versa. When the battery cycling is in normal state, the de/intercalation between two electrodes only cause the change of layered spacing without damaging the crystal structure of the cathode, and so does the graphite anode. Influenced by the type of metal oxide of the cathode, there are two forms of Li-ion intercalation consisting of a single-phase or a two-phase conversion. The former one requires expansion or shrinkage of the unit cell during the de/ lithiation, whereas the two-phase conversion, as the name suggests, concerns phase transition during  $\text{Li}^+$  insertion/extraction such as  $\text{LiFePO}_4$  and  $\text{Li}_4\text{Ti}_5\text{O}_{12}$  compound. Also, the crystal structure of

cathode compound governs the pathway that the  $\text{Li}^+$  move into the lattice. For example,  $\text{LiMn}_2\text{O}_4$  with 3D spinel structure usually have lower mass transfer resistance than the  $\text{LiCoO}_2$  with 2D layered structure. With the continuous deepening of understanding to LIBs,  $\text{LiFePO}_4$  cathode has been demonstrated to be much safer and more stable than  $\text{LiCoO}_2$ , NMC and NCA due to its tetrahedra structure of  $\text{PO}_4^{3-}$ . And  $\text{LiFePO}_4$  is able to deliver higher practical specific capacity ( $165 \text{ mAh g}^{-1}$ ) than  $\text{LiCoO}_2$  ( $145 \text{ mAh g}^{-1}$ ) but lower than NMC ( $170 \text{ mAh g}^{-1}$ ) and NCA ( $200 \text{ mAh g}^{-1}$ ) cathode.

The advent of LIBs indeed made their contribution to responding to the explosion of portable electronics. The development of microelectronics technology has not slowed down, and miniaturization, light weight, diversified performance, and portability of devices are still the future direction of mainstream. On top of that, electric vehicles are constantly anticipated to be running with longer mileage per charge. Higher requirements were placed on battery systems to meet. Nevertheless, current state-of-the-art LIBs are approaching their theoretical limit ( $400 \text{ Wh kg}^{-1}$ ) after decades of optimization. The way of storing energy based on intercalation mechanism became unsatisfactory. Widening the voltage window of operation for LIBs is also not feasible since the decomposition of most aprotic electrolyte might occur once beyond the electrochemical window.

### 1.3 General concept of lithium-sulfur battery

Because of those limitations of current LIBs as discussed in **section 1.2.2**, alternative integration electrochemistry gradually drew interests of researchers. It is a process that has ions and electrons involved in the redox reactions on the electrode as well as chemical transformation. The theoretical specific capacities of most conversion (integration) cathodes/ anodes are greater than the intercalation cathodes/ anodes as shown in **Figure 1-3a**. The most promising candidate based on this mechanism is LSB ranking second according to **Figure 1-3b**.  $\text{Li-O}_2$  battery also belongs to this category but it is still seen as the far-future energy storage system.



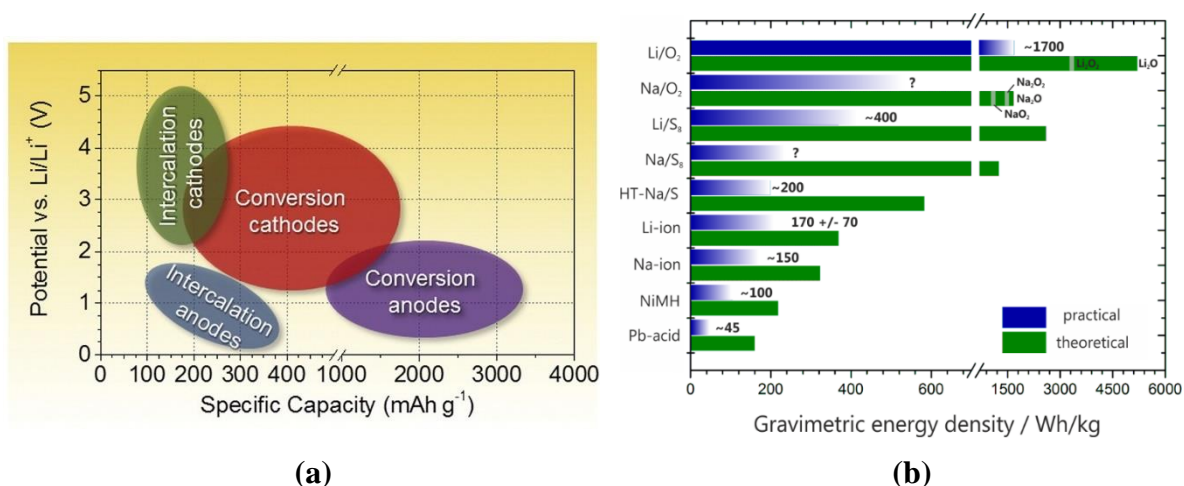


**Figure 1-3.** (a) A comparison of the average discharge potentials and specific capacities for two types of electrodes used in lithium-based batteries.<sup>7</sup> (b) An overview of the theoretical and practical energy density of different types of batteries belonging to integration or intercalation electrochemistry<sup>8</sup>. Reproduced from reference 7 and 8.

The theoretical specific capacity and energy density of LSB is  $1672 \text{ mAh g}^{-1}$  and  $2600 \text{ Wh kg}^{-1}$ , respectively, which are around 6 times higher than that of LIBs ( $280 \text{ mAh g}^{-1}$  and  $400 \text{ Wh kg}^{-1}$ ). Second advantage lies in the greatly natural abundance of elemental sulfur, and it is also vastly produced as by-product during natural gas processing and oil refining. Both contribute to its cheap price and environmental friendliness.

### 1.3.1 Working principles of Li-S battery

The first primary LSB was invented in 1962 by Herbert<sup>9</sup> and Ulam, while the first rechargeable LSB was made possible by adopting ethers<sup>10</sup> as electrolyte solvent. Traditionally, a Li-S cell is composed of a metallic lithium anode and a sulfur-containing cathode with aprotic electrolyte in between. Due to the insulating nature of elemental sulfur, it is usually mixed with conductive carbon additive to form the sulfur-composite bound by the polymer binder as shown in **Figure 1-4**.

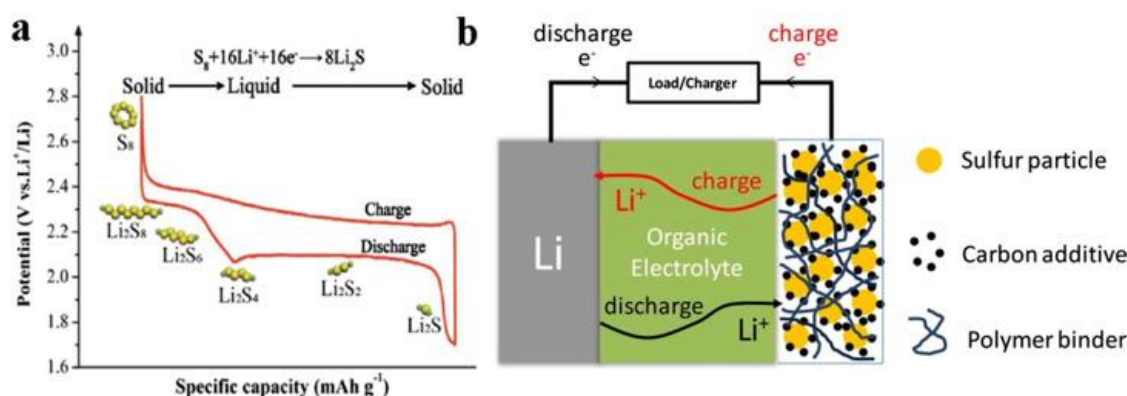
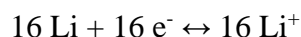


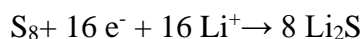
**Figure 1-4.** Schematic of material change during electrochemical process and the structure of a Li-S cell<sup>11</sup>. Reproduced from reference 11.

Electrochemical reactions during electrochemical cycling are shown per below:

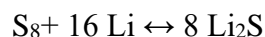
Negative electrode (lithium metal anode),



Positive electrode (sulfur cathode),



Overall reaction,



The cyclic octasulfur ( $\text{S}_8$ ) is the most stable and hence common form of solid allotrope for elemental sulfur. However, the reduction of sulfur is not a single step reaction, and there are many lithium polysulfide intermediates ( $\text{Li}_2\text{S}_x$ ,  $2 < x \leq 8$ ) forming during the cycling process. Left schematic graph in **Figure 1-4** showed the typical discharge/charge voltage profile of a Li-S cell with conventional electrolyte solvent (mixed DOL/DME, v/v=1:1). Some simplified intermediate reaction pathways were presented in **section 3.3.4 (reaction (1) and (2))**. For the first discharge plateau at around 2.4V, long-chain soluble polysulfides ( $\text{Li}_2\text{S}_n$ ,  $4 \leq n \leq 8$ )<sup>11</sup> are generated and gradually transforming to short-chain soluble polysulfides before reaching the saturation point marked by a dip of specific capacity. The second discharge plateau at around 2.1V is featured by the conversion from soluble  $\text{Li}_2\text{S}_4$  to  $\text{Li}_2\text{S}$ /  $\text{Li}_2\text{S}_2$  that are also insoluble and insulating.

Ideally, the final product should be pure  $\text{Li}_2\text{S}$  presented on the cathode, but the mixed  $\text{Li}_2\text{S}/\text{Li}_2\text{S}_2$  is usually obtained due to incomplete reaction caused by sluggish kinetics of solid-solid conversion and the passivation of cathode surface. Insoluble  $\text{Li}_2\text{S}/\text{Li}_2\text{S}_2$  are dissolved once the battery enters the charge, and elemental sulfur is redeposited at the end of the cycle. Nevertheless, there is no direct evidence to support this simple designation in this two-plateau profile without probing all the sulfur species during each stage. It is still debatable about the exact reaction mechanism even after decades of research due to the inclusion of too many intermediates ( $\text{S}_8^{2-}$ ,  $\text{S}_6^{2-}$ ,  $\text{S}_4^{2-}$ ,  $\text{S}_3^{2-}$ ,  $\text{S}_3^{\cdot-}$ ,  $\text{S}_2^{2-}$ ,  $\text{S}^{2-}$ ). The relative contents of different sulfur species or radicals vary with solvents that have different Donor Number/ dielectric constant, which may trigger different reaction scheme <sup>12</sup>. Researchers have employed some advanced in situ characterization techniques to detect sulfur species, e.g. *operando* XANES <sup>13</sup>, XPS <sup>14</sup>, UV-vis absorption spectroscopy <sup>15</sup> etc. Another cause for the fairly intricate elucidation lies in the involvement of chemical reactions in an Li-S cell that was roughly outlined in **section 3.3.4 (reaction (3) and (4))**. It must be reminded that precise reaction schemes of LSBs are yet to be understood. More related mechanistic studies are required for further exploring the reaction pathways since it might provide constructive guidance on solving challenge as laid out in next section and accelerating the commercialization of LSBs.

### 1.3.2 Great challenges towards Li-S battery

At the industrial level, however, the application of LSBs is hindered in face of some tricky challenges. Firstly, excessive amount of electrolyte is necessary for wetting the sulfur cathode with high specific area, and if the ratio of electrolyte volume to the mass of sulfur is higher than 10 as demonstrated in **Figure 1-5**, the actual energy density will be very low. Secondly, polysulfide shuttle effect severely shortens the cycle life. LiPS intermediates form and enter the electrolyte during cycling, moving back and forth between the cathode and anode without being utilized, which results in short cycle life and low coulombic efficiency. Last thing is about the safety issue, lithium metal anode

is prone to form the dendrite at this interphase between the anode and electrolyte and grow all the way up until penetrate the separator, causing the short circuit, thermal runaway and cell failure. Following is the elaboration of those challenges.

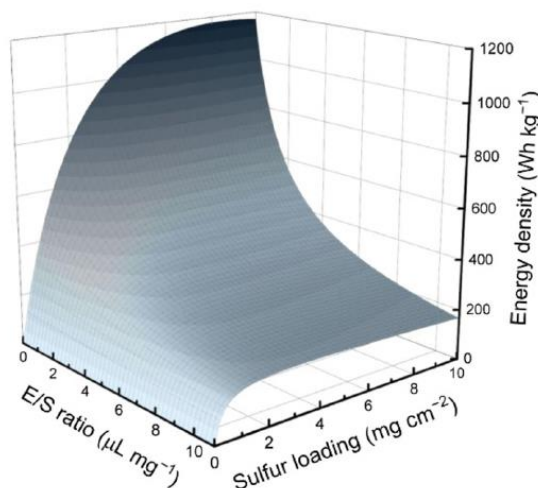


**Figure 1-5.** The relationship between calculated gravimetric energy densities and E/S ratio as well as areal sulfur loading <sup>16</sup>. Reproduced from reference 16.

### (1) Physical properties of S<sub>8</sub>/ Li<sub>2</sub>S

Starting from discharge process, the cathode is where the reduction reaction occurs. To ensure the smooth half reaction, sulfur must be reduced by accepting electrons from the external circuit and then react with Li<sup>+</sup>, which means electron transfer and Li<sup>+</sup> diffusion have to take place within the sulfur cathode. At the same time, sulfur ( $5 \times 10^{-30}$  S cm<sup>-1</sup>, 20°C) <sup>17</sup> and Li<sub>2</sub>S ( $10^{-17}$  S cm<sup>-1</sup>, 20°C) <sup>17</sup> are both very insulating in nature with rather low electronic conductivities, which results in sluggish kinetics of redox reactions and thus lower sulfur utilization. Therefore, sulfur has to be mixed with conductive carbon black <sup>18</sup> to form the composite and render intimate contact in the cathode. The fraction of conductive agent should be as low as possible because the capacity provided by the carbon black is almost equal to nothing. What is worse, same problem is encountered that insoluble discharge products Li<sub>2</sub>S<sub>2</sub>/ Li<sub>2</sub>S are electronically insulating as well. The direct consequence is the insufficient conversion from Li<sub>2</sub>S<sub>2</sub> to Li<sub>2</sub>S near the end of the

lower plateau. The deposition of the discharge product takes place on the surface of the cathode, which tends to cover and passivate the sulfur cathode and increase the impedance and polarization, which blocks the proceeding of discharge prior to utilizing all of the loaded sulfur <sup>19</sup>. Therefore, how to realize controllable deposition and morphology of Li<sub>2</sub>S has recently been a heated research topic. Plus, due to the large density disparity between sulfur (2.03 g cm<sup>-3</sup>) and Li<sub>2</sub>S (1.67 g cm<sup>-3</sup>), the resulting issue of volume expansion/ shrinkage occurring at the cathode could not be neglected. The considerable volume change ( $\approx 80\%$ ) undermines the structural stability of the cathode and further aggravates the capacity decay.

## **(2) Dissolution of polysulfide intermediates and resulting shuttle effect**

As discussed in **section 1.3.1**, the LiPS intermediates generated before being reduced to Li<sub>2</sub>S<sub>2</sub>/ Li<sub>2</sub>S are highly soluble in the typical ether electrolyte due to its long hydrophilic chain. After the dissolution, LiPSs can readily permeate through the separator driven by the concentration gradient and make contact with the metallic lithium anode where LiPSs are reduced to short-chain soluble LiPSs in the electrolyte and/or to Li<sub>2</sub>S/ Li<sub>2</sub>S<sub>2</sub> insulating layer on the anode surface, and the latter one prevents the transport of lithium ions to the liquid electrolyte. Besides, more arriving long-chain polysulfides also react with the Li<sub>2</sub>S/ Li<sub>2</sub>S<sub>2</sub> layer and become short-chain LiPSs as reflected by **reaction (3)** of **section 3.3.4**. As the concentration of short-chain LiPSs at the anode side increases coupled with the electric field during charging, they swim back to the cathode side and get re-oxidized to long-chain LiPSs. This repetitive parasitic process called “shuttle effect” of polysulfides leads to loss of active materials, low columbic efficiency and further poor cycling stability. A great deal of research has been conducted on cathode materials or structures and electrolytes to chemically or physically capture these polysulfides.

### **(3) Use of metallic lithium anode**

As mentioned in **section 1.3.1**, LSBs employ lithium metal as the negative electrode acting as the reservoir of  $\text{Li}^+$ . Although lithium locates in the first row of alkali metal column in the periodic table, it is still highly reactive to water and oxygen even with only trace amount in the electrolyte, leading to fire or explosion. Furthermore, the problem of dendritic lithium growth caused by non-uniform deposition of  $\text{Li}^+$  remained unresolved, which was mainly responsible for the explosion of battery warehouse of Moli company as mentioned in **section 1.2.2**. The risk is high that lithium dendrites penetrate the separator and cause internal short-circuiting. In terms of the stripping/plating process of  $\text{Li}^+$ , this repeating process is believed to engender the formation of “dead” lithium and pulverization on the surface, which markedly worsens the cycling stability. Other than aforementioned common challenges posed by lithium anodes of any LMBs during cycling, there are also some other problems occurring specifically for the lithium metal anode of LSBs. The infamous shuttle effect was brought up in last paragraph, and the formation of insulating  $\text{Li}_2\text{S}_2$ /  $\text{Li}_2\text{S}$  layer exacerbates the uneven deposition of  $\text{Li}^+$ , deteriorating the morphology on the lithium anode surface with more cracks and pores<sup>20</sup>. Overall, the use of lithium metal limits the commercialization of LSBs at the industrial level.

## **1.4 Current approaches on electrolyte and binder**

### **1.4.1 Functional electrolyte solvent**

The criteria for selecting the solvent consist of good chemical stability against LiPSs<sup>21</sup> and lithium anode as well as solubility for lithium salt and LiPSs. Among many classes of ethers that had been introduced and investigated in LSBs system, e.g., tetrahydrofuran (THF), dimethoxyethane (DME, G1), diglyme (G2), tri(ethylene glycol) dimethyl ether (triglyme, G3), tetra(ethylene glycol) dimethyl ether (TEGDME, tetraglyme, G4), DME stood out for the higher solubility and reaction kinetics it offered to LiPSs. DOL was chosen as the common co-solvent due to its lower viscosity and participation to the

formation of beneficial SEI layer on the surface of lithium anode that could avoid further parasitic reactions of Li anode with the electrolyte <sup>22</sup> as shown in **Figure 1-6**. Barchasz et al. <sup>23</sup> revealed that the solvation ability of ethers to  $\text{Li}^+$  was enhanced as the number of oxygen atoms in the solvent increased, which partially increased the solubility of LiPSs and delayed the passivation of cathode, benefiting the initial specific capacity. It was also reported <sup>24</sup> that the longer the chain of ether is, the slower the LiPSs diffuses in this ether-based electrolyte. Although ether with shorter chain (DME) enables faster diffusion for LiPSs, the polysulfides shuttle effect is aggravated. Therefore, the most commonly used electrolyte solvent for LSBs is the mixture of two ethers, DOL/DME (v/v=1:1) because using single-component solvent cannot balance the solubility and undesired LiPSs shuttle effect to achieve higher capacity and cycling stability.

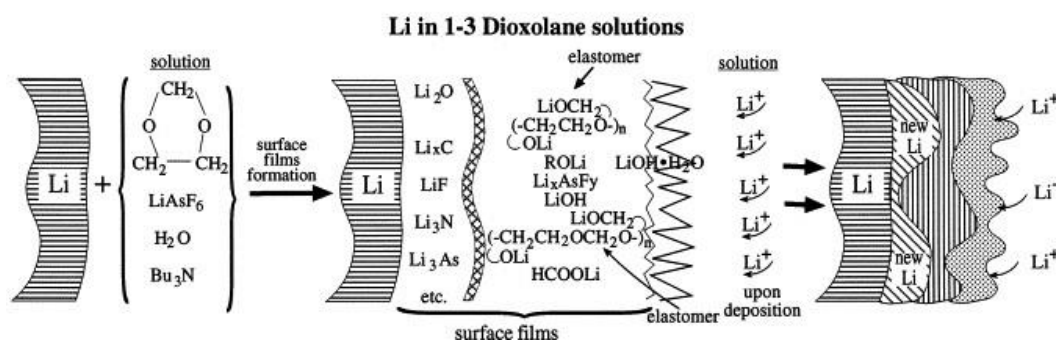


**Figure 1-6.** A schematic illustration of surface film formation on Li electrodes in DOL solutions <sup>25</sup>. Reproduced from reference 25.

The dissolution of LiPSs into electrolyte during electrochemical cycling is always regarded as a double-edged sword. On one hand, since both elemental sulfur and  $\text{Li}_2\text{S}/\text{Li}_2\text{S}_2$  are insulating in nature and insoluble in the mixed DOL/DME solvent, the solution-based redox reaction from intermediate LiPSs to the discharge product nucleated on the cathode substrate is a faster process with accelerated redox kinetics. On the other hand, it does cause the serious polysulfides shuttle problem, which shortens the cycle life of batteries and reduces the sulfur utilization as detailed in **section 1.3.2**.

As a result, there are two major directions going on (**Figure 1-7**) in terms of tackling the polysulfides of LSBs.

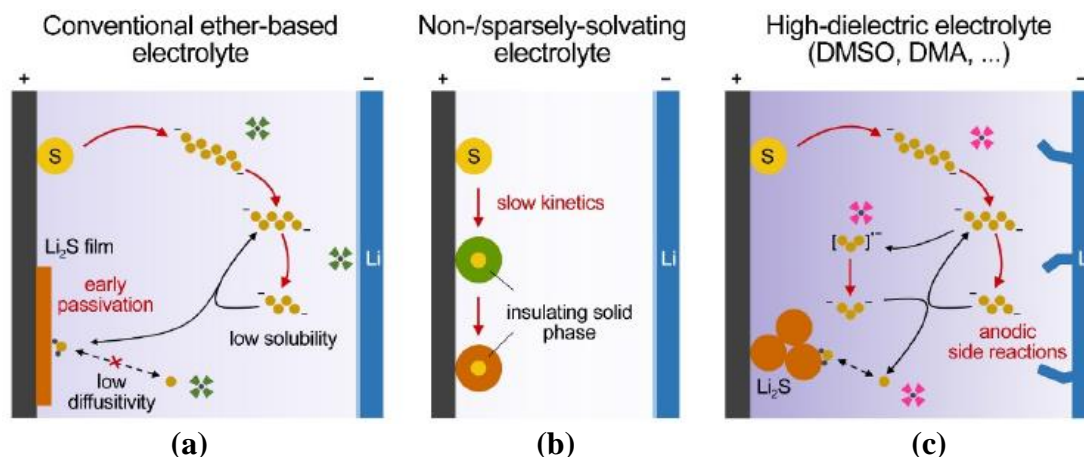


**Figure 1-7. Three types of electrochemical reaction schemes for LSBs** <sup>26</sup>. (a) Di-anion route in conventional ether-based electrolyte with poor solubility of short-chain polysulfides and  $\text{Li}_2\text{S}$  causes early passivation of the cathode surface. (b) Quasi-solid-state route in non/sparsely-solvating electrolyte with negligible soluble intermediates. (c) Radical route in high DN or dielectric constant electrolyte with  $\text{S}_3^{\bullet-}$  radical intermediate. Reproduced from reference 26.

The first one is to fully take advantage of this solution-mediated reaction pathways by enhancing the dissolution of both short-chain and long-chain LiPSs. It is particularly significant under high sulfur loading and low E/S ratio in order to accommodate more LiPSs in the electrolyte. Gupta et al.<sup>27</sup> used several electrolytes with high DN for increasing the solubility of LiPSs, they found that the DN and dielectric constant of electrolyte solvent could also affect the polysulfide speciation, e.g. the increased concentration of  $\text{S}_3^{\bullet-}$  radical altered the reaction pathways. Zhang et al.<sup>26</sup> followed this thinking and developed the tetramethylurea (TMU) with high dielectric constant as co-solvent with DOL. By solvating more LiPSs and stabilizing the existence of  $\text{S}_3^{\bullet-}$  in the electrolyte, they achieved  $324 \text{ Wh kg}^{-1}$  of energy density from pouch cell. Besides, TMU was more compatible with lithium metal than DMA and DMSO. Cheng et al.<sup>28</sup> went one step further. They realized the full dissolution of all the sulfur species during the electrochemical reactions including  $\text{Li}_2\text{S}/\text{Li}_2\text{S}_2$  by using a class of eutectic solvent that is safe in nature. Such an electrolyte system addressed issues such as huge volume



change and cathode passivation caused by  $\text{Li}_2\text{S}$ /  $\text{Li}_2\text{S}_2$ . It must be pointed that these researches were still in the proof-of-concept stage. All those three papers mentioned the incompatibility with lithium anode and only showed limited cycles of LSBs since solvents with high DN or dielectric constant are more aggressive toward lithium metal and tend to decompose faster, leading to depletion of electrolyte and battery failure.

The second direction to deal with the polysulfides is to prevent the LiPSs from dissolving into the electrolyte. Sun et al.<sup>29</sup> reported the use of ethers with high carbon/oxygen ratio as cosolvent for the electrolyte to hinder the dissolution of LiPSs, which also achieves better performance than previous literatures. By doing so, they detected less sulfur species on the anode and improved the morphology of lithium anode after long-term cycling. As mentioned in the first paragraph of **section 1.4.1**, the role of DOL is to form a protective SEI layer. Although DOL has very low solubility of LiPSs, the conductivity of  $\text{Li}^+$  in the electrolyte is not compromised. Therefore, there was a report<sup>30</sup> using pure DOL as the electrolyte solvent with 2M LiTFSI and no addition of  $\text{LiNO}_3$ . This scenario rendered very low solubility of the polysulfide (5.5 g/100g) and outstanding reversibility of lithium anode. Fluorinated ethers are also very advantageous and promising for LSBs for their low viscosity and flammability<sup>31</sup>, excellent wettability as well as almost no solubility to LiPSs. Azimi et al.<sup>32</sup> replaced DME with TTE to mix with DOL without adding  $\text{LiNO}_3$ , and the as-assembled battery was able to be charged to cut-off voltage compared to the conventional DOL/DME solvent, suggesting the confinement of LiPSs shuttling. Moreover, the fluorinated solvent was believed to decompose<sup>33</sup> on the lithium anode and enhance the SEI protective layer. Other fluorinated ethers that had been investigated consist of TFTFE, BTFE and TFEE etc. The downside of them is the low boiling point that can cause some safety issues while operating LSBs at high temperature.

#### 1.4.2 Lithium salt and its concentration

For rechargeable lithium batteries, there are some basic requirements<sup>34</sup> that a lithium salt needs to satisfy. It should undergo complete dissolution and dissociation in the aprotic solvent, and the lithium ions that are solvated should be capable of moving with as high mobility as possible. The anion must not be reactive with solvent molecules and must have high stability to resist the oxidative decomposition at the positive electrode. Neither the anion nor cation shall be able to react with other components, e.g. current collector for electrode, package materials and separator etc. When it comes to LSBs, because LiPSs dissolve into electrolyte, lithium salts shall be inert to the intermediates, which leaves fewer options for the selection of lithium salts. For LSBs, the lithium salt in the electrolyte provides lithium ions for the ionic conduction. Some lithium salts have been used as the main lithium salt such as LiTFSI, LiPF<sub>6</sub>, LiClO<sub>4</sub> and LiCF<sub>3</sub>SO<sub>3</sub> etc. At present, LiTFSI is the mostly used lithium salt. The introduction of those normal lithium salts will be elaborated in **section 3.1**.

In response to the challenges raised in **section 1.3.2**, some advancement about the lithium salts had been made. The operation of LSBs requires the formation of robust SEI layer for avoiding the occurrence of parasitic reactions and rapid degradation on the lithium anode. Researches focusing on the influence of selection of lithium salts were very less, but it is generally believed that solely relying on reactions between solvent/lithium salt and lithium anode is not enough to produce SEI layer that promises acceptable cycle life and high capacity. That is why the LiNO<sub>3</sub> is widely employed as efficient additive in the electrolyte for LSBs. However, adding LiNO<sub>3</sub> is not a permanent solution because it poses potential safety hazard, and is consumed each cycle by reacting with exposed lithium metal. Besides, uncontrollable and inhomogeneous deposition of Li<sup>+</sup> remains unresolved. Researchers started to turn their attention to the development of lithium salts and the anion-derived SEI layer. LiHFDF was reported<sup>35</sup> as the new lithium salt in LSBs to induce the LiF-rich interface on the lithium anode that suppressed

the growth of dendritic lithium efficiently. LiHFDF has lower LUMO and higher HOMO than the LiTFSI, which leads to easier reduction on the lithium anode. Ma et al.<sup>36</sup> also firstly introduced the LiTNFSI as the new lithium salt that could form more stable SEI films on the lithium metal and afford higher capacity retention than LiTFSI.

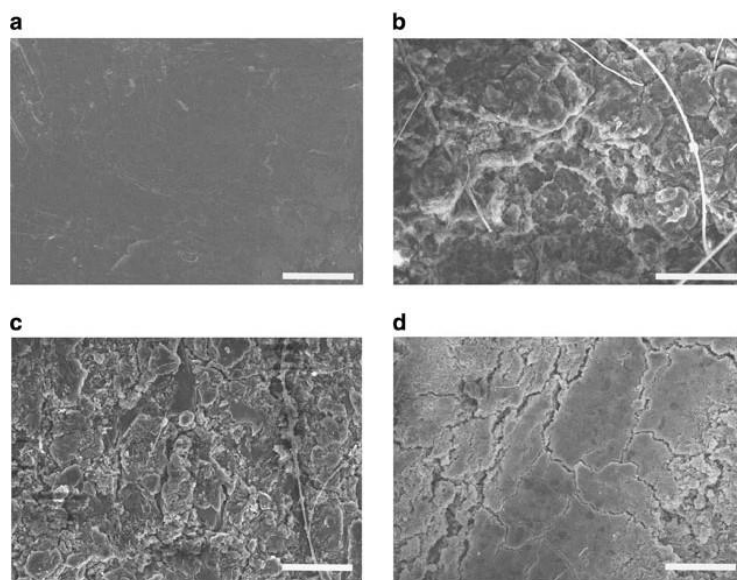


**Figure 1-8. Scanning electron microscopy images of metallic lithium anodes<sup>37</sup>.** (a) Fresh lithium metal, (b) Lithium metal with 2M LiTFSI after 278 cycles. (c) Lithium metal with 4M LiTFSI after 183 cycles. (d) Lithium metal with 7M LiTFSI electrolyte after 280 cycles. Reproduced from reference 37.

Other than the replacement of lithium salt, the variation on the concentration of lithium salt had also been validated to tailor the SEI structure and improve the uniformity of lithium deposition as well as suppress the dissolution of LiPSs. The concept of “solvent in salt”, also called highly-concentrated electrolyte (HCE), was firstly proposed by Suo et al.<sup>37</sup>. Maximum 7M of LiTFSI in DOL/DME (1:1 by volume) achieved the dendrite-free lithium anode as shown in **Figure 1-8** after 280 cycles and better cycling stability. Pang et al.<sup>38</sup> proved that quasi-solid sulfur conversion could be enabled by sparingly designing the electrolyte structure. 8.7M saturated LiTFSI were dissolved in G2 (G2:LiTFSI = 0.8:1 (mol/mol)) with TTE as diluent so that the solvent activity was minimized, which attained no dendrite growth on the lithium anode and excellent 100 cycles performance at 0.2C with extremely low E/S ratio (5  $\mu\text{L mg}^{-1}$ ). Localized high-

concentration electrolyte (LHCE) is another similar system where inert co-solvent is added into HCE system. Hydrofluoroether is the popular option as the inert solvent because it does not have the solvation ability toward  $\text{Li}^+$  and PS anion. Zheng et al. firstly reported the OFE-based LHCE electrolyte with 1M LiFSI in DME/OFE (5:95 by volume ratio). This nonflammable electrolyte was favorable to form the LiF-rich SEI film and lower the cost of lithium salts. Contrary to HCE system, dilute electrolyte was also investigated for LSBs. Wu et al.<sup>39</sup> found that diffusion rate of LiPSs in 0.1M LiTFSI in DOL/DME (1:1 by volume ratio) was the smallest compared to 1M and 3M. It was ascribed to the aggregation of  $\text{Li}_2\text{S}_2$  and  $\text{Li}_2\text{S}_4$  in a phase-divided area in this fairly dilute electrolyte system, suggesting the inhibited dissolution of short-chain LiPSs. As a result, this unexpected phenomenon gave rise to enhanced cycling stability of the battery and rather intact and smooth surface of both electrodes after cycling.

#### 1.4.3 Additive and anode protection

In LSBs, the uses of additive is mainly for stabilizing and passivating the lithium metal anode by reacting with Li anode and forming a protective SEI layer. Those additives usually have lower LUMO and higher HOMO to ensure their preferred reaction with lithium anode. As-formed SEI should have high stability to compositions of electrolyte. Since the ideal case for SEI is to cover the whole surface of Li anode completely, the equivalent volume of SEI building materials should be larger than that of the anode material<sup>40</sup>. And SEI should have a robust and dense mechanical structure without fractures on the surface. The introduction of  $\text{LiNO}_3$  to LSBs system was a breakthrough as mentioned in **section 1.4.2**. After several further studies, the compositions of the  $\text{LiNO}_3$ -derived SEI layer consist of  $\text{Li}_3\text{N}$ ,  $\text{Li}_2\text{O}$  and  $\text{Li}_x\text{NO}_y$ <sup>41</sup>. Only if the lower cut-off voltage is above 1.6V could the  $\text{LiNO}_3$  help to render more reversible LSBs<sup>42</sup>. In **section 1.4.2**, it has been discussed that  $\text{LiNO}_3$  would be used up after certain cycles, after which the Coulombic efficiency of LSBs started to decrease<sup>43</sup> because some fresh lithium were exposed to the electrolyte after the weakening of SEI layer. Polysulfides were also an

effective additive when being used together with  $\text{LiNO}_3$  in the electrolyte, the synergetic effect <sup>44</sup> of both components restrained the dendritic lithium growth. Some additives were reported to have beneficial effects on both sulfur cathode and lithium anode. Lithium iodide (LiI) was able to smoothen the anode surface <sup>45</sup> with no detect of sulfide species after being introduced as additive. In addition to anode, LiI also led to the formation of a homogeneous protective SEI layer <sup>45</sup> on the cathode surface, which to some extent prohibited the LiPSs moving out of the cathode.

#### 1.4.4 Functional binder

The functions of polymer binder for the sulfur cathode consist of mechanical properties, conductivity, polysulfide regulation, etc.<sup>46</sup> The basic function for the binder is to ensure the intimate contact among cathode materials including conductive carbon and elemental sulfur, and to firmly fixate the cathode materials on the current collector, which is enabled by the adhesivity of polymer binder. This adhesion ability was originated from van der Waals interaction, electrostatic incorporation and covalent bonding <sup>46</sup>. PVDF polymer belongs to the nonaqueous binder with good adhesivity. LA132 (polyacrylic latex) and sodium-alginate are common aqueous binders with better adhesive ability that is attributed to the dipolar interaction between cathode substrates and electronegative groups <sup>46</sup> on the LA132/Na- alginate molecules. Besides, hydrogen bonding formed between carboxy/ hydroxyl groups and oxide layer of aluminum substrate also heightened the adhesivity <sup>47</sup>, which relieved the stress and strain brought by huge volume change of sulfur cathode. Other than adhesivity, other mechanical properties such as swelling ratio and ductility are vital to maintain the structural stability during cycling. Polymer binders with three-dimensional structure possess enhanced mechanical properties than polymers with linear chains. Styrene-butadiene rubber (SBR) is usually added into carboxymethyl cellulose (CMC) as the plasticizing agent to improve the flexibility <sup>48</sup>. This mixed binder shows a strengthened 3D network structure for the sulfur cathode. The strongest surface interaction existing in the cathode is the

covalent bonding. Pang et al.<sup>49</sup> developed an advanced sulfur cathode using the binder generated by the crosslinking reaction between -OH groups in the CMC and the -COOH in citric acid. Excellent adhesion and elasticity promised very compact cathode structure without cracks (**Figure 1-9**) and stable inter-particle electrical connection at ultrahigh sulfur loading ( $14.9 \text{ mg cm}^{-2}$ ).

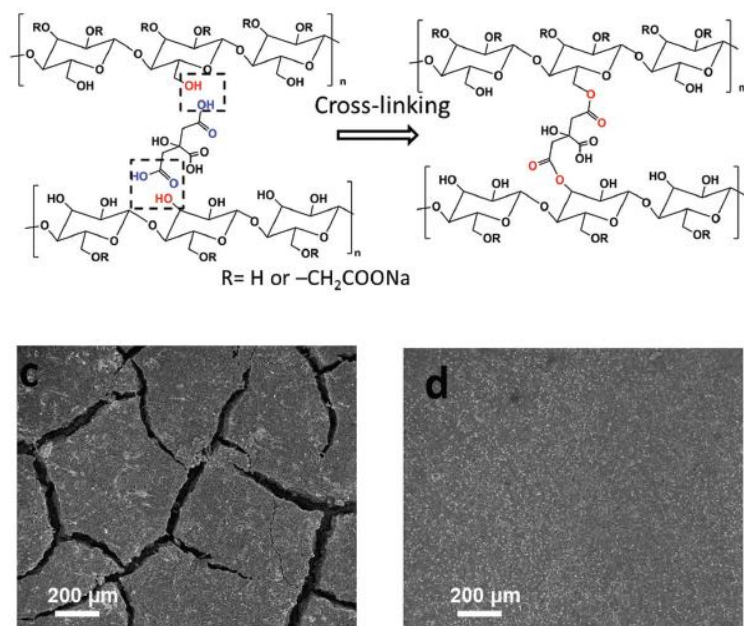


**Figure 1-9.** A schematic illustration of the cross-linking of CMC binder with CA as the linker, based on the esterification of the -OH groups in CMC and the -COOH groups in CA at  $150^\circ\text{C}$ , and the SEM images of sulfur cathode surface using PVDF and cross-linked CMC-CA binder<sup>49</sup>. Reproduced from reference 45.

At present, most of binders for LSBs are not conductive, which might increase the electrode resistance and negatively impact the redox kinetics. Thus, some binders were designed to be electronically conductive or to improve the ionic conductivity. Poly(3,4-ethylenedioxythiophene) (PEDOT) is a well-known conductive polymer, which had been verified to be able to reduce the internal resistance and the charge transfer resistance of sulfur cathode<sup>50</sup>. Based on the PEDOT polymer, a combination of polyacrylic acid (PAA) and poly(3,4-ethylenedioxythiophene):poly(styrene sulfonate) (PEDOT:PSS) was recently applied as binder<sup>51</sup> for the cathode. PEDOT:PSS

established the 3D conductive structure that enhanced the electronic conductivity, while the PSS played the role of promoting wettability of the cathode to the electrolyte so that the mass transfer of  $\text{Li}^+$  and the kinetics of redox reactions could be improved. Finally, the battery performance was attained with an initial specific capacity of  $1121 \text{ mAh g}^{-1}$  and  $830 \text{ mAh g}^{-1}$  left after 80 cycles at  $0.5\text{C}$ . However, this type of conjugated polymer usually lacks good elasticity and flexibility, leading to ineffective cushion<sup>46</sup> to the stress/ strain caused by the volume change of the sulfur cathode during cycling. In terms of the improvement of  $\text{Li}^+$  diffusion brought by the binder, poly(ethylene oxide) (PEO) is a typical example that reduced the mass transfer resistance of  $\text{Li}^+$  because of its strong swellability and even partial dissolution to the electrolyte<sup>52</sup>. After this enhancement on the electrolyte uptake of electrode, the contact between the electrolyte and active material became more intimate so that the access of  $\text{Li}^+$  to the elemental sulfur is much easier. The downside of too much swelling of the binder was that the cathode became more vulnerable to the structural damage. Other than this indirect mechanism to increase the  $\text{Li}^+$  transfer, there was also the binder system that contained polymers that are  $\text{Li}^+$ -conductive. For example, the  $\text{Li}^+$ -doped Nafion coupled with polyvinylpyrrolidone (PVP) and nano  $\text{SiO}_2$  was invented by Li et al.<sup>53</sup> Herein, PVP and  $\text{SiO}_2$  functioned as the LiPSs regulator to inhibit the polysulfide shuttling. The as-assembled battery delivered  $470 \text{ mAh g}^{-1}$  at  $5\text{C}$  galvanostatic cycling.

Due to the notorious shuttle effect of LiPSs, it is desired that functional binders are able to interact with LiPSs and immobilize them. A very common technique is to adopt binders with heteroatom-containing polar functional groups. LiPSs could be trapped either through lithium atom or the polysulfide anion/sulfur atom. The interaction between lithium atom and the electron-donating functional groups was rendered by the formation of lithium bond elucidated by Park et al.<sup>54</sup> And considering the strong electronegativity of sulfur atom in the LiPSs molecule, functional groups (such as carboxy groups) that contains oxygen atom linked with hydrogen atom could also

interact with sulfur atom through the formation of hydrogen bond <sup>55</sup>. Yuan et al.<sup>46</sup> had already summarized the binding energy of Li<sub>2</sub>S and Li-S• species with different functional groups in order to give a more direct comparison. Representative polymers include PAA binder <sup>56</sup> having a large portion of carboxy group and polyethylenimine (PEI) - hexamethylene diisocyanate (HDI) <sup>15</sup> with abundant amine groups, etc. Thus, another promising idea is to rationally select functional binders with different polar groups in the side chains <sup>57</sup>. As such, not only can those polar binders trap the polysulfides and mitigate the shuttle effect, but also would the structural robustness and conductive structure be improved due to the intermolecular forces among those functional polar groups and nanocomposite materials in the cathode <sup>46</sup>.

### **1.5 Objective and structure of this thesis**

In Chapter 2, electrochemical characterization methods and other techniques that were utilized in this thesis were briefly introduced.

In Chapter 3, the objective of this chapter was to evaluate the electrochemical performance of LSBs with five different lithium salts in the electrolyte, including long-term cycling stability, rate capability etc. And the most promising one (LiBr) was screened out for further investigation.

In Chapter 4, the objective of this chapter was to identify and fix the problems caused by the LiBr salt based electrolyte for LSBs and set up a baseline research scenario of sulfur cathode for the future LiBr-related research.

In Chapter 5, the conclusions of this thesis was summarized, and future work was proposed for further improvement.



## Chapter 2. Electrochemical Characterization Methods and Other Techniques

### 2.1 Coin cell configuration

CR2032 coin cell was used to study the electrochemical performance of new research systems of LSBs with the configuration shown in **Figure 2-1**. The first letter “C” is from IEC standard system, representing the chemical composition of the batter, and the second letter “R” and “2032” symbolize a cylindrical shape with 20 mm diameter and 3.2 mm height. A homogeneous slurry was prepared by mixing active material composites, conductive carbon additives and polymer binders in a certain weight ratio in a solvent. The suitable viscosity of the slurry was ensured for facilitating subsequent casting process by doctor blade where the carbon-coated aluminum foil (thickness of carbon coating: 1  $\mu\text{m}$ ) or carbon paper (Toray) was used as current collector. The thickness for this wet film was adjusted to change the areal sulfur loadings of the dry electrode. The wet electrode film was then dried overnight at 50  $^{\circ}\text{C}$  to evaporate the solvent. After punching out the dry circular electrode (12 mm diameter), batteries were assembled using different components as per below in a glove box filled with inter gases (Argonne) with oxygen and water content both below 0.3 ppm.

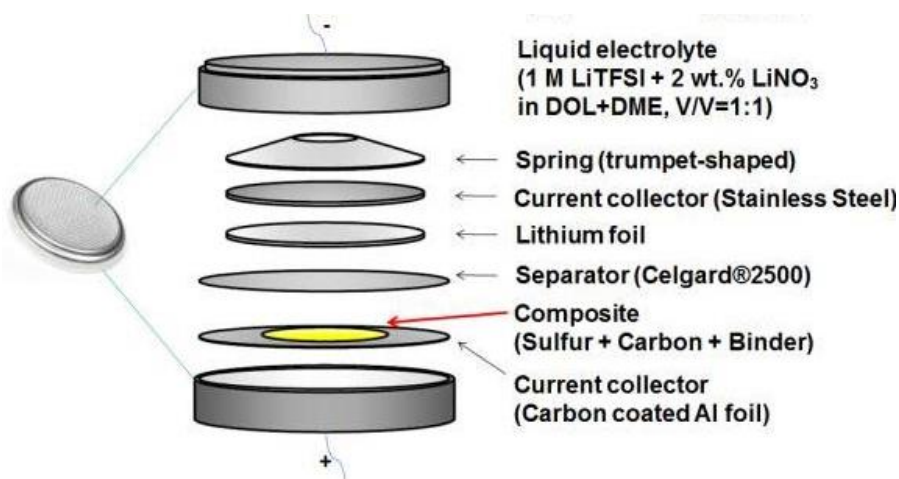


**Figure 2-1.** Schematic diagram of the Li-S coin cell adopted for this research <sup>58</sup>. Reproduced from reference 58.

## 2.2 Galvanostatic discharge/ charge

Galvanostatic cycling is the standard technique being most commonly used to evaluate the electrochemical performance including capacity, retention and cycling life et al. A constant current density and the voltage window for charge and discharge are set, and the battery is cycled in this mode. Once reaching the pre-set cut-off voltage, the current would be reversed and continue cycling. To realize those functions, some parameters are recorded including the battery voltage, cycling numbers, specific capacity and the step time. There are two type of plots that are usually extracted from the galvanostatic cycling. The plot of cell voltage vs. step time or specific capacity helps researchers to identify the voltage plateau related to electrochemical reactions during cycling process that has been discussed in **section 1.2.1**. And the plot of specific capacity delivered (y-axis) versus cycle number (x-axis) provides information about the long-term stability of battery performance. By increasing the current from a low rate for a same number of cycles followed by recovering to the initial c-rate, the rate performance of the battery can be evaluated by plotting retained specific capacity vs. cycle number. Good rate capability means minimal change on capacity during current change and uncompromising capacity at high rate.

## 2.3 Cyclic voltammetry

Cyclic voltammetry is a potentiodynamic electrochemical measurement where the current of the battery is recorded versus applied voltage that changes in a linear manner and specific rate with time to give the CV curves. It is usually conducted in a three-electrode system in which the applied voltage refers to the potential between the working electrode and reference electrode, while the current is measured between the working electrode and counter electrode. As always, a voltage window is set before the measurement. When the voltage increases, oxidation scan happens to the cell, and anodic current starts to appear at a certain voltage. After increasing to the cut-off voltage,

it turns to the opposite direction that is called reduction scan where the cathodic current will present in a certain range but with opposite polarity to the anodic current.

Cyclic voltammetry is a very powerful tool that can provide much useful information. The actual onset potential of peaks could be compared with the equilibrium potential of an electrochemical reaction to judge whether this reaction is practically favourable to occur or not. The potential difference between cathodic and anodic peak symbolizes the degree of reversibility of electrochemical reactions. Plus, the peak current density is indicative of reaction rate that is in relation to electronic conductivity on the electrode surface. The degree of overlapping for curves of multiple cycles signifies the structure stability of an electrode, and a high degree of overlapping represents the stable cathode structure. Moreover, by calculating the area of a certain CV peak, the amount of materials participated in the reaction can be assessed. The current-voltage profile can be also converted into current-time profile in order to calculate the quantity of electric charge being consumed or supplied by integrating the area of peaks.

#### **2.4 Potentiostatic electrochemical impedance spectroscopy (PEIS)**

Impedance is usually denoted as  $Z_\omega = E_\omega / I_\omega$ , referring to the type of resistance that is frequency-dependent, which represents the ability of a circuit element to resist the current flow. In the course of PEIS measurement, a small sinusoidal perturbation (alternating current potential) is applied to the cell with frequency from high to low, while the current response is recorded at the open circuit voltage<sup>59</sup>. Since there are non-linear equivalent electric components in a battery, the linear current response to voltage might not be obtained as shown in the CV diagram in **section 3.3.4**. Therefore, in order to enable pseudo-linear process, a much smaller potential amplitude (1 mV-10 mV) is applied instead, and the corresponding current response is computed by adding up the sinusoidal functions at each frequency. Furthermore, the impedance  $Z_\omega$  can be represented by the form of a complex with real and imaginary parts,  $Z_\omega = Z_0 \cos\phi + Z_0 j \sin\phi$ . There are two types of plot that are used to present the PEIS data, Bode plot

and Nyquist plot. The Nyquist plot is more accessible and hence used more frequently. It has imaginary part of the impedance as y-axis and real part as x-axis <sup>59</sup>. For electrochemical cells, the Nyquist plot is normally comprised of a number of semicircles at high and middle-frequency area on the left and a slope line with a certain angle at low frequency area on the right <sup>59</sup>. The former is determined by the resistance and capacitance in the electrode and at the interface between electrode and electrolyte, and the latter is associated with resistance of ion transport in the electrolyte. Equivalent circuit is often used to simulate and analyze the PEIS results with components like electrolyte resistance ( $R_s$ ), charge transfer resistance ( $R_{ct}$ ), double layer capacitance ( $C_{dl}$ ) and Warburg diffusion impedance ( $Z_w$ ).

## **2.5 Ultraviolet–visible absorption spectroscopy (UV-vis)**

Ultraviolet-visible spectrophotometry is a characterization method for analysis and determination by letting molecules of certain substances absorb radiation in the spectral region from 200 to 800 nm. This molecular absorption spectrum is produced by the valence electrons and electrons on molecular orbitals jumping between energy levels, which is widely used in both qualitative and quantitative determination of inorganic and organic substances. The composition, content and structure of the material can be determined or inferred by analyzing the spectrum and absorbance generated by molecules or ions absorbing ultraviolet and visible light.

Different materials have different structures, and so do their energy of molecular energy levels (the sum of energy from each energy levels). Thus, different materials selectively absorb external radiation from different wavelengths or energy, which is the basis of qualitative analysis by UV-Vis. Qualitative analysis is performed by passing the lights of different wavelengths through the object to be measured. After being absorbed by the object, the extent of absorption (absorbance  $A$ ) of lights with different wavelengths are measured. Subsequently, absorbance  $A$  (y-axis) is plotted as the function of the light wavelength (x-axis) so that the absorption spectrum of the material is obtained. The

molecular structure could be studied according to the characteristics of the absorption curve (peak strength position and number, etc.).

UV-vis can be also used for quantitative analysis based on Beer–Lambert law. The most commonly used quantitative analysis method is the standard curve method. First thing is to prepare a solution of a certain concentration with standard substances and then dilute the solution into a series of standard solutions. At a certain wavelength, the absorbance of each standard solution is tested to draw the standard curve with the absorbance as the y-axis and the corresponding concentration value of the standard solution as the x-axis. The last thing is to measure the absorbance of the sample solution according to the standard curve and find out the corresponding concentration or content of the sample solution on the standard curve. In LSBs, this technique is usually utilized for measuring concentration of different polysulfide anion.

## Chapter 3. Impact of Different Lithium Salts on the Cycling Performance of Li-S Batteries

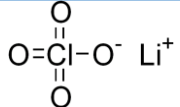
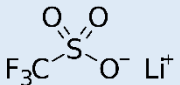
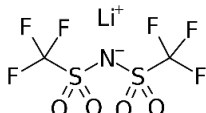

### 3.1 Introduction

Rechargeable batteries have been increasingly used as power sources for portable electronics and electric vehicles <sup>60,61</sup>. In particular, the energy density or specific energy of Li-ion batteries (LIBs) has been improved significantly, which helped promote the EV industry worldwide in the past few years. However, the rather low theoretical energy density of the current LIBs will soon become a hurdle for developing high energy batteries that can provide a satisfactorily long driving distance per charging. Therefore, the quest for ultra-high energy density batteries has intensified in recent years. Among several candidates of high energy density batteries, Li-S batteries (LSBs) are most promising <sup>62</sup> because of the high theoretical capacity <sup>63</sup> of 1672 mAh g<sup>-1</sup> of sulfur, which corresponds to a specific energy of 2600 Wh Kg<sup>-1</sup> of the battery. In addition, sulfur is naturally abundant and has low toxicity, making LSBs more attractive.

However, the application of LSBs is severely hindered by lower practical energy density and shorter battery life than LIBs. Firstly, a “flooded” system<sup>64</sup> with excess electrolyte is usually a prerequisite for the operation of LSBs as it could increase the discharge capacity based on active material and cycling stability. Meanwhile, all the soluble intermediates, that are lithium polysulfides (Li<sub>2</sub>S<sub>x</sub>, where x = 4-8), are solvated by typical ether solvent of the electrolyte to render chemical transformation <sup>65, 66</sup> readily proceed with faster reaction kinetics during cycling, but it always comes at the cost notorious “shuttle effect” as detailed in **section 1.3.2**, which leads to low Coulombic efficiency and battery degradation <sup>18, 62</sup>. Lastly, the growth of lithium dendrites <sup>67</sup> is a safety issue for LSBs, which happens on the interface between the electrolyte and lithium anode. Therefore, electrolyte plays a significant role in governing the electrochemical performance of LSBs. It serves as the “blood” for LSBs with the function of providing path for Li<sup>+</sup> conduction and diffusion. In order to address

aforementioned problems and improve the performance of LSBs, various strategies have been employed regarding different compositions of electrolyte such as aprotic solvent<sup>26, 68, 69</sup> and functional additives<sup>47, 70-74</sup> that have been reviewed in **section 1.4**. Lithium salt relatively received less attention compared to the solvent and additives, but in fact it could contribute to the formation of beneficial anion-derived electrode-electrolyte interface<sup>35, 36, 75</sup> thereby suppressing the dendritic lithium growth and physically restricting the sulfur species within the cathode structure. Besides, there were also reports<sup>76,77</sup> about the distinct morphologies of Li<sub>2</sub>S deposition induced by different anion donicity. Lithium salts with high donor number (DN) enabled 3D growth of Li<sub>2</sub>S particles, leading to delayed cathode passivation and hence enhanced sulfur utilization.

**Table 3-1.** A summary of basic information and properties of different lithium salts in this work<sup>78-80</sup>.

Formula	Structure	Molecular Weight (g mol <sup>-1</sup> )	Ionic conductivity (20-25°C) of 1M LiX in DOL/DME (v/v=1:1) [mS/cm]	Safety
LiBr	Li <sup>+</sup> ---Br <sup>-</sup>	86.85	1.05	Psychoactive and somewhat corrosive
LiClO <sub>4</sub>		106.39	7	Strong oxidizing properties
LiCF <sub>3</sub> SO <sub>3</sub>		156.01	2.38	Corrosive to Al
LiC <sub>2</sub> F <sub>6</sub> NO <sub>4</sub> S <sub>2</sub>		287.09	11.2	Corrosive to Al
LiPF <sub>6</sub>	Li <sup>+</sup> 	151.91	16.8	Thermally unstable

For Li-S batteries, the dominant lithium salt is LiTFSI. But whether this lithium salt is an optimal choice for LSBs is unclear because other lithium salts are rarely used and thus poorly understood. Chance exists that other lithium salts might be a better fit for LSBs. So, understanding more lithium salts for LSBs is necessary, which arouse many interests among researchers. The best way of doing it is to pick up more lithium salts

and conduct a systematic study to evaluate their impacts on Li-S batteries. As such, both advantages and disadvantages of more lithium salts could be known, and researchers are able to have an explicit sense on which one could better fit different research systems. It is critical to conduct a systematic study for the purpose of gaining insights on the influence of different lithium salts on performance of LSBs.

Nonetheless, few researches had been conducted previously to provide a comprehensive understanding about influences of commonly used lithium salts on LSBs. Chu et al.<sup>77</sup> chose three lithium salts, LiBr, LiTf and LiTFSI, based on their donicity of anions from high to low. The influence of donor number of anion in the electrolyte on battery performance was investigated using the form of Li-Polysulfide liquid cell. Kolosnitsyn et al.<sup>81</sup> picked five different lithium salts with sulfolane as the sole solvent and probed the correlation of physicochemical properties of electrolyte with the performance of LSBs. Kim et al.<sup>80</sup> used different combinations of lithium salt and solvent including LiClO<sub>4</sub>, LiTFSI and LiTf dissolved in a binary solvent system without adding LiNO<sub>3</sub>, and assessed the correlation between physiochemical properties of the electrolyte and electrochemical performance of LSBs. However, above-mentioned researches<sup>80-82</sup> had their limitations. Some were conducted without LiNO<sub>3</sub> additive or based upon electrolyte solvent that is not the predominant mixed DOL/DME. Others used the format of Li-Polysulfide cell using LiPSs as starting active material, which is not commensurate with the industry protocol that will be detailed at the next paragraph. The introduction of LiNO<sub>3</sub><sup>41, 72</sup> to electrolyte system of LSBs as additive was deemed as an important step because of its protective effect on metallic lithium anode by participating in the formation of SEI layer thereby enhancing cyclability of LSBs. Ever since then, LiNO<sub>3</sub> has become an indispensable component to resist the shuttle effect. After the determination of basic composition (DOL/DME solvent and LiNO<sub>3</sub> additive) of electrolyte for LSBs, there is no such a comprehensive research being conducted to evaluate the performance of LSBs under different lithium salts.



In terms of the selection of lithium salts for this study, there are two crucial criteria including whether it is commonly used, its practical value and if it is promising in LSBs field.  $\text{LiPF}_6$  is the most dominant lithium salt for LIBs due to its well-balanced properties<sup>83</sup>. Nevertheless,  $\text{LiPF}_6$  is far away from being the perfect lithium salt by virtue of poor thermal stability and high sensitivity<sup>83, 84</sup> to moisture.  $\text{LiClO}_4$  has been gradually excluded for practical use in industry given its toxicity and safety issue<sup>84</sup>, but it is prevalent in laboratory-scale experiments owing to easiness for operation, economical price and high ionic conductivity. Imide salts have also been employed extensively, especially  $\text{LiTFSI}$  salt, in LSBs research. The lattice energy<sup>37</sup> of  $\text{LiTFSI}$  was relatively low accompanied with reduced Lewis basicity due to electron-withdrawing capability<sup>83</sup> of N-substituents, leading to facile dissociation of the lithium salt and hence higher solubility. Besides,  $\text{LiTf}$ <sup>85</sup> also belongs to this category, which features the simplest imide structure but very low ionic conductivity<sup>34</sup> as shown in **Table 3-1**. The major drawback for the imide salt lies in the corrosion to aluminum current collector under voltage larger than 4V<sup>86</sup>. However, the lower potential range of sulfur species transformation makes it possible for the application of imide salts without corroding the current collector. The last lithium salt for this study is  $\text{LiBr}$  mentioned earlier with great promise. Chu et al.<sup>77</sup> obtained excellent electrochemical performance while using  $\text{LiBr}$  as the main lithium salt. They ascribed it to the high sulfur utilization resulted from the delay of passivation in the cathode, which is due to the three-dimensional growth of  $\text{Li}_2\text{S}$  instead of film-like morphology. But they used Li-Polysulfide liquid cell with  $\text{Li}_2\text{S}_8$ -containing catholyte and carbon paper or freestanding carbon nanotube electrode without the slurry casting process. Casting active materials on the current collector by a traditional slurry process is a more feasible method because it maximizes the packing efficiency and is commensurate with current industrial protocols<sup>87</sup> for manufacturing electrodes of LIBs. For the current lithium battery industry, it is impossible to employ carbon paper as the cathode due to its high cost, low packing efficiency and high bulk

density. In this research, more practical sulfur/Super P cathode was instead utilized to evaluate the LiBr salt.

Herein, we evaluated the impacts of five different electrolytes with above-mentioned lithium salts on LSBs. At the same concentration, coin cells with same configuration were assembled and tested by a variety of electrochemical techniques. During the cycle process, stability, Coulombic efficiency and rate capability were compared. Corresponding capacity ratio and sulfur utilization was calculated and ranked. It was found that the battery using LiBr electrolyte had the best galvanostatic cycling performance but experienced severe “overcharge” problem at the early stage. LiTf and LiBr electrolyte have relatively low ionic conductivity as laid out in **Table 3-1**, leading to their poor cycle performance during high C-rate cycling. Li/Li symmetric coin cells were also adopted to investigate compatibility of changing lithium salts with metallic lithium anode. Finally, kinetics of redox reactions under different electrolytes were examined and analyzed by CV. And charge transfer process was probed by EIS for batteries after finishing CV test.

### 3.2 Experimental section

**Electrode preparation:** Elemental sulfur and Super P carbon black was uniformly mixed at a weight ratio of 65:35 in an agate mortar using a grinding pestle for 15 min, and then the mixture was transferred into a hydrothermal reactor that was subsequently placed in a convection oven for a 12-hour heat treatment at 155°C. Intimate electric contact between insulating sulfur and conductive carbon was assured by this melt-diffusion method. After cooling down to room temperature, the mixture was blended with additional Super P and PVDF solution (5 wt%) in *N*-methyl-2-pyrrolidone (NMP) to make a slurry, which has a solid composition of 50% sulfur, 40% Super P, and 10% PVDF. The slurry obtained was blade coated onto a carbon-coated aluminum foil as current collector. The thickness of the wet film determined the ultimate sulfur loading. The cathode film was placed in a convection oven at 50°C for 16 h to remove the solvent

and cut into circular disks with diameter of 12 mm. Then disks were dried in a vacuum oven for 2 h to remove residual solvent. Sulfur loading of the cathode was 1-1.2 mg cm<sup>-2</sup>.

**Electrolyte preparation:** Lithium salts including lithium bromide (LiBr), lithium perchlorate (LiClO<sub>4</sub>), bis(trifluoromethane)sulfonimide lithium salt (LiTFSI), lithium trifluoromethanesulfonate (LiTf), lithium hexafluorophosphate (LiPF<sub>6</sub>), and lithium nitrate (LiNO<sub>3</sub>) as well as anhydrous solvents, 1,3-dioxolane (DOL) and 1,2-dimethoxyethane (DME) were purchased from commercial sources and used as received. 1M electrolyte solutions of different lithium salts containing 2wt% of LiNO<sub>3</sub> as the additive in DOL/DME (v : v = 1:1) were prepared in a glove box filled with argon with both moisture level < 0.2 ppm and oxygen level < 0.5 ppm.

**Cell assembly:** R2032 Li-S coin cells were assembled in the glove box filled with argon using the prepared cathode and electrolyte with an E/S ratio of 20  $\mu\text{L mg}^{-1}$ . E/S ratio was specified as the ratio of electrolyte volume to weight of elemental sulfur. Assembly of the coin cell started from anode case, followed by spring, spacing, lithium metal anode with diameter of 15.8 mm, Celgard 2500 membrane with diameter of 19 mm as the separator, cathode and cathode case. This sequence of assembly ensured that spring was positioned firmly without possible dislocation that might cause cell failure while crimping.

**Electrochemical testing:** After assembly and sitting for 3 h, Li-S coin cells were cycled galvanostatically on a LAND battery tester between 1.7 V and 2.8 V. C-rate for Li-S batteries during charging or discharging process was defined based on 1C = 1672 mA g<sup>-1</sup>. Specific capacity of the coin cell was based on the mass of elemental sulfur. The Coulombic efficiency of the coin cell was defined as the percentage (%) of discharge capacity to the following charging capacity. Electrochemical impedance spectroscopy (EIS) and cyclic voltammetry (CV) measurements for batteries were performed on the Bio-logic electrochemical potentiostat/ galvanostat (VSP). Two-electrode EIS

measurement was conducted in a frequency range from 100 mHz to 200 kHz at  $V_{OC}$  with a perturbation degree of 10 mV. CV was carried out within a voltage range from 1.7 V to 2.8 V at the scan rate of 0.2 mV/s after the batteries were assembled and rested for 3 h.

The compatibility of lithium metal anode with different electrolytes was probed by using a Li/Li symmetric coin cell configuration. Two fresh lithium foils (450  $\mu\text{m}$  thick) with a diameter of 15.8 mm were used as positive and negative electrodes, respectively, and a Celgard 2500 membrane with diameter of 19 mm was utilized as the separator between two lithium foils. A Li/Li symmetric cell contains 75  $\mu\text{L}$  electrolyte. A fixed amount of lithium was plated and stripped on the Li electrode at a galvanostatic condition of 0.5  $\text{mA cm}^{-2}$  for 1 h for each plating and stripping cycle.

**Ionic conductivity measurement:** The ionic conductivity of different electrolytes was measured by electrochemical impedance spectroscopy (EIS) using Bio-logic electrochemical potentiostat/ galvanostat (VSP). A Celgard 2500 separator saturated with 30  $\mu\text{L}$  of electrolyte was sandwiched between two stainless steel electrodes in 2032-type coin cells, and its ionic conductivity was calculated based on the formula shown below:

$$\sigma = l / (R_b A)$$

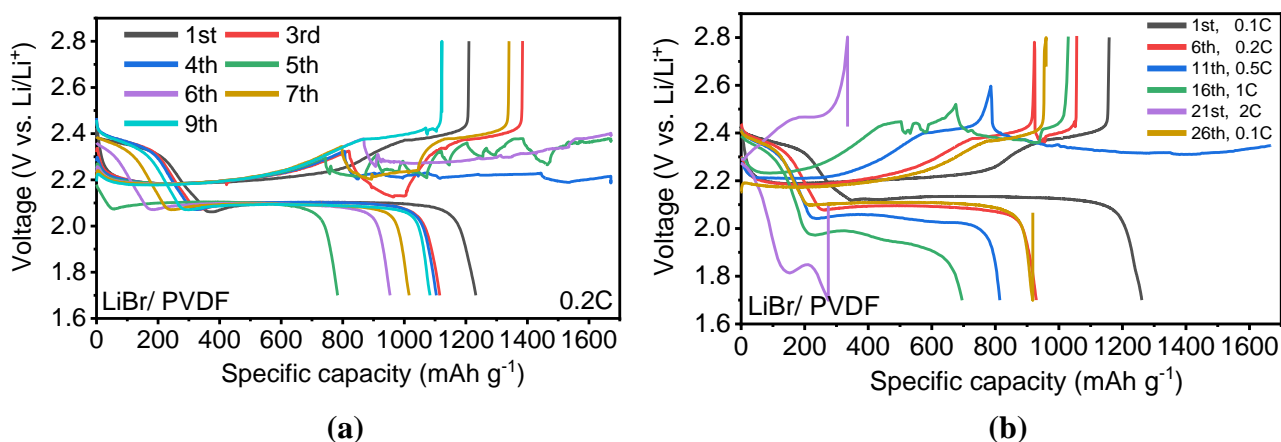
where  $\sigma$  represents ionic conductivity,  $l$  stands for the thickness of the membrane,  $A$  referred the area of the stainless steel electrode, and  $R_b$  was the bulk resistance.

### 3.3 Results and discussion

#### 3.3.1 Cycling performance comparison of five lithium salts

**Figure 3-2 a-f** are some electrochemical results of batteries with five lithium salts. The LiBr battery has the highest initial discharge capacity of 1232  $\text{mAh g}^{-1}$  and retention rate of 71.0% after 100 discharge/charge cycles, followed by  $\text{LiClO}_4$  (1165, 68.1%), LiTf (1120, 65.9%), LiPF<sub>6</sub> (1035, 65.0%), and LiTFSI (1035, 64.4%). Noticeably, an

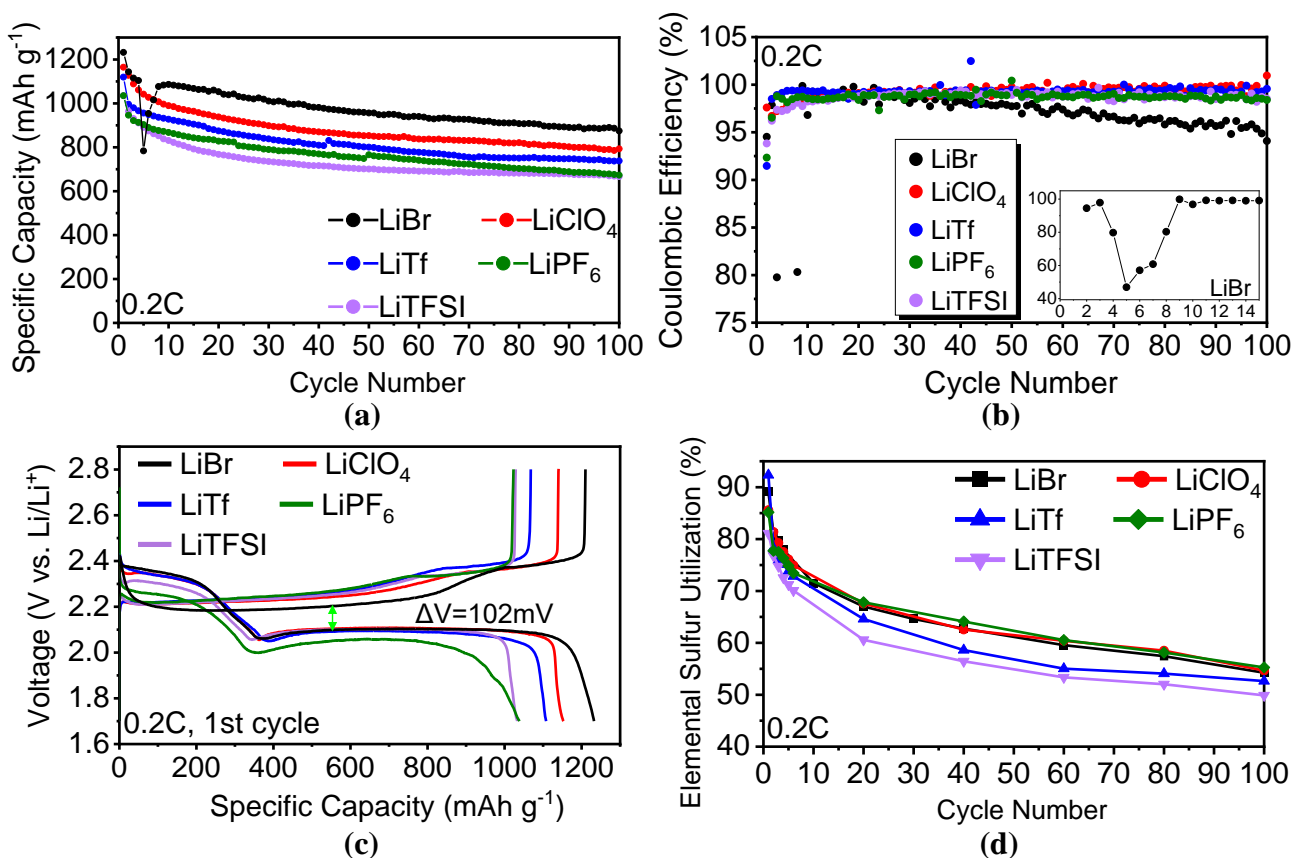
unusual thing for LiBr occurred from 3rd to 8th cycle during charging process in which so-called “overcharge” phenomenon<sup>38, 49</sup> took place prior to cut-off voltage. It was featured by a sudden voltage drop during charge along with many fluctuations (**Figure 3-1**) instead of reaching the cut-off voltage in a sharp and straight way as shown in **Figure 3-2c**. As a result, there was a ceaseless charging process unless a cut-off charging time was pre-set. In **Figure 3-2a**, this problem directly led to the sudden discharge capacity drop in 3<sup>rd</sup> cycle because the discharge started from a lower voltage.



**Figure 3-1.** Charge and discharge voltage profiles of several overcharged cycles for LiBr battery during (a) 0.2C galvanostatic cycling and (b) rate performance test. The fluctuation of voltage would not stop unless a cut-off charging time was set before the cycling.

Coulombic efficiency comparison of batteries with varying lithium salts was presented in **Figure 3-2b**. It was calculated by dividing charge capacity with subsequent discharge capacity. All batteries manifested a noticeably increasing tendency for first few cycles starting from a relatively low value except for LiClO<sub>4</sub> battery. The trend of curve to decrease first and then increase of LiBr battery in the inset of **Figure 3-2b** coincided with **Figure 3-2a**, elucidating the appearance of overcharge problem. Besides, the efficiency decline of LiBr battery was the most appreciable among five batteries with only 94% for the last cycle. Unstable lithium surface in the LiBr electrolyte was possibly responsible for the decline of efficiency verified by its rapidly accumulation of impedance in Li/Li symmetric cell (**Figure 3-4**). For the rest of four batteries with

different electrolytes, the average Coulombic efficiency was all higher than 98.0%. That is because after using  $\text{LiNO}_3$  as an additive for the electrolyte of LSB<sup>72</sup>, protective SEI layer forms on the surface of anode that passivates and protects lithium metal anode. This layer could suppress the side reactions of high-valent soluble polysulfide anions with lithium metal and, therefore, avoid forming irreversible  $\text{Li}_2\text{S}$  /  $\text{Li}_2\text{S}_2$  on the surface of the lithium anode. Accordingly, Coulombic efficiency and discharge capacity of LSB were improved. Judging from **Figure 3-2b**, specific ordering is  $\text{LiClO}_4$  (99.26%)>  $\text{LiTf}$  (99.23)>  $\text{LiTFSI}$  (98.70%)>  $\text{LiPF}_6$  (98.65%)>  $\text{LiBr}$  (95.70%).



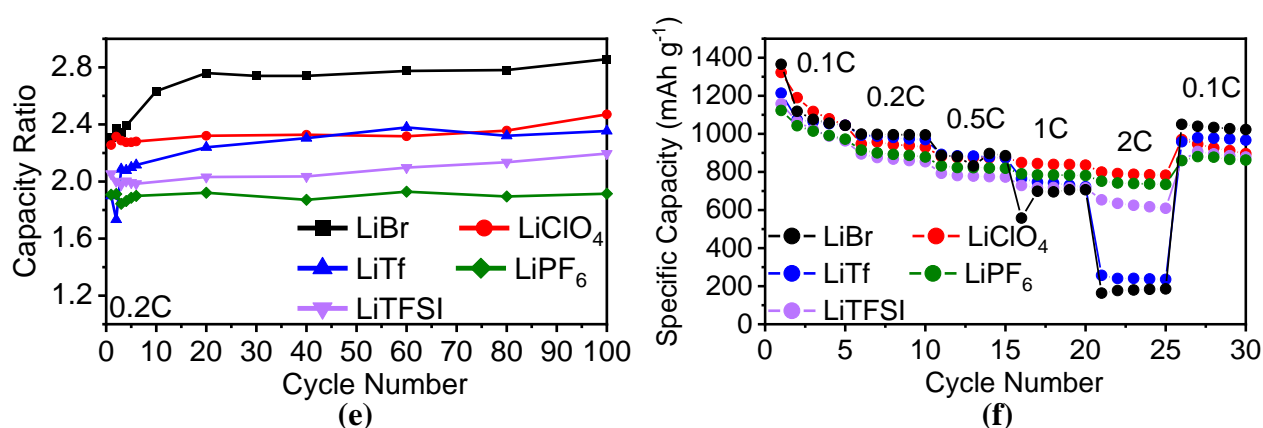


**Figure 3-2. Electrochemical characteristics of Li-S batteries with different lithium salts.** Electrolyte comprises following compositions, 1 M lithium salt in 1,3-dioxolane (DOL) + 1,2-dimethoxyethane (DME), (1:1 by volume) and 2wt% LiNO<sub>3</sub> as additive. **a)** Specific discharge capacity of batteries over 100 cycles at 0.2C. **b)** Coulombic efficiency values for 100 charge/discharge cycles at 0.2C. **c)** Charge and discharge voltage profile of batteries for 1<sup>st</sup> cycle at 0.2C. **d)** Elemental sulfur utilization defined by specific discharge capacity drawn from first discharge plateau divided by theoretical value for 100 cycles at 0.2C. **e)** Capacity ratio of batteries with different lithium salts for 100 discharge/charge cycles. **f)** Rate performance test for 30 discharge/charge cycles in total with current density ranging from 0.1C to 2C, then returning to 0.1C.

Also, LiBr battery displayed the smallest voltage hysteresis compared to that of the rest of four batteries in **Figure 3-2c**. Voltage hysteresis is defined as the disparity of voltage between charging and discharging process, which is associated with the diffusion of soluble polysulfides<sup>88</sup> and redox kinetics of electrochemical reactions on the cathode<sup>18, 89</sup>. Voltage hysteresis is able to reflect the degree of reversibility for electrochemical reactions. Reduction of the voltage hysteresis signifies a decrease of polarization for the electrochemical reaction, which represents the promoted redox kinetics<sup>90</sup> and higher sulfur utilization as well as energy efficiency. The improvement of LiBr battery can be ascribed to the three-dimensional growth of Li<sub>2</sub>S particle leading to delayed electrode passivation and faster charge transfer process<sup>77</sup>. The rest of lithium salts were ranked in following order as LiClO<sub>4</sub>, LiTFSI, LiTf and LiPF<sub>6</sub> from small to large.

**Figure 3-2d** and **3-2e** represent the utilization of elemental sulfur and reduction ability of lithium salt on short-chain polysulfides, respectively. Elemental sulfur utilization was

calculated based on the ratio of first-plateau specific capacity to theoretical value (418 mAh g<sup>-1</sup>), which estimated how much elemental sulfur was utilized and transformed to LiPSs. Capacity ratio (also called plateau ratio) was defined as the value of discharge specific capacity drawn from second plateau divided by that of first plateau, which evaluated the degree of reduction reaction from short-chain LiPSs to Li<sub>2</sub>S. The theoretical value for this capacity ratio is 1:3.

Two plateaus are divided by a saturation point that is marked by a voltage dip. As cycle proceeded, the elemental sulfur utilization gradually decreases resulting from the loss of active material, but the capacity ratio increases, exhibiting enhanced ability to reduce short-chain soluble polysulfide to Li<sub>2</sub>S / Li<sub>2</sub>S<sub>2</sub>. Still, LiBr battery ranks first in terms of capacity ratio even though LiBr did not display outstanding elemental sulfur utilization. For LiTFSI battery, the utilization of elemental sulfur is the worst (**Figure 3-2d**), and its capacity ratio is second-to-last outperforming the LiPF<sub>6</sub> battery (**Figure 3-2e**). LiTf battery is the opposite case featuring low elemental sulfur utilization but high capacity ratio.

As to rate performance comparison in **Figure 3-2f**, both LiTf and LiBr battery had poor performance under high C-rate discharge in **Figure 3-2f** with a noticeable drop (187 mAh g<sup>-1</sup> for LiBr battery and 124 mAh g<sup>-1</sup> for LiTf battery) during 1C and even more pronounced decline after switching to 2C (only 160 – 260 mAh g<sup>-1</sup> left for discharge). The fluctuation of capacity in 13<sup>th</sup> and 16<sup>th</sup> cycle for LiBr battery was indicative of overcharge prior to the discharge. On the contrary, LiPF<sub>6</sub> and LiClO<sub>4</sub> battery showed high specific capacity under 1C and 2C discharge, which can be attributed to its excellent ionic conductivity<sup>34</sup>. LiPF<sub>6</sub> battery kept 728.7 mAh g<sup>-1</sup> and 653.4 mAh g<sup>-1</sup>, while LiClO<sub>4</sub> battery remained 849.2 mAh g<sup>-1</sup> and 799.4 mAh g<sup>-1</sup> at 1C and 2C discharge, respectively. The battery with LiTFSI electrolyte behaved in a normal way with acceptable rate capability overall. After turning back to 0.1C at 26<sup>th</sup> cycle, all five batteries are capable of recovering their discharge capacity compared with 5<sup>th</sup> cycle



when the C-rate change began. But the recovery rate is different, LiBr (100.5%) > LiClO<sub>4</sub> (92.8%) > LiTf (91.7%) > LiTFSI (89.4%) > LiPF<sub>6</sub> (88.4%).

### 3.3.2 Voltage barrier at the beginning of oxidizing Li<sub>2</sub>S

**Figure 3-2c** showed the 1<sup>st</sup> cycle charge and discharge voltage profiles for batteries with five different lithium salts. Specifically, the charge profile for LiBr battery was prominent with a large voltage spike up to 2.41 V at the onset stage of charging process, where insoluble and non-conductive Li<sub>2</sub>S was oxidized. This phenomenon could be attributed to the three-dimensional growth of Li<sub>2</sub>S under LiBr electrolyte <sup>77</sup>, which would increase the Li<sub>2</sub>S particle size to micrometer level and thereby increase the difficulty of oxidation. It has been previously reported <sup>91-93</sup> that initial charging is difficult for rechargeable batteries based on Li<sub>2</sub>S as starting active material. An activation process is always required with a large voltage spike at the beginning of charge. Yang et al. <sup>93</sup> investigated the possible mechanism behind this initial barrier for activating the Li<sub>2</sub>S cathode and illustrated it is thermodynamically originated from the phase nucleation. And it is common knowledge that formation of a new phase, which is the polysulfide phase in this case, relies upon extra impetus input as seen in other typical two-phase reaction of material <sup>94</sup>.

Two factors affect the magnitude of this potential barrier, charge transfer between electrolyte and surface of Li<sub>2</sub>S particles and diffusion of lithium ion inside Li<sub>2</sub>S particles <sup>95</sup>. Both processes are associated with particle size of Li<sub>2</sub>S and its electronic conductivity and ionic diffusivity of Li<sup>+</sup> in Li<sub>2</sub>S <sup>91-96</sup>. The insulating and electrochemically inactive nature of Li<sub>2</sub>S results in sluggish charge transfer on the surface and hampered lithium-ion diffusion in Li<sub>2</sub>S <sup>96</sup>. After the activation of Li<sub>2</sub>S is finished, polysulfides will be present in the electrolyte and serve as the polysulfide nuclei that gives rise to instantaneous separation of phases in which increasing number of lithium ions appear on the Li<sub>2</sub>S particle surface [<sup>95</sup>]. Meanwhile, charge transfer at the electrode-electrolyte

interface is also facilitated, which accounts for the small overpotential <sup>[93]</sup> presented in the rest of the first charge after activation.

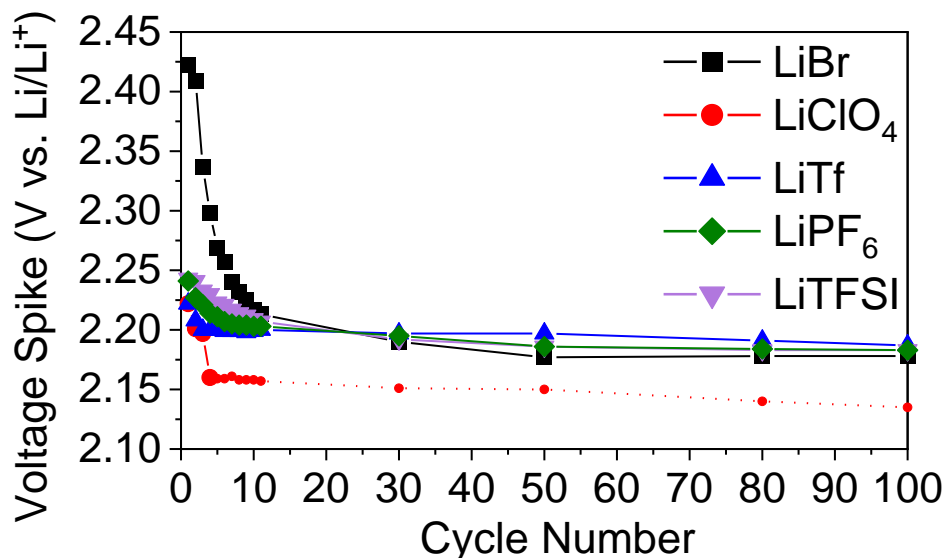


**Figure 3-3.** Variation trend of voltage spike at onset of charge for batteries with different electrolytes.

**Figure 3-3** revealed the variation trend of initial voltage spike during each charging of five batteries as the cycle progressed. Except for LiClO<sub>4</sub> battery, the voltage spike of four other batteries was determined to be the corresponding maximum voltage in a range from the beginning to 20 mAh g<sup>-1</sup> of each charge cycle. Because the voltage barrier for LiClO<sub>4</sub> battery in this range disappeared after the 3<sup>rd</sup> cycle, the rest of data points were picked from the voltage value at 0 mAh g<sup>-1</sup> of each charge cycle, which are marked as smaller circular dots being connected by dashed line.

Of note, despite the formation of agglomerates of Li<sub>2</sub>S in LiBr electrolyte (with the high-DN anion), it did not produce initial voltage spike as high as the batteries directly using Li<sub>2</sub>S<sup>91-93</sup> as active material. The reason lies in the polysulfides existing in the electrolyte or not during the first charging. Considering that we adopted elemental sulfur as the active material for this work, the batteries start with discharge process. Elemental sulfur undergoes step-by-step lithiation, being converted into final redox product, Li<sub>2</sub>S. Soluble long-chain polysulfides are generated as intermediates that dissolve in the

electrolyte from the very beginning of the first discharging. However, not all polysulfides were utilized. Some of them stayed in the electrolyte, leading to “shuttle effect” as mentioned in the introduction part. Those polysulfides form phase nuclei on the vicinity of  $\text{Li}_2\text{S}$  particles during the first charge, which facilitates the oxidation of  $\text{Li}_2\text{S}$ . As for LSBs directly using  $\text{Li}_2\text{S}$  as active material, this voltage spike for subsequent charging cycles become lower owing to the existence of a certain amount of polysulfides in the electrolyte, which removes the additional energy for the formation of new phase<sup>93</sup>. This phenomenon echoes our experimental finding in **Figure 3-3**. It is evident that the voltage spike gradually decreased and stabilized at a certain value, which means the voltage barrier was dying down until it disappeared. It could possibly be interpreted by the fact that more polysulfides stay in the electrolyte without utilized within each cycle. Additionally, Gorlin et al.<sup>97</sup> also delved deeper on the redox mechanism for  $\text{Li}_2\text{S}$  electrode using Spatially Resolved Operando X-Ray Absorption Spectroscopy and showed that the process of oxidizing  $\text{Li}_2\text{S}$  particles is promoted by abundant polysulfides existing in the electrolyte as well as separator, in a way that they are involved in a chemical step during this process.

### 3.3.3 Compatibility with lithium anodes and self-discharge behavior

To explore the compatibility of different lithium salts with lithium metal anode,  $\text{Li}/\text{Li}$  symmetric cell was utilized for evaluation as shown in **Figure 3-4**. Lithium stripping and plating occurred during charging and discharging, and the amplitude of overpotential is indicative of impedance inside the  $\text{Li}/\text{Li}$  symmetric cell.

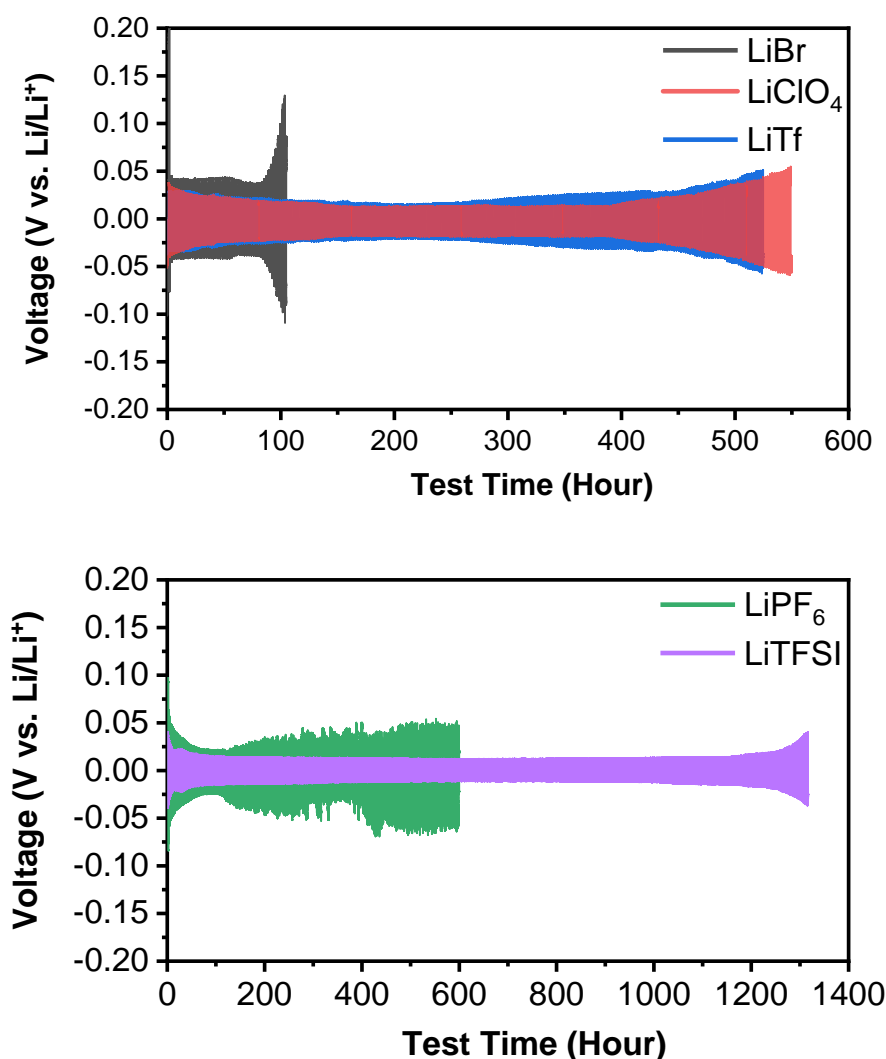


**Figure 3-4. Compatibility of lithium metal electrode and electrolyte with varying lithium salts.** Voltage variation curves of Li/Li symmetric cell during Li plating and stripping process in different electrolyte at a galvanostatic condition of  $0.5 \text{ mA cm}^{-2}$ . Electrolyte system includes 1 M varying lithium salt + 2wt%  $\text{LiNO}_3$  in DOL/DME (1:1 by volume ratio). Five lithium salts were presented in two separate figure for the purpose of clarity.

It is evident that LiBr battery behaved worst in terms of cycling performance since it had the largest overpotential (43 mV) and shortest stable duration less than 100 hours.  $\text{LiPF}_6$  battery also surprisingly showed only about 110 hours of stable time followed by jagged voltage fluctuation unlike the sudden voltage build-up of LiBr cell. Battery with  $\text{LiClO}_4$  electrolyte exhibited slightly better performance than that of LiTf electrolyte in which the former one presented smaller overpotential (13mV) and longer stable time

(400 hours) in comparison to the latter one, while both demonstrated gradual increase of impedance thereafter. LiTFSI cell was the most stable one throughout the test with the smallest overpotential (10mV) and no impedance build-up until 1200 hours under this moderately aggressive cycling condition.

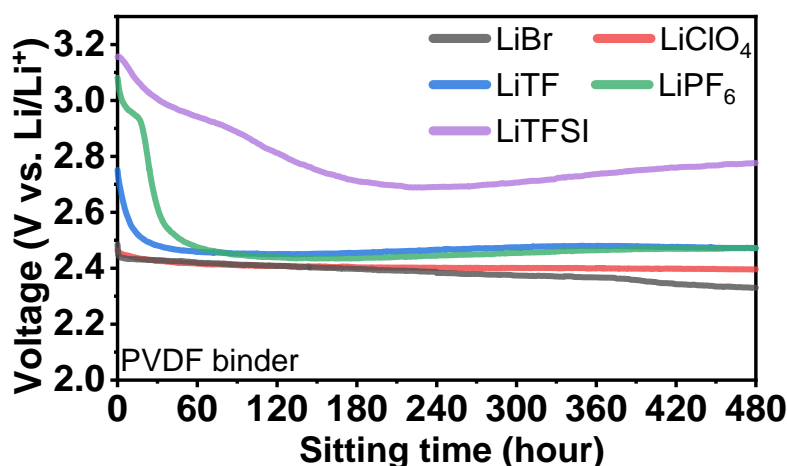


**Figure 3-5. Variation of open circuit voltages ( $V_{oc}$ ) of LSBs using different lithium salts during the self-discharge measurement.** Electrolyte system includes 1 M varying lithium salt + 2wt%  $\text{LiNO}_3$  in DOL/DME (1:1 by volume ratio).

Additionally, self-discharge behaviors of LSBs using varying lithium salts were evaluated as well. Even during the storage/ sitting time, elemental sulfur still gradually transforms into soluble long-chain LiPSs and readily dissolves into the electrolyte. They would be reduced or even irreversibly precipitated as  $\text{Li}_2\text{S}$ /  $\text{Li}_2\text{S}_2$  once reaching the Li anode, resulting in the loss<sup>98</sup> of the battery capacity. This process can be reflected by the change of  $V_{oc}$  of LSBs during the self-discharge experiments as shown in **Figure 3-5**. LiBr battery and  $\text{LiClO}_4$  battery have more severe self-discharge than other three batteries because the  $V_{oc}$  started with around 2.5V at the beginning of the test, which are obviously lower than other three batteries. Besides, the  $V_{oc}$  of LiBr battery and  $\text{LiClO}_4$  battery remained lower than other three batteries throughout the storage time. LiTF battery and  $\text{LiPF}_6$  battery both underwent sharp decline from 0 to 60th hour and had similarly almost flat  $V_{oc}$  trend afterwards. LiTFSI battery showed the least self-

discharge phenomenon among five batteries with the gradual decline until roughly 240th hour and slow increase starting from there. The  $V_{oc}$  of LiTFSI battery was above 2.68V all the time in the test, suggesting almost no occurrence of electrochemical reactions. The ranking of severity of self-discharge behavior should be  $LiBr > LiClO_4 > LiTf > LiPF_6 > LiTFSI$ .

### 3.3.4 Kinetics of electrochemical reactions for different lithium salts

**Figure 3-6** suggested that five batteries with different lithium salts had different electrochemical characteristics in terms of the peak voltage and the onset potential drawn from cyclic voltammograms. The 2<sup>nd</sup> cycle was chosen to ensure that the electrode reaction had already stabilized. The onset potential was picked based on a current density of  $10 \mu A cm^{-2}$  beyond the baseline current [99], which is a method commonly adopted in electrocatalysis field.

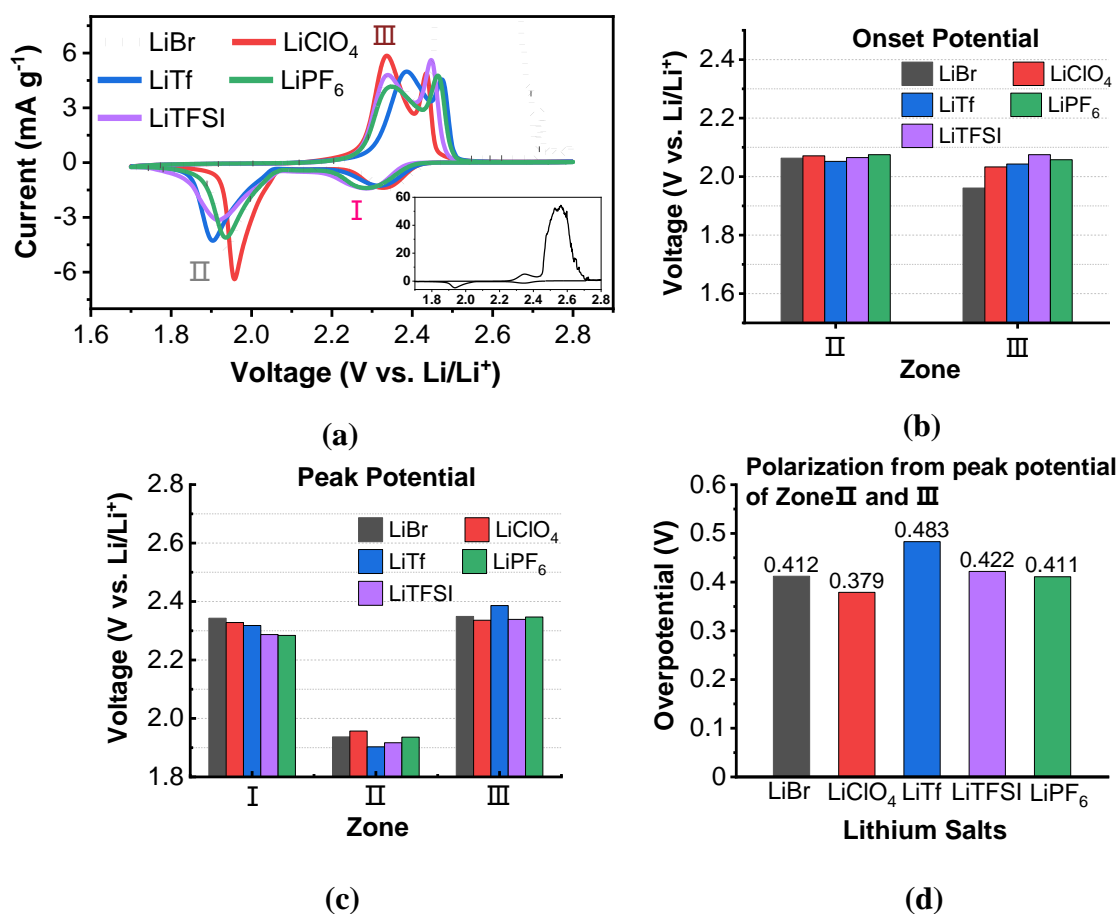


**Figure 3-6. Cyclic voltammograms of Li-S batteries with varying lithium electrolyte salts.** a) 2<sup>nd</sup> cycle of cyclic voltammetry (CV) at a sweep rate of 0.2 mV/s. b) Peak potential obtained from Zone I, II and III. c) Onset potential extracted from Zone I, II and III. d) Overpotential drawn from cyclic voltammograms of five different batteries where peak potential of Zone III minus peak potential of Zone II.

In our case, there are mainly two redox processes involved during cathodic and anodic scan for Li-S batteries as per below:



For the cathodic scan, first reduction peak at higher potential range is ascribed to the generation of high order lithium polysulfides from elemental S<sub>8</sub> simplified as reaction (1), and second reduction peak is the transformation from lithium polysulfides to insoluble lithium sulfide/ disulfide that can be described by reaction (2). During the anodic scan, two peaks were overlapped to a certain extent, which can be roughly represented by backward reaction (1) and (2). The equilibrium potential for two electrochemical reactions can be used as benchmark to assess the degree of difficulty for those reactions to happen in practical.

**Figure 3-6d** shows the difference between the second cathodic peak potential and first anodic peak potential. This difference suggests the degree of reversibility of reaction (2) that is corresponding to the second plateau in **Figure 3-2c** during galvanostatic cycling of Li-S batteries, accounting for 75% of theoretical capacity. It is noticeable that LiClO<sub>4</sub> battery possessed the lowest overpotential while LiTf battery had the highest overpotential, and the other three batteries held similar value. Those results demonstrate reaction (2) has the highest reversibility under LiClO<sub>4</sub> electrolyte. Five batteries can be ranked as follows in terms of reversibility of reaction (2), LiClO<sub>4</sub> > LiPF<sub>6</sub> > LiBr > LiTFSI > LiTf.

With respect to the peak current density, five batteries all had similar value at Zone I. At Zone II and III, LiClO<sub>4</sub> battery displayed the highest current density and very sharp peak shape, representing the fastest reaction rate of reaction (2). LiBr battery ranks 2<sup>nd</sup> for both Zone II and III followed by LiTf battery in 3<sup>rd</sup> place. The most notable phenomenon was the occurrence of current overflow for LiBr battery after 2.4 V in the middle of charging process. It could be linked to the overcharge phenomenon during rate performance (**Figure 3-2f**) and 0.2C galvanostatic test (**Figure 3-1**) where it also took place near 2.4V at the finish of lithium sulfide oxidation and the formation stage of elemental sulfur on the cathode side. It is possibly due to the scatter and damage of cathode structure stemming from the three-dimensional growth<sup>77</sup> of lithium sulfide under LiBr electrolyte that gives rise to the formation of large-sized particles.

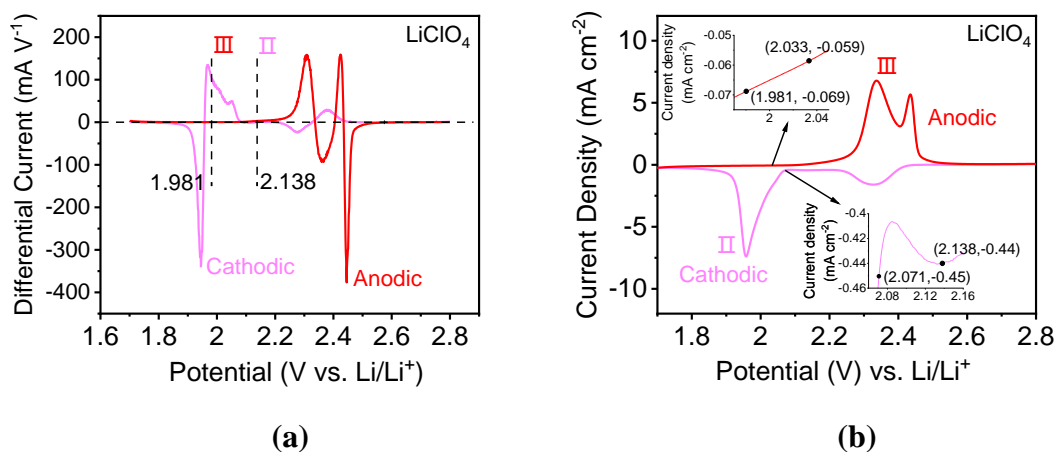


**Figure 3-7. Onset potential for electrochemical reactions of Li-S battery with LiClO<sub>4</sub> electrolyte. a)** Differential CV curves. **b)** Normal CV curves with mA/cm<sup>2</sup> unit for y-axis.

The onset potential of each redox reaction was extracted from the CV curves as demonstrated in **Figure 3-7**, and they were compared to the equilibrium potential. LiClO<sub>4</sub> battery was chosen as an example above to demonstrate how the onset potential of redox reactions was extracted from the CV peak. As the **Figure 3-7a** exhibited, 2.138V and 1.981V were determined as the baseline voltages for cathodic Zone II and anodic Zone III before the electrochemical peaks, respectively. These baseline voltages correspond to the minimum rate of change of current density on the CV curve prior to a



peak. In other words, the derivative value ( $dI/dV$ ) is the lowest at baseline voltages. **Figure 3-7b** insets reveal the process of determining the value of onset potential by referring to a prevalent definition in electrocatalysis field, where the current density exceeds (for anodic peaks) or falls behind with<sup>99</sup> (for cathodic peaks) the corresponding baseline current density for  $10 \mu\text{A cm}^{-2}$ . The value of onset/baseline voltage and corresponding current density are annotated in the insets next to the highlighted data point. Thus, the onset potential for cathodic peak II and anodic peak III are 2.071V and 2.033V, respectively.

The accurate value for the equilibria potential of reaction (1) and (2) were difficult to be determined for two reasons. Firstly, there are both electrochemical and chemical reactions<sup>100, 101</sup> (disproportionation) involved in those CV peaks as described by reaction (1) - (4).



Plus, sulfur species with multiple valences are involved in each step, leading to difficulty and unclarity in terms of the determination of equilibrium potential. It could be numerous sub-reactions happening at one time at the cathode. Furthermore, it is impossible to measure the concentration of species that are incorporated in those reactions. Despite this, Moy et al.<sup>102</sup> came up with an analytical model and provided equilibrium voltage range for all reversible sub-reactions encompassing sequential sulfur species during reduction process. After applying their findings in our case, reaction (2) has an approximate equilibrium voltage of 1.9 V. **Figure 3-6b** shows onset potential measurements of two zones from CV graph. Analysis was focused on reaction (2) that corresponds to Zone II and III. Onset potential at Zone II is very similar among five batteries demonstrating comparable degree of difficulty for forward reaction to occur. On the other hand, different result was produced in Zone III. LiBr battery exhibited the lowest onset potential and closest value to 1.9V, manifesting LiBr's

electrocatalytic effect for diminishing the degree of difficulty for reverse reaction (2). The rest of lithium salts were ranked as  $\text{LiClO}_4 > \text{LiTf} > \text{LiPF}_6 > \text{LiTFSI}$ .

### 3.3.5 Charge transfer process of batteries with different lithium salts

Also, the electrochemical impedance spectroscopy (EIS) technique was exploited to acquire information about interfacial behavior for batteries with different lithium salts after completing cyclic voltammograms of the same measurement condition. All batteries were at full charge state while operating the EIS test. Due to the unique electrochemistry of Li-S batteries, which is the dissolution-precipitation reaction on both electrodes, the cycle performance of Li-S batteries is relying on the interfacial phenomenon to a large extent. SEI layer<sup>43, 103, 104</sup> and insulating  $\text{Li}_2\text{S}/\text{Li}_2\text{S}_2$  film can form on the surface of lithium anode owing to the lowest standard reduction potential of metallic lithium and the notorious shuttle effect as mentioned in **section 1.4.3** and **section 1.3.2**. Besides, the deposition morphology of  $\text{Li}_2\text{S}/\text{Li}_2\text{S}_2$  on the surface of cathode also plays a significant role in the cycle stability<sup>76, 100, 105</sup>. The sulfur cathode is set as working electrode where electrochemical reactions happen and deliver capacity by transforming elemental sulfur to  $\text{Li}_2\text{S}/\text{Li}_2\text{S}_2$ . Moreover, for half-cell configuration, lithium metal anode, as counter electrode, is in much larger excess compared with the amount of active material in the working electrode. In other words, the metallic lithium anode contains greater capacity and electrode surface so as to rule out its possible interference during the test of working electrode. Thus, little information could be extracted from the EIS spectrum concerning metallic lithium anode side, and the principal interpretation of EIS constituent parts is related to the kinetics of redox reactions on the sulfur cathode side. As shown in **Figure 3-8**, Nyquist plots are comprised of two semicircles in the high-frequency range and an inclined straight line in the low-frequency area for cycled coin cells. It was widely accepted that the semicircle in the higher frequency region (left semicircle) accounts for the formation of cathode electrolyte interface<sup>106</sup>, while the semicircle in the medium-high frequency

domain (right semicircle) could be designated to charge transfer process<sup>72, 107, 108</sup> on the interface between cathode and electrolyte that is determined by insulating  $\text{Li}_2\text{S}/\text{Li}_2\text{S}_2$  layer and cathode electrolyte interface.

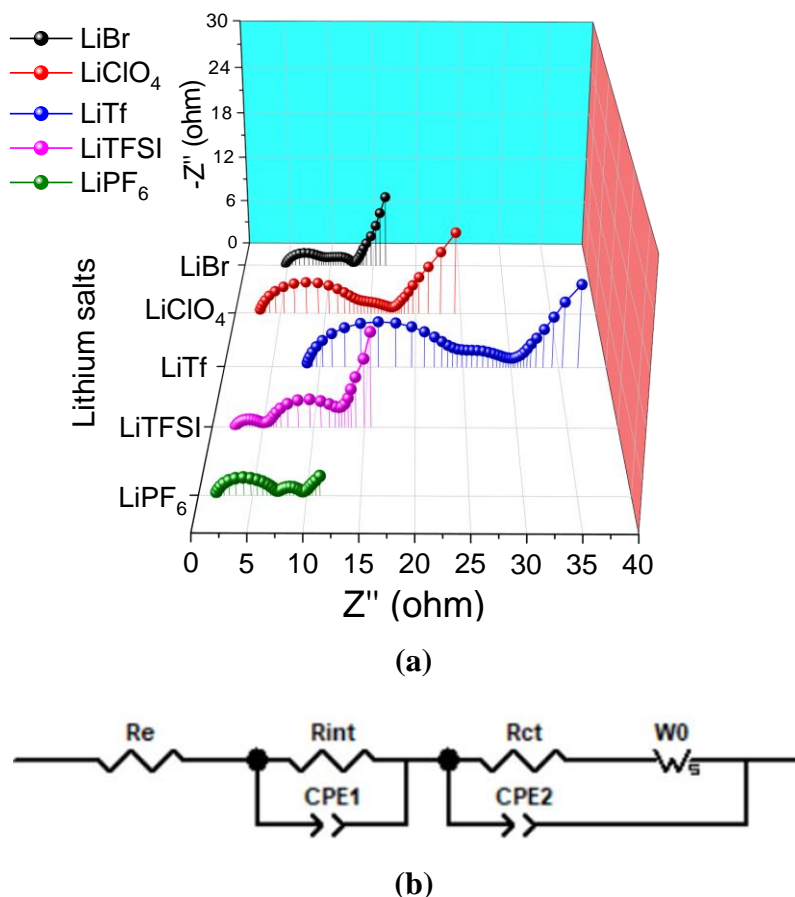


**Figure 3-8.** (a) Electrochemical impedance spectrum of batteries after cyclic voltammetry test for four cycles. (b) The equivalent circuit model for EIS analysis based on two-electrode Li-S coin cells.

**Table 3-2.** A summary of resistance values simulated by ZView for batteries with different electrolytes.

Electrolyte	$R_e$ (ohm)	$R_{int}$ (ohm)	$R_{ct}$ (ohm)	$W_o$ -R (ohm)
LiBr	4.8	4.0	4.1	34.4
$\text{LiClO}_4$	2.7	9.4	5.2	26.6
LiTf	8.5	14.4	7.1	34.7
LiTFSI	2.3	3.0	8.3	94.7
$\text{LiPF}_6$	1.7	5.1	3.1	11.6

$R_e$ : resistance of electrolyte solution

$R_{int}$ : interfacial resistance

$R_{ct}$ : charge transfer resistance

$W_0$ -R: Warburg resistance

**Table 3-2** listed the summary of electrochemical parameters from batteries with different lithium salts, which were collected by using ZView software simulation combined with equivalent Randles circuit <sup>109</sup> displayed under the table. The impedance of electrolyte solution was denoted as  $R_e$  that is equal to x-intercept of the EIS curve, while  $R_{int}$  and  $R_{ct}$  were equivalent to the diameter of each corresponding semicircle. Battery with  $LiPF_6$  electrolyte demonstrates the lowest value that can be explained as electrolyte having the smallest viscosity after cycling.  $LiTFSI$  and  $LiClO_4$  batteries also bore comparably small value, while batteries with  $LiBr$  and  $LiTf$  electrolytes displayed larger  $R_e$  that might partly account for their inefficiency during discharge under high C-rate in **Figure 3-2f**. by the cause of limited ionic conductivity. When it comes to  $R_{ct}$ ,  $LiTFSI$  battery surprisingly showed the biggest resistance whereas  $LiPF_6$  had the best behavior. One thing worth mentioning is that  $LiBr$  battery presented both rather low  $R_{int}$  and  $R_{ct}$ , which was possibly the reflection of impaired cathode structure and scattered conductive carbon as a consequence.

**Table 3-3.** The comparison of key performance parameters of LSBs with different lithium salts

Name	Initial specific capacity (0.2C, mAh g <sup>-1</sup> )	Retention (%)	Average Coulombic efficiency (%)	High C-rate Performance	Capacity ratio	Compatibility with lithium
LiBr	1232.2 (1 <sup>st</sup> )	71.0 (1 <sup>st</sup> )	95.7 (5 <sup>th</sup> )	5 <sup>th</sup>	1 <sup>st</sup>	5 <sup>th</sup>
LiClO <sub>4</sub>	1164.8 (2 <sup>nd</sup> )	68.1 (2 <sup>nd</sup> )	99.26 (1 <sup>st</sup> )	1 <sup>st</sup>	2 <sup>nd</sup>	2 <sup>nd</sup>
LiTf	1119.5 (3 <sup>rd</sup> )	65.9 (3 <sup>rd</sup> )	99.23 (2 <sup>nd</sup> )	4 <sup>th</sup>	3 <sup>rd</sup>	3 <sup>rd</sup>
LiTFSI	1035.3 (4 <sup>th</sup> )	64.4 (5 <sup>th</sup> )	98.70 (3 <sup>rd</sup> )	3 <sup>rd</sup>	4 <sup>th</sup>	1 <sup>st</sup>
LiPF <sub>6</sub>	1035.1 (5 <sup>th</sup> )	65.0 (4 <sup>th</sup> )	98.65 (4 <sup>th</sup> )	2 <sup>nd</sup>	5 <sup>th</sup>	4 <sup>th</sup>

### 3.4 Conclusion

To sum up, **Table 3-3** lists the comparison of key performance parameters being discussed. We have evaluated the influences of more lithium salts on electrochemical performance of LSBs with  $\text{LiNO}_3$  as additive, including  $\text{LiPF}_6$ ,  $\text{LiClO}_4$  that are already widely employed in LIBs and two types of imide salts ( $\text{LiTFSI}$  and  $\text{LiTf}$ ) as well as a halide lithium salt ( $\text{LiBr}$ ). We have found that  $\text{LiBr}$  battery has the No.1 initial specific capacity and retention rate owing to its highest capacity ratio, but it suffers from the poor rate performance and compatibility with metallic lithium anode, plus overcharge problem during the cycle process.  $\text{LiClO}_4$  is able to offer the best high C-rate performance and Coulombic efficiency, but its strong oxidation property has been the biggest concern.  $\text{LiTf}$  is in the middle ranking for all indexes among five lithium salts except for low capacity during high C-rate discharge.  $\text{LiTFSI}$  owns excellent compatibility with lithium metal anode and could afford moderate performance in general, which makes it a base and universal lithium salt for LSBs.  $\text{LiPF}_6$  is in fact not very suitable for LSBs as demonstrated by all the results especially the compatibility test. It can easily react with the cyclic ether solvent under trace amount of water or dissolution heat yielding polymerized products<sup>110</sup> that is undesired for the operation of LSBs. This work can provide more guidance to researchers on choosing appropriate lithium salt for LSB-related studies.

## Chapter 4. Troubleshooting and Optimization for LiBr-based Li-S Batteries

### 4.1 Introduction

From what had been discussed in **Chapter 3** and outlined in **Table 3-3**, the Li-S battery using LiBr electrolyte had the highest initial discharge specific capacity, sulfur utilization and capacity retention in 100 cycles throughout the 0.2C galvanostatic test. These are performance parameters to be valued most for judging whether if this lithium salt is worth delving deeper. Thus, LiBr was screened out as the most promising one among five lithium salts that were evaluated for LSBs. At the same time, LiBr salt also brought some unavoidable problems during the operation of LSBs as described below.

1. Sudden drop of discharge specific capacity caused by failure of charging the battery to cut-off voltage, fluctuation of charging voltage and formation of overcharge.
2. Unusual current soar during reduction scan of cyclic voltammogram
3. Poor cycling performance at higher c-rate (1C and 2C).
4. Shortest stable duration indicated by cycling performance of Li/Li symmetric cell among five different lithium salts

Due to the enormous potential that LiBr could bring to LSBs community, my interests were drawn on trying to solve those problems while improving the electrochemical performance.

### 4.2 Experimental section

In this part, some experimental operations were the same as **Chapter 3** that had already been elaborated in **section 3.1**.

**Preparation of cathodes with PEI-Araldite 506 epoxy resin binder:** Elemental sulfur/Super P nanocomposite was firstly prepared by melt-diffusion method as introduced in **section 3.2**. The mixture was then blended with additional Super P and

solution of PEI and Araldite 506 (5 wt% with different mass ratio) in *N*-methyl-2-pyrrolidone (NMP) to make a slurry, which has a solid composition of 50% sulfur, 40% Super P, and 10% PEI-Araldite 506. The slurry was blade coated onto a carbon-coated aluminum foil. The wet cathode film was placed in a convection oven at 50°C for 16 h to remove the solvent while enabling in situ crosslinking reaction. Afterwards, the dry film was cut into circular disks with diameter of 12 mm, which were then further dried in a vacuum oven for 2 h to remove residual solvent. Sulfur loading of the cathode was roughly 1.3 mg cm<sup>-2</sup> for all the Li-S cells in this chapter unless noted otherwise.

**Preparation of cathode with high sulfur loading:** Elemental sulfur and Super P carbon black was uniformly mixed at a weight ratio of 70:30 in an agate mortar using a grinding pestle. Then the mixture was transferred into a hydrothermal reactor that was subsequently placed in a convection oven for a 12-hour melt-diffusion at 155°C. After cooling down to room temperature, the mixture was blended with PEI and Araldite 506 epoxy resin in *N*-methyl-2-pyrrolidone (NMP) to make a slurry. The cathode material has a solid composition of 63% sulfur, 27% Super P, and 10% PEI-Araldite 506. The as-obtained slurry was casted onto a carbon-coated aluminum foil/carbon paper from commercial source as current collectors by using blade coating. Subsequent steps are the same as last paragraph. Sulfur loading of the cathode was 3.5-6.3 mg cm<sup>-2</sup>.

### 4.3 Results and discussion

#### 4.3.1 Exploration of possible reasons for problems of Li-S cells using LiBr salt

As shown in **Figure 3-1**, the occurrence of overcharge was reflected in the voltage profile by the fluctuations of charging voltage and ceaseless charging process without reaching the cut-off voltage (2.8V). After consulting relevant literature, under two conditions did the LSBs present similar shape of curve during charge, which could be used for reference to speculate possible reasons of those problems in my case.

#### *4.3.1.1 Corrosion of lithium anode caused by LiPSs shuttling*

The first scenario came to my mind that might cause the overcharge was the notorious but very common polysulfides “shuttle effect” in the LSBs, which had been elaborated in **section 1.3.2**. The dissolution of PS intermediates into ether electrolyte does indeed facilitate the conversion electrochemistry given the extremely low conductivity of both elemental sulfur and  $\text{Li}_2\text{S}/\text{Li}_2\text{S}_2$ , and solution-based conversion has faster redox kinetics than solid phase conversion. However, this phenomenon also results in short cycle life, low sulfur utilization and coulombic efficiency since the PS intermediates react with the lithium anode to produce short-chain soluble PS and an  $\text{Li}_2\text{S}/\text{Li}_2\text{S}_2$  insulating layer as well as “dead” lithium on the anode surface, which aggravates the growth of lithium dendrite with larger specific area and thus higher reactivity toward all components of electrolyte. This phenomenon accompanied the cycling process of LSBs from the very beginning. Yuriy et al.<sup>111</sup> conducted a series of both simulations and experiments for providing a quantitative analysis of polysulfide shuttle phenomenon. They proposed a parameter called charge-shuttle factor ( $f_c$ ) that is related to charge current and shuttle constant/heterogeneous reaction constant. Their simulation results about the correlation between voltage and current density, heat transfer coefficients and lithium salt concentration during charge process were incorporated. During overcharge, two types of curve shape in the voltage profile were introduced including voltage fluctuation and direct leveling. However, the lithium anode they used for the research is unprotected, which enabled the lithium anode to readily react with LiPSs. The introduction of  $\text{LiNO}_3$ <sup>41</sup> to the electrolyte system was regarded as an important step for LSB community. The protective SEI layer derived from the reaction of lithium anode with  $\text{LiNO}_3$  effectively prevents the direct contact between anode and electrolyte, thus avoiding the occurrence of overcharge in the LSBs. As a result, LSBs employing  $\text{LiNO}_3$  as additive are able to be charged to the cut-off voltage with a sharp rise at the end of charge process contrary to the voltage leveling (**Figure 4.1**) or fluctuation for LSBs<sup>111</sup> without the addition of  $\text{LiNO}_3$ . In my case, the LiBr electrolyte was prepared with 2wt% of  $\text{LiNO}_3$  additive



(0.3M), complying with general electrolyte configuration. Thus, the assumption of lithium polysulfides corroding the unprotected lithium anode that leads to the occurrence of overcharge in the LiBr batteries was ruled out.

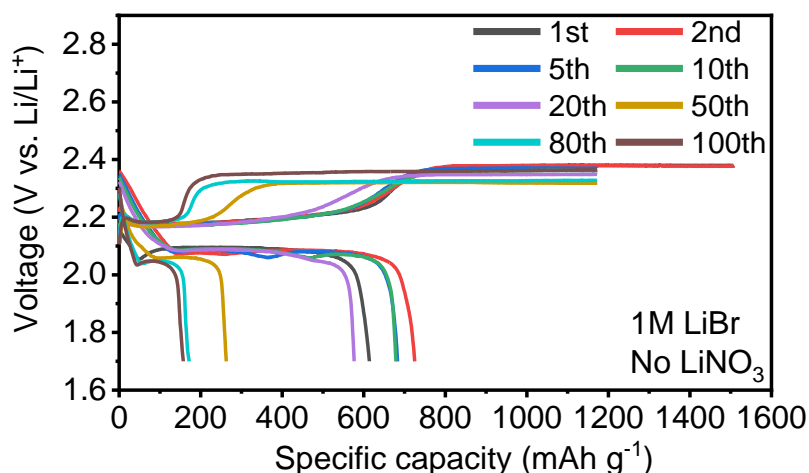
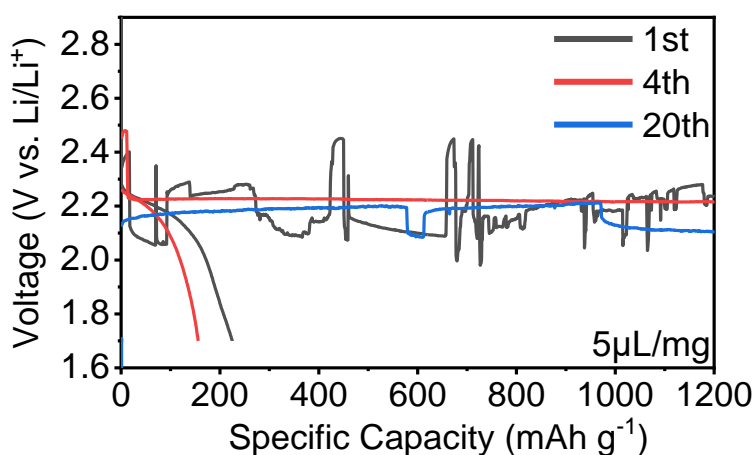


**Figure 4-1.** Voltage profiles of Li-S cell using electrolyte without adding LiNO<sub>3</sub> at 0.2C. The electrolyte composition includes 1M LiBr in DOL/DME (1:1 by volume ratio).

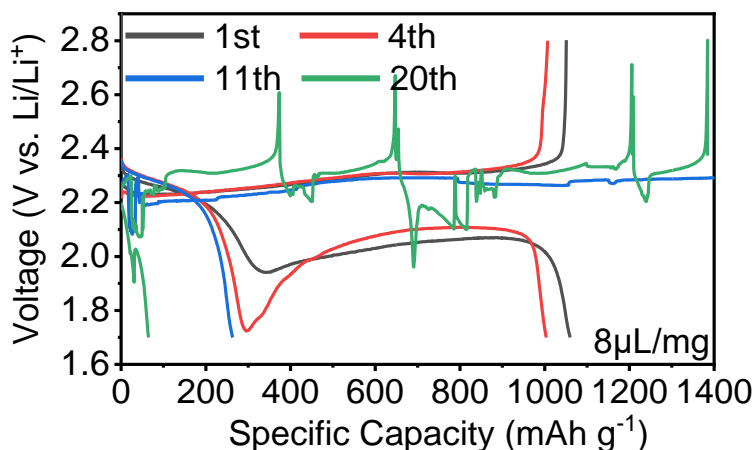
#### 4.3.1.2 Degradation of lithium anode under high concentration of LiPSs in the LiNO<sub>3</sub>-containing electrolyte

However, the addition of LiNO<sub>3</sub> is not omnipotent. Similar voltage fluctuation and long overcharge process for LSBs were also reported in several papers<sup>38,49,112</sup>, in which they used the electrolyte with a normal amount of LiNO<sub>3</sub> additive. But distinctions in their research system lay in the areal sulfur loading and the E/S ratio (**section 3.2**). For LSBs, lean electrolyte (E/S ratio < 5  $\mu\text{L mg}^{-1}$ ) and high areal sulfur loading (> 6  $\text{mg cm}^{-2}$ ) are desired for achieving practically competitive specific energy density. Pang et al.<sup>38</sup> added small amount of conventional 1M LiTFSI+2wt% LiNO<sub>3</sub> electrolyte in the LSB with 2  $\text{mg cm}^{-2}$  of sulfur loading and 5  $\mu\text{L mg}^{-1}$  of E/S ratio. The as-prepared battery could not even complete the 1<sup>st</sup> charge due to the fluctuation of charging voltage without reaching cut-off voltage. They attributed this failure of charge to the high concentration of dissolved polysulfides and resultant severe shuttle effect. Due to the lean electrolyte condition, the concentration of polysulfides in the electrolyte could be at least 4 times

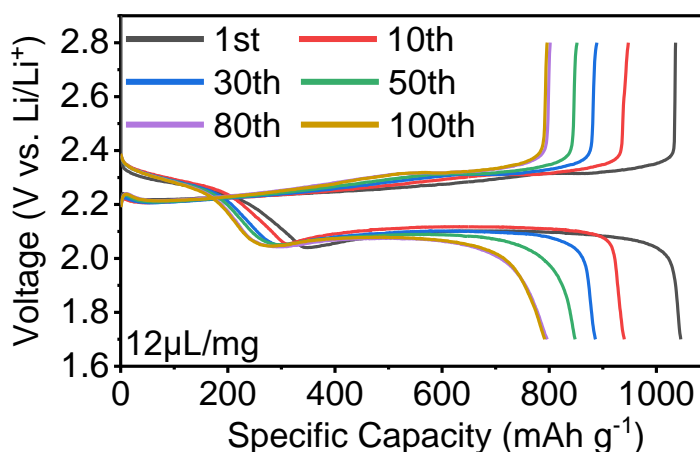
higher than normal condition during the cycle of the battery. In a separate study, Pang et al.<sup>49</sup> adopted a comprehensive approach for the cathode and increased the areal sulfur loading to  $14.9 \text{ mg cm}^{-2}$  combined with only  $3.5 \text{ } \mu\text{L mg}^{-1}$  of E/S ratio. Starting from 11<sup>th</sup> cycle of this battery, significant fluctuation of voltage on charge was observed that were ascribed to the formation of lithium dendrite because the overcharge happened in the middle of lithium deposition on the anode side. They further explained that LSB with high sulfur loading renders a very high areal capacity on the lithium metal anode, which exacerbated the growth of dendritic lithium and accumulation of impedance. Those lithium dendrites rapidly react with not only lithium polysulfides to form insulating  $\text{Li}_2\text{S}_2/\text{Li}_2\text{S}$  layer but also all the components of electrolyte that results in unnecessary loss of electrolyte and fluctuated charge voltage. What is worse, those side reactions were further aggravated by the extremely low E/S ratio. To sum up, the addition of  $\text{LiNO}_3$  works well only when the concentration of polysulfides in the electrolyte is not very high, which is also part of the reason why excess electrolyte is usually required for the successful operation of LSBs, i.e. the large E/S ratio (usually higher than  $10 \text{ } \mu\text{L mg}^{-1}$ ). When the E/S ratio was too small or the areal sulfur loading was too high, the corresponding LSBs might be subject to overcharge reflected in the voltage profile similar to LiBr battery in my research during charge.



(a)



(b)



(c)

**Figure 4-2.** Voltage profiles of Li-S batteries using different E/S ratios at 0.2C. (a)  $5\mu\text{L mg}^{-1}$ . (b)  $8\mu\text{L mg}^{-1}$ . (c)  $12\mu\text{L mg}^{-1}$ . The electrolyte composition includes 1M LiTFSI+2wt%  $\text{LiNO}_3$  in DOL/DME (v/v=1:1).

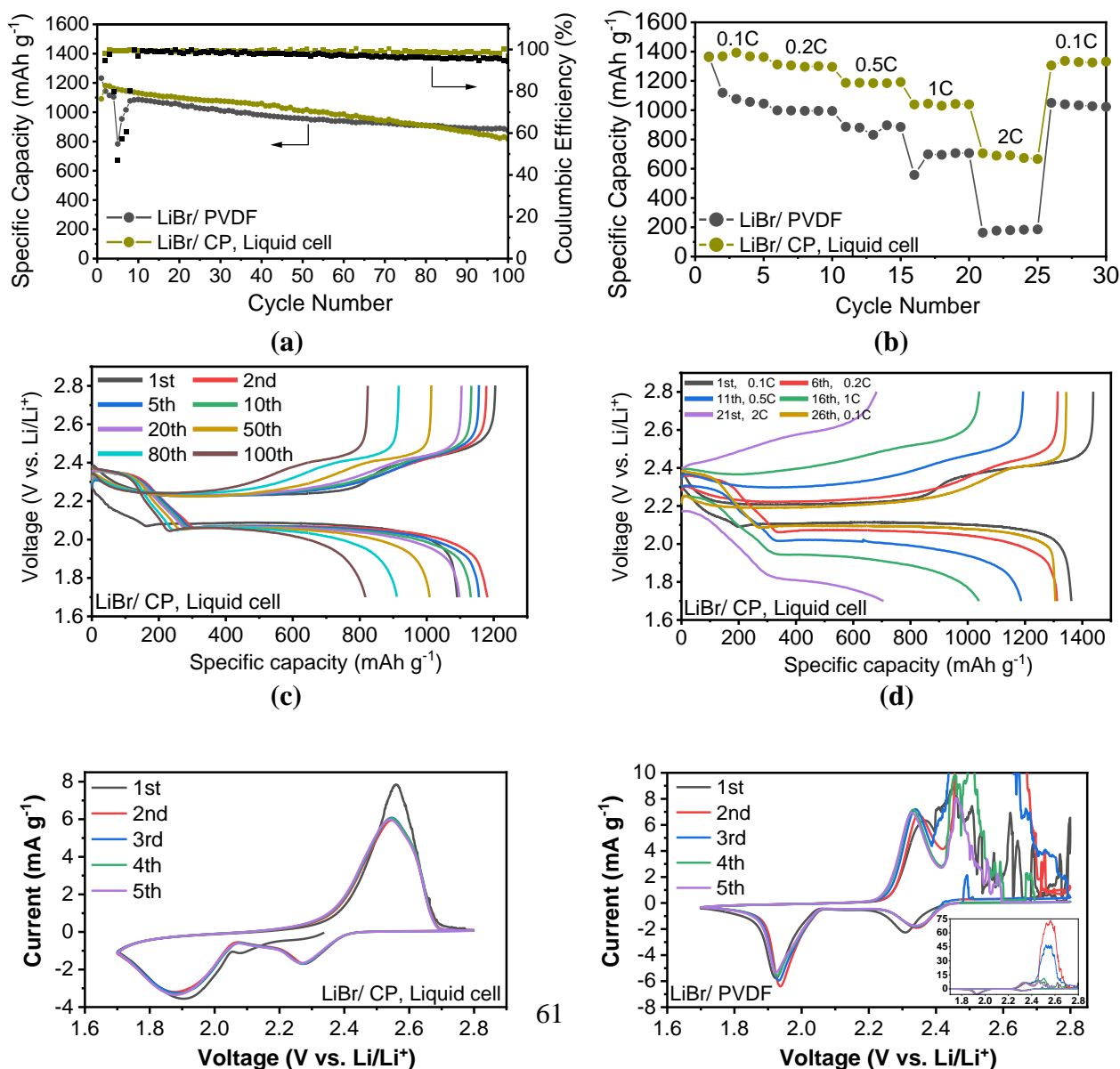
Confirmatory experimental results shown in **Figure 4-2** echoed one of the aforementioned statements. Three different E/S ratios were conducted based on conventional 1M LiTFSI+2wt%  $\text{LiNO}_3$  electrolyte and low sulfur loading ( $1.2\text{mg cm}^{-2}$ ). It was clearly observed that the LSB with  $5\mu\text{L mg}^{-1}$  of E/S ratio could not even finish the 1<sup>st</sup> charge, and the charge curve was full of sudden rise and falls of voltage. After

increasing the E/S ratio to  $8 \mu\text{L mg}^{-1}$ , the battery was able to behave normally for 3 cycles, but followed by an unusual discharge curve in 4<sup>th</sup> charge. The joint between first and second plateau in the 4<sup>th</sup> discharge curve, also called the saturation point, was uncommonly small down to almost 1.7V. This abnormality indirectly suggested the high concentration of polysulfides in the electrolyte since they got more easily to be reduced and form  $\text{Li}_2\text{S}_2/\text{Li}_2\text{S}$  on the cathode even during the first plateau. Starting from 11<sup>th</sup> cycle, the overcharge problem occurred frequently. As for the battery with  $12 \mu\text{L mg}^{-1}$  of E/S ratio, it had been running smoothly throughout the cycling test without overcharge. To conclude, this series of experiments justified that the Li-S cell would seriously suffer from the problem of charge failure under low E/S ratio based on conventional battery configuration. Nevertheless, for LSBs using LiBr electrolyte, neither did I use lean electrolyte condition (E/S ratio =  $20 \mu\text{L mg}^{-1}$ ) nor did I adopt sulfur cathode with high areal sulfur loading ( $1.2 \text{ mg cm}^{-2}$ ). Two possible reasons discussed above could not explain why overcharge problem occurred in LiBr batteries.

#### *4.3.1.3 Identification of the origin of problems on the cathode*

At the time when the troubleshooting work seemed to enter a dead end, I started looking back to the research paper from which my project was inspired. In the paper<sup>77</sup> that the LiBr was firstly adopted as the promising lithium salt for LSBs, the research team utilized the form of Li-Polysulfide liquid cell with carbon paper or freestanding CNT electrode as positive electrode and polysulfide-containing electrolyte, which means the slurry coating process was skipped, and no binder was involved. After going through this traceback, an assumption was come up that the problem of overcharge and current surge had nothing to do with the anode side. If these problems were caused by severe dendritic lithium growth or degradation of lithium metal, etc., they would happen no matter which type of battery were adopted. Apparently, those problems did not occur in the paper mentioned earlier in this paragraph. Some verification experiments were again conducted as shown in **Figure 4-3**. LiBr/ PVDF represents the conventional Li-S battery

that the sulfur cathode was obtained by traditional slurry casting on the Al current collector. LiBr/ CP represents the liquid Li-S cell with carbon paper and polysulfide-containing electrolyte. According to the green curve in **Figure 4-3 (a)** and **Figure 4-3 (b)**, no sudden drop of discharge capacity occurred during 0.2C cycling and rate performance test. **Figure 4-3 (c)** and **Figure 4-3 (d)** also exhibited no voltage fluctuations and long overcharge plateau throughout the tests. Stark contrast appeared from the CV graph in **Figure 4-3 (e)** and **Figure 4-3 (f)**. Liquid cell displayed rather smooth CV curves in **Figure 4-3 (e)** with no current surge, while the conventional Li-S battery showed serious current soar during reduction scan at the moment when the voltage got to 2.4V~2.5V and the current density reached 4 mA g<sup>-1</sup>~6 mA g<sup>-1</sup>.



(e)

(f)

**Figure 4-3. Comparison of conventional Li-S cell and Li-Polysulfide liquid cell.** (a) 0.2C galvanostatic cycling. (b) Rate performance test. (c, d) Voltage profile of Li-Polysulfide liquid cell from 0.2C cycling and rate performance. (e, f) CV scan results. The electrolyte composition for conventional Li-S cell includes 1M LiBr+2wt% LiNO<sub>3</sub> in DOL/DME (v/v=1:1), while the catholyte composition for Li-Polysulfide liquid cell 1M LiBr+0.3M LiNO<sub>3</sub>+0.3MLi<sub>2</sub>S<sub>6</sub> in DOL/DME (v/v=1:1). The scan rate for CV was 0.2mV/s.

By doing this series of confirmatory experiments, it is safe to conclude that the overcharge and current surge problem occurring in the conventional Li-S cell had nothing to do with the lithium anode. Now that the lithium metal anode side was ruled out, the attention should be turned to the sulfur cathode side. Continuing from the last paragraph about the research team<sup>77</sup> that firstly utilized LiBr as main lithium salt for LSBs, the reason of using liquid cell instead of conventional Li-S cells was that the growth pattern and morphological evolution of the Li<sub>2</sub>S could be observed and identified more clearly, which was very important for authors to explain why LiBr improved the cycling performance of LSBs. In this perspective, using liquid cell with polysulfide as staring active material was a very smart choice. Authors put emphasis of their research on proof-of-concept and mechanism exploration. But the form of Li-Polysulfide liquid cell was apparently not commensurate with present industrial protocols. Distributing active material through traditional preparation of slurry and subsequent casting on the current collector is still considered as a more feasible method and is widely employed industry-wise due to the maximized packing efficiency<sup>87</sup>. Besides, the use of carbon paper reduced the energy density by large thus it is impossible to adopt carbon paper as current collector in the industrial operation.

It is evident that the cathode structure between conventional Li-S cells and Li-Polysulfide liquid cells is very different. Since the slurry casting process is not necessary for liquid cell, there are no binders in its system. The first discharge process only had one lower plateau during galvanostatic cycling that marks “Li<sub>2</sub>S<sub>6</sub> → Li<sub>2</sub>S/ Li<sub>2</sub>S<sub>2</sub>”. Three-

dimensional carbon paper was used as positive electrode for providing polysulfides with reaction sites and the host for  $\text{Li}_2\text{S}$ /  $\text{Li}_2\text{S}_2$  deposition. This commercial carbon paper is made of carbon microfibers bound by adhesives with complicated manufacturing process. The most important indicator for the carbon paper is its strength and it has been widely utilized for high performance fuel cells as the gas diffusion layer <sup>113</sup>. During the electrochemical cycling of liquid Li-Polysulfide battery, it is impossible for the carbon paper to experience the problem of structural damage and collapse. On the contrary, the sulfur cathode that is prepared by conventional slurry casting on 2D Al current collector is known to be constantly bothered by the delamination and detachment of active material due to the dramatic volume change (~80%) in the course of cycling. This phenomenon was originated from enormous density difference between discharge products ( $\text{Li}_2\text{S}$ ) and elemental sulfur (**section 1.3.2**), which often results in the disruption of structural integrity like pulverization of nanocomposite cathode.

**Table 4-1.** A comparison of particle size of conductive agent and pore diameter of separator <sup>114, 115</sup>.

Item	Super P	Celgard 2500 Separator
Particle size/ Pore diameter (nm)	~ 40	200 - 300

At low sulfur loading ( $\sim 1.2 \text{ mg cm}^{-2}$ ) and limited cycle numbers, the structural problem might not be critical, and all the lithium salts other than LiBr showed smooth cycling as what had been discussed in **Chapter 3**. Only LiBr gave rise to the overcharge problem in some cycles and current surge problem during CV test at the low sulfur loading. It could be explained by the different growth trajectories <sup>77</sup> of  $\text{Li}_2\text{S}$  and its resulting particle size. Electrolyte with high Donor-Number anion increases the partial solubility of  $\text{Li}_2\text{S}$ , which induces the 3D growth of  $\text{Li}_2\text{S}$  particles instead of film-like  $\text{Li}_2\text{S}$  spread and thus delayed passivation of conductive network in the cathode structure. With more conducting carbon surface being exposed, the sulfur utilization increases very much and so does the discharge capacity. However, the direct consequence of 3D growth is to form the sizable aggregation (micrometer scale) of  $\text{Li}_2\text{S}$  particles that is more inclined

to squeeze the surrounding material, generating more stress/strain to impact the structural stability. Upon charging, even more remarkable volume shrinkage surpasses the adhesivity and buffer ability of the polymer network enabled by Van der Waals force among linear chains, finally leading to detachment or even pulverization of the cathode materials. What is worse, since the conductive agent during slurry making for LSBs is usually in nano scale such as Super P or Ketjen Black, it is hard to secure them on the 2D current collector. Plus, their particle size are much smaller than the pore size of separator (Celgard 2500) as indicated in **Table 4-1**, hence the chance exists for those detached conductive carbon nanoparticles to permeate through the separator and make contact with the negative electrode <sup>116</sup>, causing the short-circuiting and corresponding voltage fluctuations.

#### 4.3.2 Attempts to solve the cathode structural problem

After confirming that the LiBr battery failure is concerning with cathode side instead of anode side, changes needed to be made for the purpose of strengthening the structural stability. Binder plays a vital role in withstanding the detachment and pulverization of cathode materials by cushioning the stress/strain resulted from the volume change and retaining the structural cohesion among those nano-sized composites. PVDF polymer is the most widely used binder in the LSBs world. It does have some advantages such as wide electrochemical window, good thermal stability and satisfied adhesive ability <sup>46</sup>. However, it was reported that PVDF binder could dissolve <sup>117</sup> into the organic electrolyte or even react with polysulfides <sup>118</sup>, leading to continuous degeneration of cathode material and even collapse of cathode structure. Lacry et al. <sup>119</sup> specifically investigated the downsides with PVDF homopolymer to the porous sulfur cathode and appealed to the immediate substitution of PVDF binders for LSBs. In addition, PVDF binder falls short on other mechanical properties such as elasticity and stretchability.



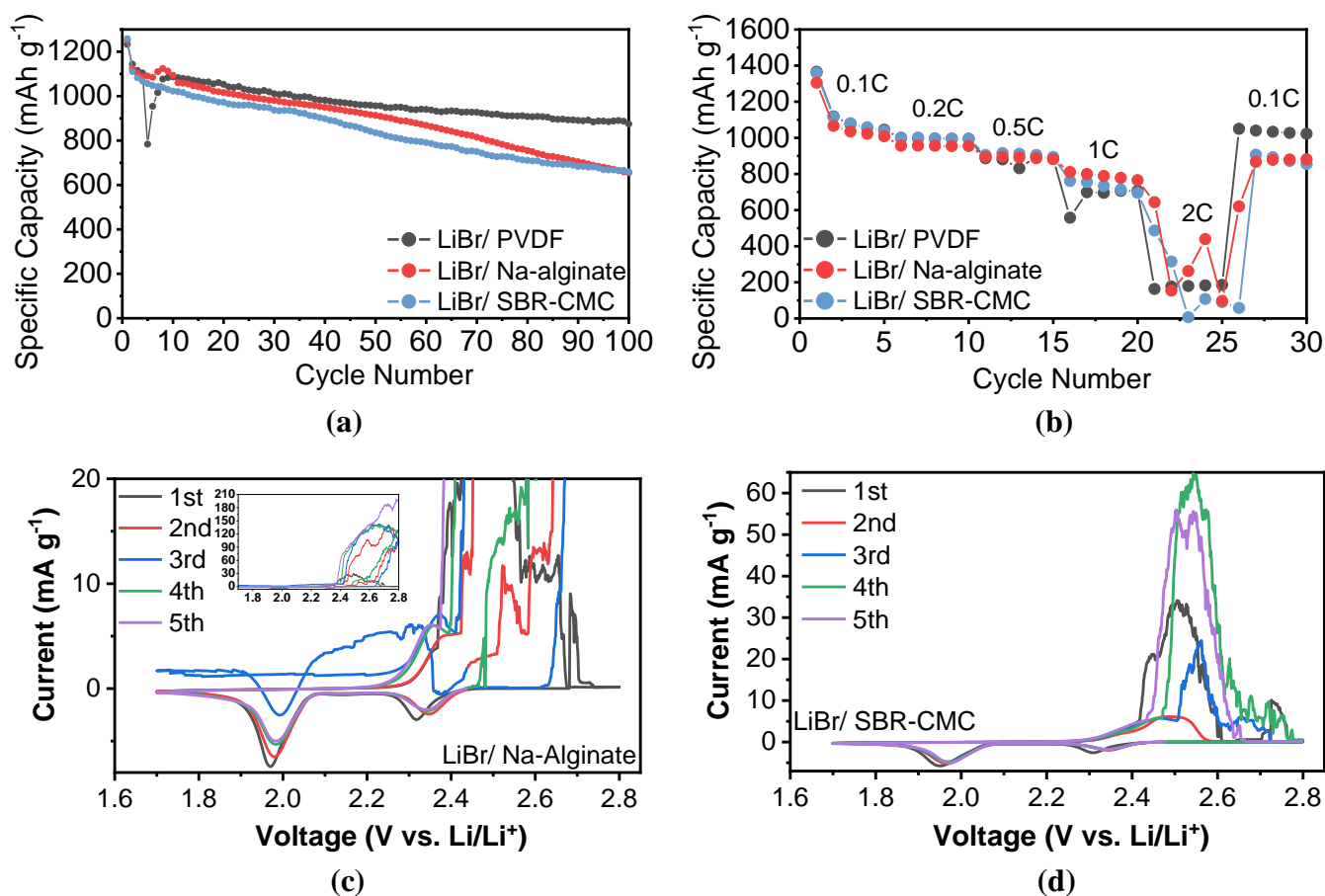


**Figure 4-4. Comparison of conventional Li-S cells using LiBr electrolyte and PVDF/Na-alginate/SBR-CMC binder.** (a) 0.2C galvanostatic cycling. (b) rate performance test. (c, d) CV scan results. The electrolyte composition includes 1M LiBr+2wt% LiNO<sub>3</sub> in DOL/DME (v/v=1:1). The scan rate for CV was 0.2mV/s.

Two other different binders with better mechanical strength were adopted to replace the PVDF in order to address the structural issues brought by LiBr electrolyte. Na-alginate is considered to have higher adhesive ability than PVDF polymer. Polar groups in the Na-alginate increase the surface electronegativity and contribute to the stronger adhesivity by boosting physical interactions amid S/C nanocomposites, binders and current collectors<sup>120</sup>. Na-alginate had been previously demonstrated to function better in sulfur cathodes and other types of electrode. It not only provided better buffer ability to the sulfur cathode<sup>121</sup> than PVDF binder after 50 cycles but also enhanced the electrochemical cycling stability. For other electrodes, it immensely improved the

structural integrity and electronic conductivity of CuO electrode <sup>122</sup>, and it also realized more stable electrochemical performance of graphite and silicon anode <sup>123</sup>. For the SBR-CMC binder, as the name suggests, is made of two water-soluble polymers. Carboxymethyl cellulose (CMC) was commonly adopted as the sole binder for LIBs. But it is not favorable to be applied in the LSBs because of its poor elastic strength. After combining with styrene-butadiene rubber (SBR), the binary binder system could afford a more stable sulfur cathode in mechanical property. The introduction of SBR as plasticizing agent brings the ductility to improve the structural robustness of the cathode and to maintain the intact 3D conductive structure <sup>46</sup> during cycling of LSBs. The function of CMC polymer in the binder system is to promise uniform dispersion of S/C nanocomposites <sup>124</sup> on the cathode so that the ionic and electronic resistance could be reduced.

After the replacement of PVDF binder, corresponding batteries were cycled in the tester and scanned by CV as shown in **Figure 4-4**. Both LiBr batteries with SA and SBR-CMC binder were not subject to the charge failure problem and the cycling was smooth at 0.2C (**Figure 4-4a**), which indicates these two binders had some positive effects in relieving the stress caused by the giant Li<sub>2</sub>S particles and preventing structural collapse to happen. This improvement was also reflected in the rate performance before 2C with no overcharging occurring in **Figure 4-4b**. However, two batteries started to undergo severe charge failure problem and fluctuation of voltage after switching to 2C, which was also accompanied by the extremely low discharge capacity with only minimum 154.1 mAh g<sup>-1</sup> (25<sup>th</sup>) for battery using SA binder and 7 mAh g<sup>-1</sup> (23<sup>rd</sup>) for battery using SBR-CMC. In addition, two batteries presented similar current surge in the CV graph as per **Figure 4-4d, e**. When the reduction scan reached around 2.4~2.5V accompanied by larger current density, the curve suddenly became out of control and began skyrocketing. Battery with SBR-CMC demonstrated more hopeful curve than PVDF and SA binder since the 1<sup>st</sup> CV cycle did not show such a current surge, which illustrated

the binder with higher elasticity works better, but with limited effects, in retaining the structure stability of sulfur cathode during the CV test. To sum up, it has been justified that binder change is a right direction and an effective strategy for solving the problem induced by LiBr electrolyte. Replacing PVDF to other binders with better mechanical properties is somewhat beneficial to address the overcharge problem during 0.2C cycling, but it was realized at the cost of worse cycling stability, which was undesired. Moreover, SA and SBR-CMC binder are incapable of fundamentally avoiding the damage of the sulfur cathode under LiBr electrolyte when the current density running through the cell became larger. The journey to seek more appropriate binder to couple with LiBr electrolyte was still ongoing, and adhesion and elasticity of the binder might be the focus of consideration.

#### 4.3.3 The solution to the structural problem of sulfur cathode

As discussed above, SA polymer has higher adhesive ability than PVDF, and SBR-CMC possesses decent stretchability. But apparently, they all failed to satisfy the requirement of sustaining the structural distortion originated from the LiBr electrolyte. It is worth mentioning that all the three above-mentioned binders are linear chain polymers. The fixation of cathode material onto current collector and close contact among S/C nanocomposites are realized through the polymer network that is enabled by the intertwining of macromolecule chains<sup>125</sup> and the existence of van der Waals forces among those chains. This molecular force is considered too weak to endow the binder enough adhesion and elasticity to maintain the stability of cathode structure given the nano-scale particles. The strongest molecular interaction is the covalent bonding, which elicited the next attempt for solving the overcharge problem of LiBr battery.

Polymer binder formed by in situ crosslinking reaction was introduced to LSBs mainly for the sulfur cathode with a high areal loading ( $>5 \text{ mg cm}^{-2}$ ) of active material, which is one of the basic requirements for the practical application of LSBs. High sulfur content in the cathode material and thick electrode are two typical strategies for

achieving the cathode with high sulfur loading, in which some common problems occur frequently. Firstly, the conductivity of the cathode might decrease due to the increased mass ratio of insulating sulfur to conductive additive, which demands more homogeneous dispersion of cathode material and more compact cathode structure. Furthermore, the weak adhesive ability enabled by linear polymer for binding as mentioned in the last paragraph aggravates the cracking and delamination problem during the preparation of thick cathodes and subsequent electrochemical cycling. The introduction of crosslinked polymer binder is a precise response to those challenges. The excellent structural robustness of cathode is ensured by the crosslinked macromolecule network with the strongest covalent bonding among polymer chains <sup>126</sup>. The stress and strain of the sulfur cathode could be efficiently accommodated by this type of reticular structure. The use of binder with crosslinked structure had been reported in several papers such as the polyacrylamide <sup>126</sup>, polymer formed through esterification <sup>49</sup> between CMC (-OH) and citric acid (-COOH) as well as the in situ-formed polymer by crosslinking reaction between Polyethylenimine (PEI) and Araldite 506 epoxy resin <sup>125</sup>. Considering the importance of adhesion and ductility on constructing the sulfur cathode, it is natural to think about replacing the PVDF binder with crosslinked polymer.

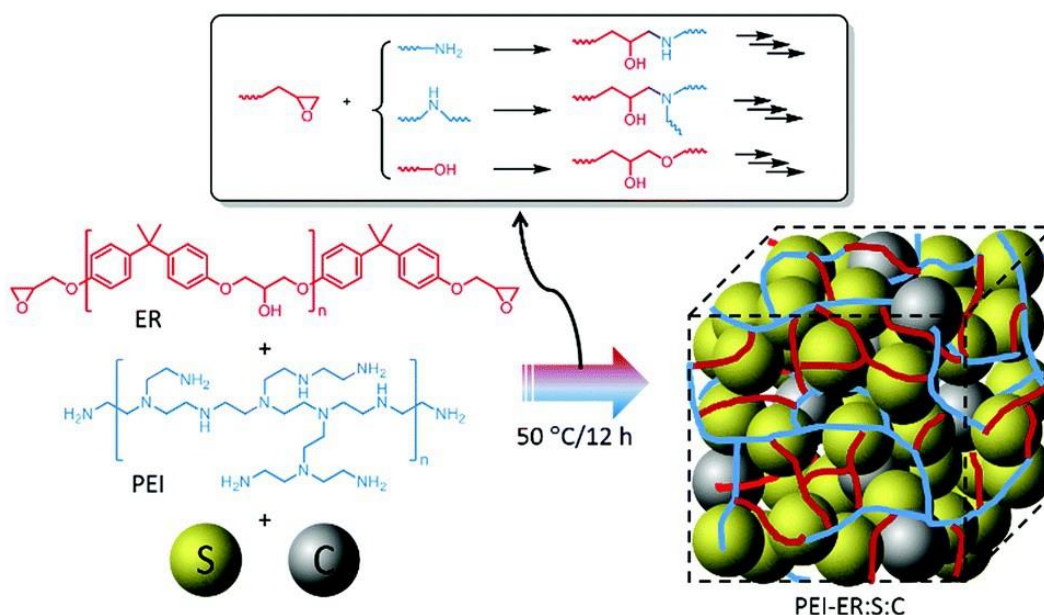


**Figure 4-5. Schematics of in situ step-growth polymerization of polyethylenimine (PEI) and Araldite 506 epoxy resin (ER) in the presence of sulfur (S) and conductive carbon black (C) to form a PEI-ER:S:C cathode composite material. S and C particles are tightly held by the cross-linked 3D PEI-506 network <sup>125</sup>. Reproduced from reference 125.**

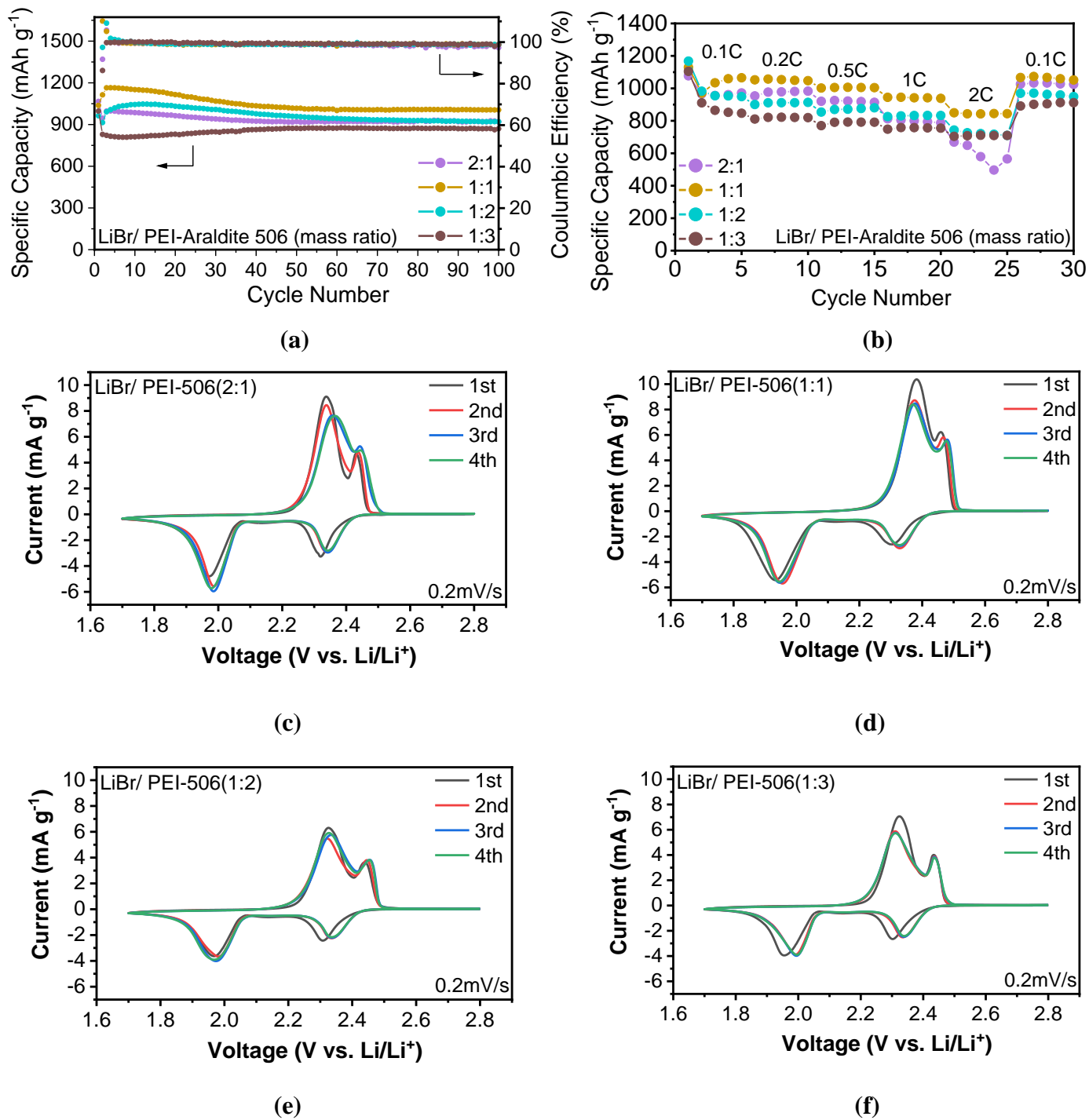


**Figure 4-6. Comparison of conventional Li-S batteries using LiBr electrolyte and crosslinked binders with different mass ratios of PEI to Araldite 506.** (a) 0.2C galvanostatic cycling. (b) rate performance. (c-f) CV scan results. The electrolyte composition includes 1M LiBr+2wt% LiN<sub>3</sub>O<sub>3</sub> in DOL/DME (v/v=1:1). (a) 0.2C cycling performance. (b) Rate performance. (c-f) Cyclic voltammogram at the scan rate of 0.2 mV s<sup>-1</sup>.

The first crosslinked polymer that appeared in my mind is the in situ-formed epoxy resin through curing between PEI and Araldite 506 (**Figure 4-5**) that was developed<sup>125</sup> in our group previously. The net structure linked by chemically covalent bonds was forming in the sulfur cathode during the drying process. After changing the binder to PEI-Araldite 506, 0.2C galvanostatic cycling, rate performance test and CV were adopted to examine if the overcharge and current surge problem were solved. A total of four mass ratios were tried for LSBs combined with LiBr electrolyte. Different mass ratios represent different degree of crosslinking and thus different mechanical properties. According to the experimental results shown in **Figure 4-6a**, all four batteries enabled smooth 0.2C cycling with no sudden capacity drop and occurrence of overcharge after the binder substitution. Likewise, when it comes to harsher conditions such as higher c-rate charge and higher current density during reduction scan of CV, those problems still vanished. No charge failure and fluctuations of charging voltage were observed during rate capability test (**Figure 4-6b**) for LiBr/ PEI-506 batteries. “Uncluttered” CV curves were obtained for the LiBr/ PEI-506 batteries with no current surge occurring throughout the test (**Figure 4-6c-f**). This series of successful experiments corroborated the assumption that the malfunction of cathode resulted in the overcharge and current surge problems. The large agglomeration of Li<sub>2</sub>S particles creates more stress and strain in the cathode that harmfully influenced the structural integrity and aggravates the delamination/ pulverization problems. Substituting the binder with stronger and more outstanding mechanical strength such as adhesion and stretchability could effectively maintain the structural integrity. More importantly, it could also prevent the detachment/ pulverization of the cathode material and thus avoid the possible contact of conductive agent to the opposite electrode during charging process.

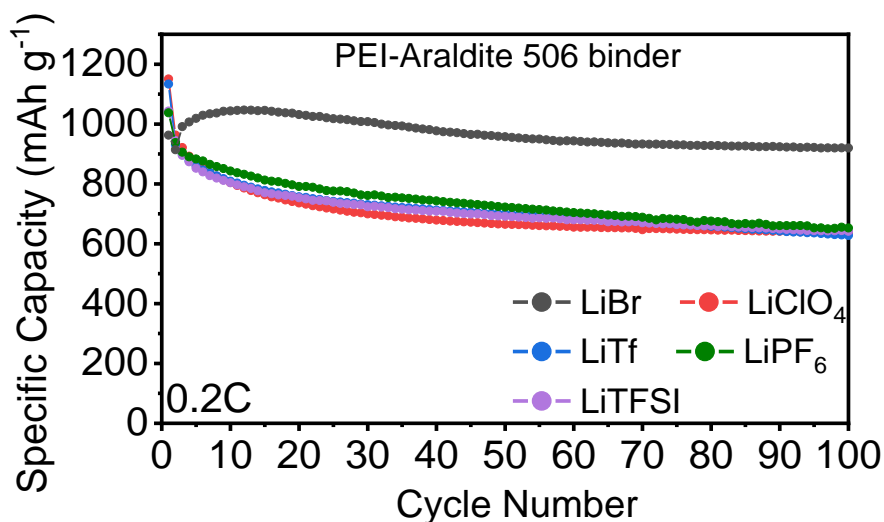


**Figure 4-7.** Comparison of conventional Li-S batteries using PEI-Araldite 506 binder with different lithium electrolyte salts during 0.2C. The electrolyte composition includes 1M LiX+2wt% LiNO<sub>3</sub> in DOL/DME (v/v=1:1).

After confirming the positive effects of PEI-Araldite 506 binder on the above-mentioned problems during cycling and measurement of LiBr batteries, other lithium salts investigated before in **Chapter 3** were tried again with this crosslinked binder in order to compare their long term performance at the absence of interference brought by the overcharge problem. The results further validated the superiority of LiBr salt in long term cycling performance as demonstrated in **Figure 4-7**. LiBr battery still had the No.1 0.2C cycling stability within 100 cycles, largely outperforming that other lithium salts. The rest of batteries with four different lithium salts manifested similar trend of decay as the cycling proceeded. The substitution of the binder from PVDF to PEI-Araldite 506 did not affect the conclusion. Once again, the enormous potential of LiBr to the Li-S battery field was further substantiated by this experiment.

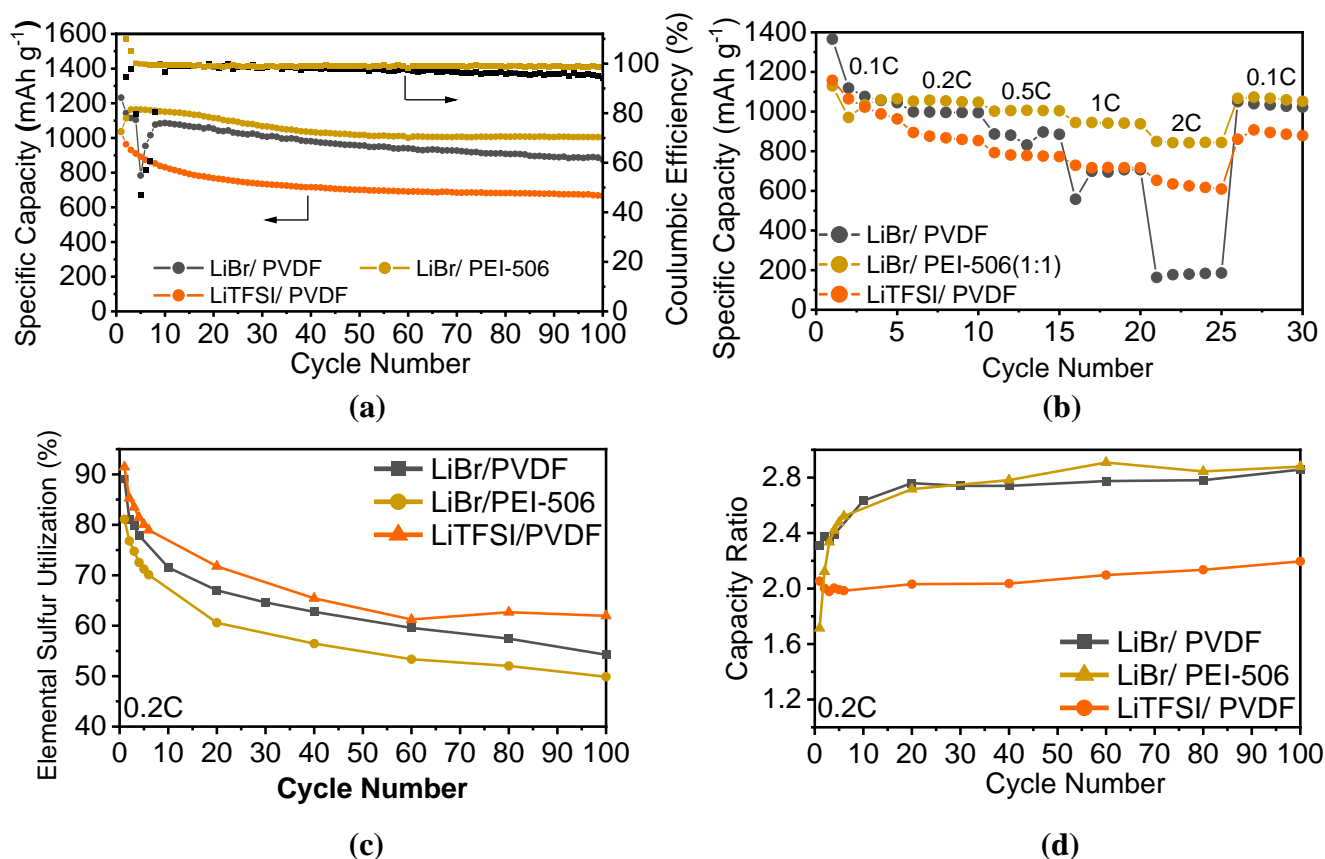


**Figure 4-8. Comparison of conventional Li-S batteries using LiBr electrolyte and PVDF binder/PEI-Araldite 506 binder during (a) 0.2C galvanostatic cycling and (b) rate performance test. (c) Elemental sulfur utilization and (d) capacity (plateau) ratio under three different combinations. The electrolyte composition includes 1M LiBr/ LiTFSI+2wt%  $\text{LiNO}_3$  in DOL/DME (v/v=1:1).**

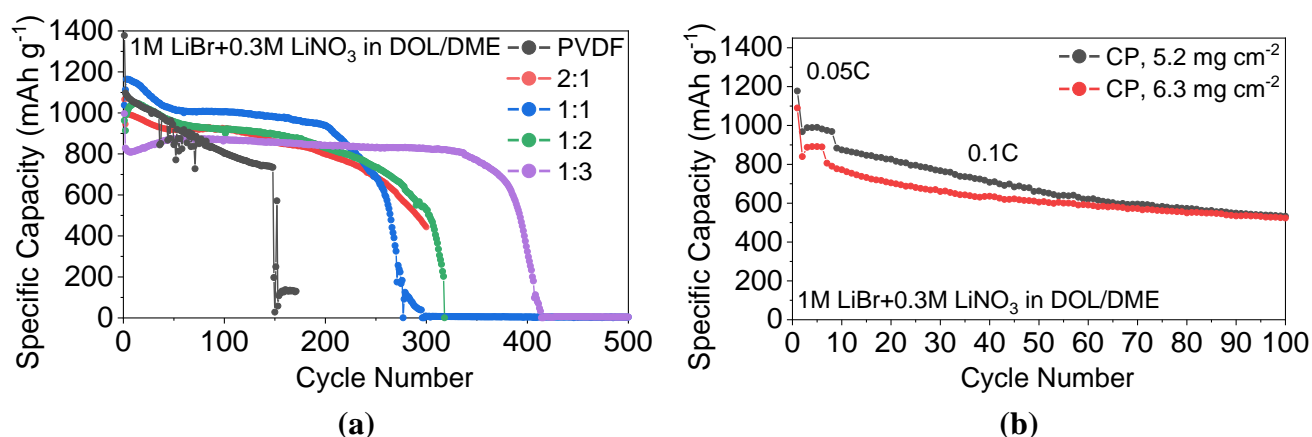


**Figure 4-9. (a) Comparison of 0.2C cycle performance of LSBs using LiBr electrolyte with PVDF binder and PEI-506 binder (different mass ratios) at extended cycles. Batteries were kept cycling until being subject to a sharp decline of capacity, which were considered as “dead”. (b) 0.1C cycle**



**performance of LSBs using LiBr electrolyte with higher sulfur loading based on carbon paper.** First several cycles were for activation at 0.05C.

It is worth mentioning that the solution to the overcharge problem could not be based on compromising electrochemical performance of LiBr battery. The original intention of using LiBr is to take advantage and accomplish high sulfur utilization and hence discharge capacity. Herein, the LiBr/ PEI-506 with best electrochemical performance was selected to compare with the LiBr/ PVDF battery. Only if the overcharge and current surge problem were addressed together with stability being improved was the binder change meaningful. As observed in **Figure 4-8a**, the cycling stability was boosted compared to the LiBr/ PVDF battery. The capacity retention for LiBr/ PVDF was only 70.9%, whereas the LiBr/PEI-506 battery exhibited 86.3% of retention. Surprisingly, sharper contrast was manifest during rate performance test in **Figure 4-8b**. LiBr/PEI-506 battery showed remarkable enhancement, particularly under higher c-rate (such as 0.5C, 1C and 2C). LiBr/ PVDF battery could only achieve 180 mAh g<sup>-1</sup> for discharge capacity under 2C, while 850 mAh g<sup>-1</sup> was realized for LiBr/ PEI-506 battery. The orange curve represented the performance of LSB with the common combination of lithium salt (LiTFSI) and binder (PVDF) as a reference. The yellow curve in **Figure 4-8d** suggested that PEI-506 binder did not compromise the advantage of LiBr electrolyte to extend the second plateau because the capacity ratio rapidly increased to around 2.9 within 20 cycles. **Figure 4-8c** decoupled the capacity from first plateau of each discharge, revealing the main reason for the capacity decay. Given that the capacity ratio kept increasing, it was apparent the decay of capacity from first plateau played dominant role in the overall capacity fading. Another advantage of using PEI-506 crosslinked binder is that it could elongate the cycle life of LiBr battery. **Figure 4-9a** compared the maximum cycles that LiBr-based LSBs could sustain using PVDF binder and PEI-506 binder (different mass ratios). Different mass ratios represented different crosslinking density and hence different mechanical properties. All the four mass ratios of PEI and Araldite 506 showed prolonged maximum cycles. Finally, in **Figure 4-9b**,

Li-S battery with thick cathodes were cycled using LiBr electrolyte and PEI-506 binder. There were still no voltage fluctuations occurring during the cycling with 63wt% of sulfur in the cathode material and  $6.3 \text{ mg cm}^{-2}$  sulfur loading. Decent cycling performance was obtained, and more refining work needs to be done.

#### 4.4 Conclusion

In the field of LSBs, it is reasonable that a new technological breakthrough starts with Li-Polysulfide liquid cell for proof-of-concept, but its successful application should not be limited to this form of cell. Moreover, the conventional Li-S cell should be employed to further examine the feasibility of this breakthrough as explained in **section 3.1 and 4.3.1.3**. For this type of sulfur cathode, the use of LiBr salt provided great promise but also brought some problems as laid out in **section 4.1**. The root of those problems was speculated to be structural damage of cathode that led to detachment of nanosized carbon particles. Those detached nanosized conductive particles might penetrate through the pores of separator and make contact with the negative electrode, causing sudden short-circuit and thus voltage fluctuations during cycling and current surge during CV test. Larger stress/ strain in the cathode generated by 3D colossal  $\text{Li}_2\text{S}$  particles should exacerbate the structural collapse. After the preliminary confirmation, this problem was successfully solved by replacing the linear-chain PVDF binder with crosslinked PEI-Araldite 506 binder. Linked by covalent bonds, the crosslinked network structure could accommodate the volume change of the cathode under LiBr electrolyte. Overcharge and current surge problems did not occur during 0.2C cycling, rate performance test and CV test. Besides, LiBr/PEI-506 battery gave 86.3% of retention after 100 cycles at 0.2C without compromising the inherently high capacity ratio enabled by LiBr electrolyte. For rate capability, LiBr/PEI-506 battery still showed effective discharge even at 2C with very high  $850 \text{ mAh g}^{-1}$ , and the cycle life increases a lot after replacing the PVDF binder with PEI-506 binder as shown in **Figure 4-9a**. Finally, with 63 wt% of sulfur in

the cathode material and  $6.3 \text{ mg cm}^{-2}$  of sulfur loading, the thick sulfur cathode using LiBr/PEI-506 combination was cycled and assessed.

## Chapter 5. Summary and Future Directions

The work presented in this thesis focused on lithium salt in the electrolyte and LiBr-based battery failure investigation. Researches about lithium salts of LSBs are usually neglected due to the dominant role of LiTFSI. The future successful mass production of LSBs must be the collective effects of comprehensive approaches on different components. The function of lithium salt had already been gradually developed including stabilization of interface on both electrodes and controllable  $\text{Li}_2\text{S}$  deposition on the cathode etc.

The first project as discussed in **Chapter 3** evaluated the impact of five lithium salts on the electrochemical performance of LSBs. Long-term cycling performance, rate capability, voltage barrier, compatibility with lithium anode, self-discharge behavior etc. were assessed and ranked for five different lithium salts to give a clearer picture about the characteristics of five lithium salts used in LSBs. LiBr salt was selected with great promise and potential for further studies.

For the second project of this thesis, possible mechanism and reasons of LiBr-based battery failure was explored, and a solution was provided for a common challenge accompanied with the development of LSBs. In order to increase sulfur utilization and discharge capacity (specific energy density), it is highly promising to adopt 3D- $\text{Li}_2\text{S}$ -growth-induced strategies, but ensuing problems that appear simultaneously along with this beneficial deposition pattern should be researched and fixed. Finally, a baseline research scenario for future LiBr-based optimization work in LSBs was established, which is using the crosslinked polymer for the slurry casting process. The significance of this study is to make the strategy of inducing 3D growth of  $\text{Li}_2\text{S}$  one step further to practical application. Similar strategies<sup>26, 70</sup> have been done before to induce 3D growth of  $\text{Li}_2\text{S}$ . But they were all carried out in Li-Polysulfide liquid cell using carbon paper as cathode, which is not applicable in the lithium battery industry (**section 3.1**). In this

work, the scope of application of this effective strategy was extended, making it closer to the practical application.

In the future, the actual collapse/ damage or detachment of the cathode was not visually observed as direct evidence, which should be done next. Quantitative analysis for mechanical properties of polymer binders should be conducted to get a clearer understanding about the impact of binder elasticity and adhesion on the structural stability of the cathode. Besides, initial capacity of the LiBr/PEI-506 scenario is not very high, which is worth digging deeper on how to improve it. The most important aspect is about the compatibility of LiBr electrolyte with lithium anode, e.g. the fluorinated solvent might be a good substitution. For LiBr-based LSBs, the capacity decay of first plateau ( $\sim 2.4\text{V}$ ) is mainly responsible for the overall capacity fading as discussed in **section 4.3.3**, which should be paid attention on how to maintain the elemental sulfur utilization. Finally, long-term cycling performance for high sulfur loading cathodes with LiBr electrolyte needs to be improved, and the degradation of lithium anode might be the key reason.

## Bibliography

1. Tarascon, J.-M.; Armand, M., Issues and challenges facing rechargeable lithium batteries. In *Materials for sustainable energy: a collection of peer-reviewed research and review articles from Nature Publishing Group*, World Scientific: 2011; pp 171-179.
2. Whittingham, M. S. *Science* **1976**, 192, (4244), 1126-1127.
3. Armand, M.; Touzain, P. *Materials Science and Engineering* **1977**, 31, 319-329.
4. Mizushima, K.; Jones, P.; Wiseman, P.; Goodenough, J. B. *Materials Research Bulletin* **1980**, 15, (6), 783-789.
5. Yamabe, T.; Tanaka, K.; Ohzeki, K.; Yata, S. *Solid state communications* **1982**, 44, (6), 823-825.
6. Meng, Y. S.; Arroyo-de Dompablo, M. E. *Energy Environ. Sci.* **2009**, 2, (6), 589-609.
7. Nitta, N.; Wu, F.; Lee, J. T.; Yushin, G. *Materials today* **2015**, 18, (5), 252-264.
8. Adelhelm, P.; Hartmann, P.; Bender, C. L.; Busche, M.; Eufinger, C.; Janek, J. *Beilstein journal of nanotechnology* **2015**, 6, (1), 1016-1055.
9. Danuta, H.; Juliusz, U.; Herbert, D.; Ulam, J. *US Pat* **1962**, 3043896.
10. Peled, E.; Sternberg, Y.; Gorenshtein, A.; Lavi, Y. *Journal of the Electrochemical Society* **1989**, 136, (6), 1621.
11. Manthiram, A.; Fu, Y.; Chung, S.-H.; Zu, C.; Su, Y.-S. *Chemical reviews* **2014**, 114, (23), 11751-11787.
12. Cuisinier, M.; Hart, C.; Balasubramanian, M.; Garsuch, A.; Nazar, L. F. *Adv. Energy Mater.* **2015**, 5, (16), 1401801.
13. Cuisinier, M.; Cabelguen, P.-E.; Evers, S.; He, G.; Kolbeck, M.; Garsuch, A.; Bolin, T.; Balasubramanian, M.; Nazar, L. F. *The Journal of Physical Chemistry Letters* **2013**, 4, (19), 3227-3232.
14. Liang, X.; Hart, C.; Pang, Q.; Garsuch, A.; Weiss, T.; Nazar, L. F. *Nature communications* **2015**, 6, (1), 1-8.
15. Chen, W.; Qian, T.; Xiong, J.; Xu, N.; Liu, X.; Liu, J.; Zhou, J.; Shen, X.; Yang, T.; Chen, Y. *Advanced materials* **2017**, 29, (12), 1605160.
16. Zhao, M.; Li, B.-Q.; Zhang, X.-Q.; Huang, J.-Q.; Zhang, Q. *ACS Central Science* **2020**, 6, (7), 1095-1104.
17. Dean, J. A., *Lange's handbook of chemistry*. McGraw-Hill New York: 1992; Vol. 15.
18. Ji, X.; Lee, K. T.; Nazar, L. F. *Nature Materials* **2009**, 8, (6), 500-506.
19. Xu, R.; Belharouak, I.; Zhang, X.; Chamoun, R.; Yu, C.; Ren, Y.; Nie, A.; Shahbazian-Yassar, R.; Lu, J.; Li, J. C. M.; Amine, K. *ACS Applied Materials & Interfaces* **2014**, 6, (24), 21938-21945.
20. Zheng, J.; Lv, D.; Gu, M.; Wang, C.; Zhang, J.-G.; Liu, J.; Xiao, J. *Journal of the Electrochemical Society* **2013**, 160, (11), A2288.
21. Hagen, M.; Hanselmann, D.; Ahlbrecht, K.; Maça, R.; Gerber, D.; Tübke, J. *Adv. Energy Mater.* **2015**, 5, (16), 1401986.
22. Mikhaylik, Y. V.; Kovalev, I.; Schock, R.; Kumaresan, K.; Xu, J.; Affinito, J. *Ecs Transactions* **2010**, 25, (35), 23.
23. Barchasz, C.; Leprêtre, J.-C.; Patoux, S.; Alloin, F. *Electrochimica Acta* **2013**, 89, 737-743.

24. Carbone, L.; Gobet, M.; Peng, J.; Devany, M.; Scrosati, B.; Greenbaum, S.; Hassoun, J. *ACS applied materials & interfaces* **2015**, 7, (25), 13859-13865.
25. Aurbach, D. *J. Power Sources* **2000**, 89, (2), 206-218.
26. Zhang, G.; Peng, H.-J.; Zhao, C.-Z.; Chen, X.; Zhao, L.-D.; Li, P.; Huang, J.-Q.; Zhang, Q. *Angewandte Chemie International Edition* **2018**, 57, (51), 16732-16736.
27. Gupta, A.; Bhargava, A.; Manthiram, A. *Adv. Energy Mater.* **2019**, 9, (6), 1803096.
28. Cheng, Q.; Xu, W.; Qin, S.; Das, S.; Jin, T.; Li, A.; Li, A. C.; Qie, B.; Yao, P.; Zhai, H. *Angewandte Chemie International Edition* **2019**, 58, (17), 5557-5561.
29. Sun, K.; Wu, Q.; Tong, X.; Gan, H. *ACS Applied Energy Materials* **2018**, 1, (6), 2608-2618.
30. Qu, C.; Chen, Y.; Yang, X.; Zhang, H.; Li, X.; Zhang, H. *Nano Energy* **2017**, 39, 262-272.
31. Wang, L.; Ye, Y.; Chen, N.; Huang, Y.; Li, L.; Wu, F.; Chen, R. *Advanced functional materials* **2018**, 28, (38), 1800919.
32. Azimi, N.; Weng, W.; Takoudis, C.; Zhang, Z. *Electrochemistry communications* **2013**, 37, 96-99.
33. Shin, W.; Zhu, L.; Jiang, H.; Stickle, W. F.; Fang, C.; Liu, C.; Lu, J.; Ji, X. *Materials Today* **2020**.
34. Xu, K. *Chemical reviews* **2004**, 104, (10), 4303-4418.
35. Xiao, Y.; Han, B.; Zeng, Y.; Chi, S. S.; Zeng, X.; Zheng, Z.; Xu, K.; Deng, Y. *Adv. Energy Mater.* **2020**, 10, (14), 1903937.
36. Ma, Q.; Tong, B.; Fang, Z.; Qi, X.; Feng, W.; Nie, J.; Hu, Y.-S.; Li, H.; Huang, X.; Chen, L. *Journal of The Electrochemical Society* **2016**, 163, (8), A1776.
37. Suo, L.; Hu, Y.-S.; Li, H.; Armand, M.; Chen, L. *Nature communications* **2013**, 4, (1), 1-9.
38. Pang, Q.; Shyamsunder, A.; Narayanan, B.; Kwok, C. Y.; Curtiss, L. A.; Nazar, L. F. *Nature Energy* **2018**, 3, (9), 783-791.
39. Wu, F.; Chu, F.; Ferrero, G. A.; Sevilla, M.; Fuertes, A. B.; Borodin, O.; Yu, Y.; Yushin, G. *Nano Letters* **2020**.
40. Zhang, H.; Eshetu, G. G.; Judez, X.; Li, C.; Rodriguez-Martínez, L. M.; Armand, M. *Angewandte Chemie International Edition* **2018**, 57, (46), 15002-15027.
41. Aurbach, D.; Pollak, E.; Elazari, R.; Salitra, G.; Kelley, C. S.; Affinito, J. *Journal of the Electrochemical Society* **2009**, 156, (8), A694.
42. Zhang, S. S. *Journal of The Electrochemical Society* **2012**, 159, (7), A920.
43. Adams, B. D.; Carino, E. V.; Connell, J. G.; Han, K. S.; Cao, R.; Chen, J.; Zheng, J.; Li, Q.; Mueller, K. T.; Henderson, W. A.; Zhang, J.-G. *Nano Energy* **2017**, 40, 607-617.
44. Li, W.; Yao, H.; Yan, K.; Zheng, G.; Liang, Z.; Chiang, Y.-M.; Cui, Y. *Nature communications* **2015**, 6, (1), 1-8.
45. Wu, F.; Lee, J. T.; Nitta, N.; Kim, H.; Borodin, O.; Yushin, G. *Advanced Materials* **2015**, 27, (1), 101-108.
46. Yuan, H.; Huang, J. Q.; Peng, H. J.; Titirici, M. M.; Xiang, R.; Chen, R.; Liu, Q.; Zhang, Q. *Adv. Energy Mater.* **2018**, 8, (31), 1802107.
47. Kim, H. M.; Hwang, J.-Y.; Aurbach, D.; Sun, Y.-K. *The journal of physical chemistry letters* **2017**, 8, (21), 5331-5337.
48. Guo, J.; Wang, C. *Chemical communications* **2010**, 46, (9), 1428-1430.

49. Pang, Q.; Liang, X.; Kwok, C. Y.; Kulisch, J.; Nazar, L. F. *Adv. Energy Mater.* **2017**, 7, (6), 9.
50. Liu, J.; Li, R.; Chen, T.; Wan, W.; Wei, J.; Dai, C. *Journal of The Electrochemical Society* **2018**, 165, (3), A557.
51. Pan, J.; Xu, G.; Ding, B.; Chang, Z.; Wang, A.; Dou, H.; Zhang, X. *RSC advances* **2016**, 6, (47), 40650-40655.
52. Lacey, M. J.; Jeschull, F.; Edström, K.; Brandell, D. *Chemical Communications* **2013**, 49, (76), 8531-8533.
53. Li, G.; Cai, W.; Liu, B.; Li, Z. *J. Power Sources* **2015**, 294, 187-192.
54. Park, K.; Cho, J. H.; Jang, J.-H.; Yu, B.-C.; Andreae, T.; Miller, K. M.; Ellison, C. J.; Goodenough, J. B. *Energy Environ. Sci.* **2015**, 8, (8), 2389-2395.
55. Zhang, S. S.; Tran, D. T.; Zhang, Z. *Journal of Materials Chemistry A* **2014**, 2, (43), 18288-18292.
56. Zhang, Z.; Bao, W.; Lu, H.; Jia, M.; Xie, K.; Lai, Y.; Li, J. *ECS Electrochemistry Letters* **2012**, 1, (2), A34.
57. Qiu, T.; Shao, H.; Wang, W.; Zhang, H.; Wang, A.; Feng, Z.; Huang, Y. *RSC advances* **2016**, 6, (104), 102626-102633.
58. Liao, J.; Ye, Z. *Batteries* **2018**, 4, (2), 22.
59. Mei, B.-A.; Munteshari, O.; Lau, J.; Dunn, B.; Pilon, L. *The Journal of Physical Chemistry C* **2018**, 122, (1), 194-206.
60. Etacheri, V.; Marom, R.; Elazari, R.; Salitra, G.; Aurbach, D. *Energy Environ. Sci.* **2011**, 4, (9), 3243-3262.
61. Goodenough, J. B. *Accounts of chemical research* **2013**, 46, (5), 1053-1061.
62. Gao, X.-P.; Yang, H.-X. *Energy Environ. Sci.* **2010**, 3, (2), 174-189.
63. Ji, X.; Nazar, L. F. *Journal of Materials Chemistry* **2010**, 20, (44), 9821-9826.
64. Lee, C.-W.; Pang, Q.; Ha, S.; Cheng, L.; Han, S.-D.; Zavadil, K. R.; Gallagher, K. G.; Nazar, L. F.; Balasubramanian, M. *ACS central science* **2017**, 3, (6), 605-613.
65. Bruce, P. G.; Freunberger, S. A.; Hardwick, L. J.; Tarascon, J.-M. *Nature materials* **2012**, 11, (1), 19-29.
66. Urbonaitė, S.; Poux, T.; Novák, P. *Adv. Energy Mater.* **2015**, 5, (16), 1500118.
67. Cheng, X.-B.; Zhang, R.; Zhao, C.-Z.; Zhang, Q. *Chemical Reviews* **2017**, 117, (15), 10403-10473.
68. Zheng, J.; Ji, G.; Fan, X.; Chen, J.; Li, Q.; Wang, H.; Yang, Y.; DeMella, K. C.; Raghavan, S. R.; Wang, C. *Adv. Energy Mater.* **2019**, 9, (16), 1803774.
69. Chen, J.; Yang, H.; Zhang, X.; Lei, J.; Zhang, H.; Yuan, H.; Yang, J.; Nuli, Y.; Wang, J. *ACS Applied Materials & Interfaces* **2019**, 11, (36), 33419-33427.
70. Gerber, L. C. H.; Frischmann, P. D.; Fan, F. Y.; Doris, S. E.; Qu, X.; Scheuermann, A. M.; Persson, K.; Chiang, Y.-M.; Helms, B. A. *Nano Letters* **2016**, 16, (1), 549-554.
71. Choi, J.-W.; Cheruvally, G.; Kim, D.-S.; Ahn, J.-H.; Kim, K.-W.; Ahn, H.-J. *J. Power Sources* **2008**, 183, (1), 441-445.
72. Zhang, S. S. *Electrochimica Acta* **2012**, 70, 344-348.
73. Wu, F.; Thieme, S.; Ramanujapuram, A.; Zhao, E.; Weller, C.; Althues, H.; Kaskel, S.; Borodin, O.; Yushin, G. *Nano Energy* **2017**, 40, 170-179.
74. Li, W.; Yao, H.; Yan, K.; Zheng, G.; Liang, Z.; Chiang, Y.-M.; Cui, Y. *Nature Communications* **2015**, 6, (1), 7436.



75. Lee, J. T.; Eom, K.; Wu, F.; Kim, H.; Lee, D. C.; Zdyrko, B.; Yushin, G. *ACS Energy Letters* **2016**, 1, (2), 373-379.
76. Yang, B.; Jiang, H.; Zhou, Y.; Liang, Z.; Zhao, T.; Lu, Y.-C. *ACS applied materials & interfaces* **2019**, 11, (29), 25940-25948.
77. Chu, H.; Noh, H.; Kim, Y.-J.; Yuk, S.; Lee, J.-H.; Lee, J.; Kwack, H.; Kim, Y.; Yang, D.-K.; Kim, H.-T. *Nature Communications* **2019**, 10, (1), 188.
78. Matsuda, Y.; Morita, M. *J. Power Sources* **1987**, 20, (3-4), 273-278.
79. Read, J. *Journal of the Electrochemical Society* **2005**, 153, (1), A96.
80. Kim, H.-S.; Jeong, C.-S. *Bulletin of the Korean Chemical Society* **2011**, 32, (10), 3682-3686.
81. Kolosnitsyn, V.; Kuzmina, E.; Karaseva, E.; Sheina, L. In *Effect of physicochemical properties of electrolyte systems on behavior of lithium sulfur cells*, Meeting Abstracts, 2013; The Electrochemical Society: pp 330-330.
82. Wang, W.; Wang, Y.; Huang, Y.; Huang, C.; Yu, Z.; Zhang, H.; Wang, A.; Yuan, K. *Journal of Applied Electrochemistry* **2010**, 40, (2), 321-325.
83. Xu, K. *Chemical reviews* **2014**, 114, (23), 11503-11618.
84. Younesi, R.; Veith, G. M.; Johansson, P.; Edström, K.; Vegge, T. *Energy Environ. Sci.* **2015**, 8, (7), 1905-1922.
85. Scheers, J.; Fantini, S.; Johansson, P. *J. Power Sources* **2014**, 255, 204-218.
86. Xu, G.; Shangguan, X.; Dong, S.; Zhou, X.; Cui, G. *Angewandte Chemie International Edition* **2020**, 59, (9), 3400-3415.
87. Kwok, C.; Pang, Q.; Worku, A.; Liang, X.; Gauthier, M.; Nazar, L. *ACS applied materials & interfaces* **2019**, 11, (25), 22481-22491.
88. Li, Y.; Wang, W.; Liu, X.; Mao, E.; Wang, M.; Li, G.; Fu, L.; Li, Z.; Eng, A. Y. S.; Seh, Z. W.; Sun, Y. *Energy Storage Materials* **2019**, 23, 261-268.
89. Wang, W.; Yue, X.; Meng, J.; Wang, X.; Zhou, Y.; Wang, Q.; Fu, Z. *The Journal of Physical Chemistry C* **2019**, 123, (1), 250-257.
90. Xiao, Z. B.; Yang, Z.; Wang, L.; Nie, H. G.; Zhong, M. E.; Lai, Q. Q.; Xu, X. J.; Zhang, L. J.; Huang, S. M. *Advanced Materials* **2015**, 27, (18), 2891-+.
91. Cai, K.; Song, M.-K.; Cairns, E. J.; Zhang, Y. *Nano Letters* **2012**, 12, (12), 6474-6479.
92. Yang, Y.; McDowell, M. T.; Jackson, A.; Cha, J. J.; Hong, S. S.; Cui, Y. *Nano Letters* **2010**, 10, (4), 1486-1491.
93. Yang, Y.; Zheng, G. Y.; Misra, S.; Nelson, J.; Toney, M. F.; Cui, Y. *Journal of the American Chemical Society* **2012**, 134, (37), 15387-15394.
94. Wagemaker, M.; Mulder, F. M.; Van der Ven, A. *Advanced Materials* **2009**, 21, (25-26), 2703-+.
95. Su, D.; Zhou, D.; Wang, C.; Wang, G. *Advanced Functional Materials* **2018**, 28, (38), 1800154.
96. Yan, Y. Y.; Cheng, C.; Zhang, L.; Li, Y. G.; Lu, J. *Adv. Energy Mater.* **2019**, 9, (18).
97. Gorlin, Y.; Patel, M. U. M.; Freiberg, A.; He, Q.; Piana, M.; Tromp, M.; Gasteiger, H. A. *Journal of the Electrochemical Society* **2016**, 163, (6), A930-A939.
98. Zheng, J.; Gu, M.; Chen, H.; Meduri, P.; Engelhard, M. H.; Zhang, J.-G.; Liu, J.; Xiao, J. *Journal of Materials Chemistry A* **2013**, 1, (29), 8464-8470.
99. Yuan, Z.; Peng, H. J.; Hou, T. Z.; Huang, J. Q.; Chen, C. M.; Wang, D. W.; Cheng, X. B.; Wei, F.; Zhang, Q. *Nano Letters* **2016**, 16, (1), 519-527.

100. Kong, L.; Chen, J. X.; Peng, H. J.; Huang, J. Q.; Zhu, W. C.; Jin, Q.; Li, B. Q.; Zhang, X. T.; Zhang, Q. *Energy Environ. Sci.* **2019**, 12, (10), 2976-2982.
101. Zhang, S. S. *Energies* **2012**, 5, (12), 5190-5197.
102. Moy, D.; Manivannan, A.; Narayanan, S. R. *Journal of the Electrochemical Society* **2015**, 162, (1), A1-A7.
103. Jaumann, T.; Balach, J.; Klose, M.; Oswald, S.; Eckert, J.; Giebeler, L. *Journal of The Electrochemical Society* **2016**, 163, (3), A557-A564.
104. Wu, B.; Lochala, J.; Taverne, T.; Xiao, J. *Nano Energy* **2017**, 40, 34-41.
105. Gerber, L. C.; Frischmann, P. D.; Fan, F. Y.; Doris, S. E.; Qu, X.; Scheuermann, A. M.; Persson, K.; Chiang, Y.-M.; Helms, B. A. *Nano letters* **2016**, 16, (1), 549-554.
106. Guo, J.; Du, X.; Zhang, X.; Zhang, F.; Liu, J. *Advanced Materials* **2017**, 29, (26), 1700273.
107. Guo, J.; Wen, Z.; Wu, M.; Jin, J.; Liu, Y. *Electrochemistry Communications* **2015**, 51, 59-63.
108. Zhang, S. S. *J. Power Sources* **2008**, 180, (1), 586-590.
109. Sun, Z.; Zhang, J.; Yin, L.; Hu, G.; Fang, R.; Cheng, H.-M.; Li, F. *Nature communications* **2017**, 8, (1), 1-8.
110. Yim, T.; Kang, K. S.; Yu, J.-S.; Kim, K. J.; Park, M.-S.; Woo, S.-G.; Jeong, G.; Jo, Y. N.; Im, K. Y.; Kim, J.-H. *Japanese Journal of Applied Physics* **2014**, 53, (8S3), 08NK01.
111. Mikhaylik, Y. V.; Akridge, J. R. *Journal of the Electrochemical Society* **2004**, 151, (11), A1969.
112. Sun, K.; Matarasso, A. K.; Epler, R. M.; Tong, X.; Su, D.; Marschilok, A. C.; Takeuchi, K. J.; Takeuchi, E. S.; Gan, H. *Journal of The Electrochemical Society* **2018**, 165, (2), A416.
113. Park, S.; Popov, B. N. *Fuel* **2011**, 90, (1), 436-440.
114. Cho, I.; Choi, J.; Kim, K.; Ryou, M.-H.; Lee, Y. M. *Rsc Advances* **2015**, 5, (115), 95073-95078.
115. Finegan, D. P.; Cooper, S. J.; Tjaden, B.; Taiwo, O. O.; Gelb, J.; Hinds, G.; Brett, D. J.; Shearing, P. R. *J. Power Sources* **2016**, 333, 184-192.
116. Yang, X.; Li, X.; Adair, K.; Zhang, H.; Sun, X. *Electrochemical Energy Reviews* **2018**, 1, (3), 239-293.
117. Liu, W.-R.; Yang, M.-H.; Wu, H.-C.; Chiao, S.; Wu, N.-L. *Electrochemical and Solid State Letters* **2004**, 8, (2), A100.
118. Zhang, S. S. *Journal of the Electrochemical Society* **2012**, 159, (8), A1226.
119. Lacey, M. J.; Jeschull, F.; Edström, K.; Brandell, D. *The Journal of Physical Chemistry C* **2014**, 118, (45), 25890-25898.
120. Baldan, A. *Journal of Materials Science* **2004**, 39, (1), 1-49.
121. Bao, W.; Zhang, Z.; Gan, Y.; Wang, X.; Lia, J. *Journal of energy chemistry* **2013**, 22, (5), 790-794.
122. Kang, W.; Zhao, C.; Shen, Q. *Int. J. Electrochem. Sci* **2012**, 7, (9), 8194-8204.
123. Kovalenko, I.; Zdyrko, B.; Magasinski, A.; Hertzberg, B.; Milicev, Z.; Burtovyy, R.; Luzinov, I.; Yushin, G. *Science* **2011**, 334, (6052), 75-79.
124. Wang, W.; Yue, X.; Meng, J.; Wang, X.; Zhou, Y.; Wang, Q.; Fu, Z. *The Journal of Physical Chemistry C* **2018**, 123, (1), 250-257.
125. Yan, L.; Gao, X.; Wahid-Pedro, F.; Quinn, J. T. E.; Meng, Y.; Li, Y. *Journal of Materials Chemistry A* **2018**, 6, (29), 14315-14323.

126. Zhu, X.; Zhang, F.; Zhang, L.; Zhang, L.; Song, Y.; Jiang, T.; Sayed, S.; Lu, C.; Wang, X.; Sun, J. *Advanced Functional Materials* **2018**, 28, (11), 1705015.